

# Automated Symbolic Upscaling: Model Generation for Extended Applicability Regimes, Part 1

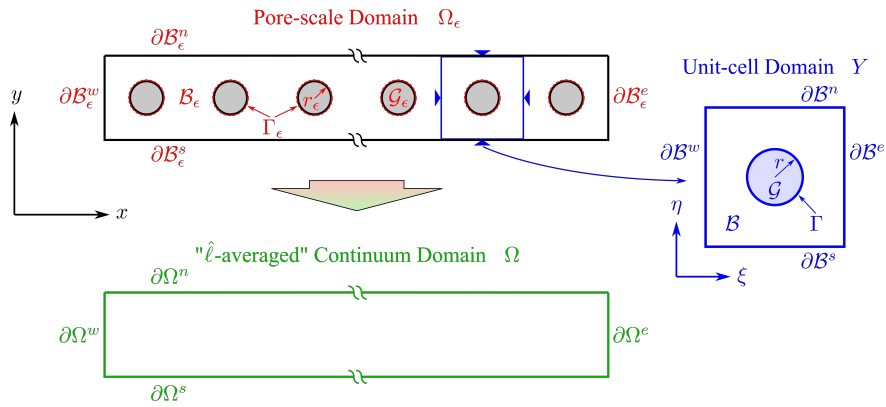
Kyle Pietrzyk<sup>1</sup> and Ilenia Battiato<sup>1</sup>

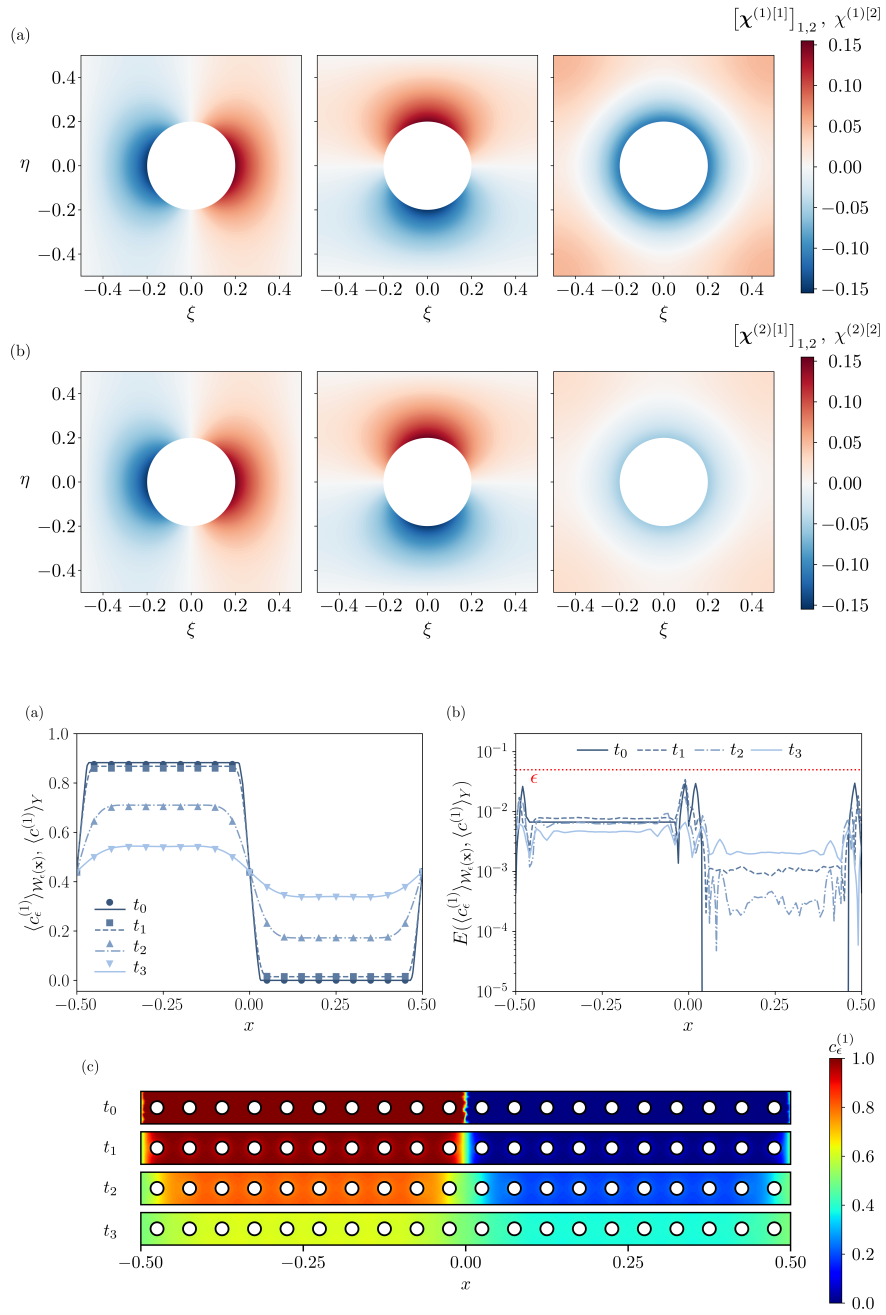
<sup>1</sup>Stanford University

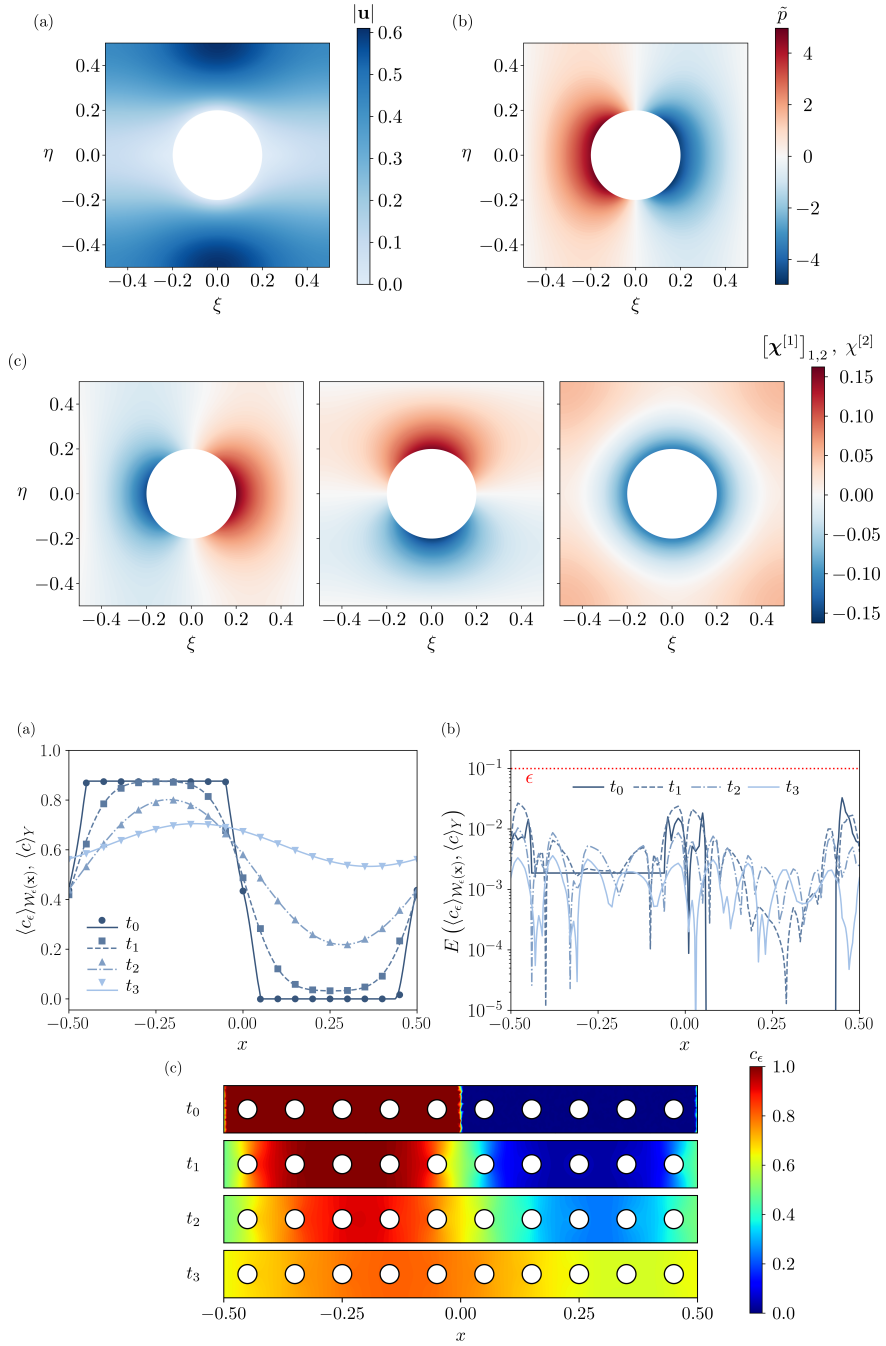
November 22, 2022

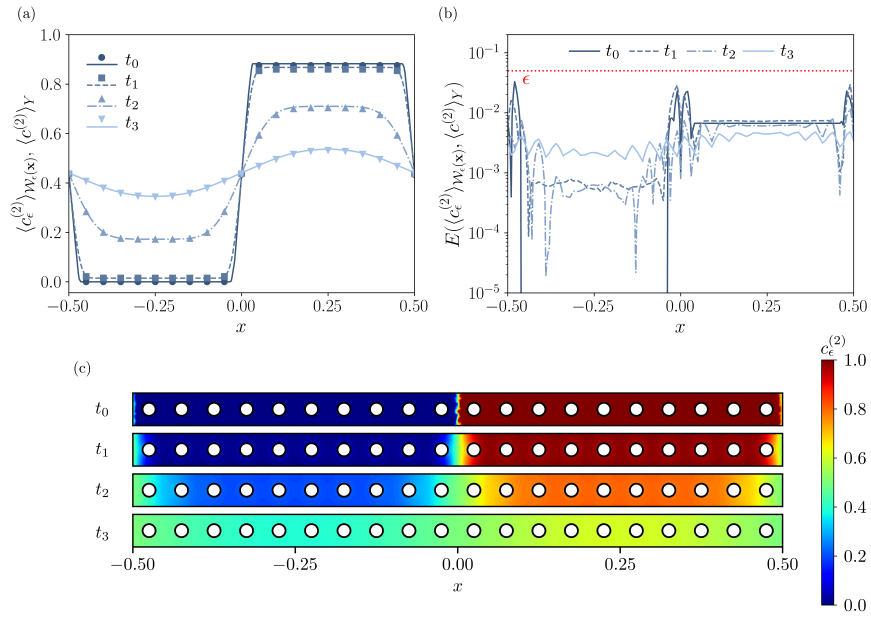
## Abstract

In porous media theory, upscaling techniques are fundamental to deriving rigorous Darcy-scale models for flow and reactive transport in subsurface systems. Due to limitations in classical upscaling methods, a number of ad hoc techniques have been proposed to address physical regimes of higher reactivity, such as moderately reactive regimes where diffusive and reactive mass transport are of the same order of magnitude. In Part 1 of this two part series, we present a strategy for expanding the applicability of classical homogenization theory by generalizing the assumed closure form. We detail the implementation of this strategy on two reactive mass transport problems with moderately reactive physics. The strategy produces nontrivial homogenized models with effective parameters that couple reactive, diffusive, and advective transport. Numerical validation is provided for each problem to justify the implemented strategy.









# Automated Symbolic Upscaling: Model Generation for Extended Applicability Regimes, Part 1

Kyle Pietrzyk<sup>1</sup>, Ilenia Battiato<sup>1</sup>

<sup>1</sup>Department of Energy Resources Engineering, Stanford University, 367 Panama St., Stanford, CA 94305

## Key Points:

- A strategy for expanding the applicability of classical homogenization theory by generalizing the assumed closure form is presented.
- The strategy is detailed and numerically validated in two reactive mass transport problems experiencing moderately reactive physics.
- Nontrivial homogenized models with effective parameters that couple reactive, diffusive, and advective transport are derived.

## Abstract

In porous media theory, upscaling techniques are fundamental to deriving rigorous Darcy-scale models for flow and reactive transport in subsurface systems. Due to limitations in classical upscaling methods, a number of *ad hoc* techniques have been proposed to address physical regimes of higher reactivity, such as moderately reactive regimes where diffusive and reactive mass transport are of the same order of magnitude. In Part 1 of this two part series, we present a strategy for expanding the applicability of classical homogenization theory by generalizing the assumed closure form. We detail the implementation of this strategy on two reactive mass transport problems with moderately reactive physics. The strategy produces nontrivial homogenized models with effective parameters that couple reactive, diffusive, and advective transport. Numerical validation is provided for each problem to justify the implemented strategy.

## 1 Introduction

Due to the vast spectra of spatiotemporal variations in subsurface processes and geological media, multiscale modeling has remained a cornerstone for analyzing flow and reactive transport beneath the surface (Scheibe et al., 2015; Molins & Knabner, 2019; Mehmani, Anderson, et al., 2021). The technical approaches set forth by this paradigm focus on translating the physical dynamics at finer scales (e.g., the pore-scale) to much larger scales where nontrivial behaviors tend to occur. By providing accurate and computationally efficient predictions of such large-scale behaviors, these analysis methods enhance the understandings of phenomena observed in geological engineering and hydrology, such as acidification reactions in carbonate rocks and biogeochemical reactions (Tang et al., 2015; Yan et al., 2017; Molins et al., 2019; Becker et al., 2022; Mehmani, Castelletto, & Tchelepi, 2021; Wang & Battiato, 2020). While many classical approaches to multiscale modeling continue to be employed (Schiller & Wang, 2018; Battiato et al., 2019), new data-driven strategies are also being developed to reap the benefits of state-of-the-art technologies (Lubbers et al., 2020; Wang & Battiato, 2021).

Within multiscale modeling, considerable efforts have focused on evolving and generalizing *upscaling* techniques, such as the method of volume averaging (MVA) (Whitaker, 1999), homogenization theory (Hornung, 1997), and thermodynamically constrained averaging theory (TCAT) (Gray & Miller, 2014), among others. These techniques provide rigorous approaches to systematically generate macroscopic partial differential equations (PDEs) from first principle equations at the microscale (Battiato et al., 2019). To formulate macroscopic PDEs, supplemental terms and effective coefficients are derived to accurately account for multiscale behaviors (Pietrzyk et al., 2021). In addition to the accuracy and computational efficiency provided by these models, *applicability conditions* (also referred to as *scaling laws* in MVA (Golfier et al., 2009; Wood, 2009) and *permissibility conditions* in TCAT (C. Miller et al., 2018)) can also be obtained during the upscaling procedures (Battiato & Tartakovsky, 2011; Boso & Battiato, 2013), which provide physical constraints under which estimates of the accrued modeling error are known *a priori*. A number of upscaling theories go beyond the derivation of classical Darcy-scale equations for reactive transport and multiphase flow (e.g., modeling nonhysteretic capillary pressure behavior (C. T. Miller et al., 2019)). Some of these include deterministic and stochastic nonlocal modeling techniques (Gelhar & Axness, 1983), such as dual and multicontinuum modeling (Cushman & Ginn, 1993; Neuman, 1993; Haggerty et al., 2000), continuous time random walk modeling (Berkowitz et al., 2006), moment methods (Neuman, 1993), and projector operator methods (Cushman & Ginn, 1993). Even advanced methods for physics-based multiscale modeling with various degrees of coupling have used upscaling techniques as their primary machinery for model development (Battiato et al., 2011; Yousefzadeh & Battiato, 2017; Ahmed et al., 2022).

With continued interest in upscaling and related modeling methods, attention has centered around extending the applicability of such techniques to physical regimes in which the accuracy of effective-medium models has been questioned (Battiato et al., 2009; Arunachalam et al., 2015; Pietrzyk et al., 2021). In particular, significant progress has been made toward extending the applicability of upscaling techniques to highly advective and reactive regimes. In the context of homogenization theory (Hornung, 1997), problem-specific techniques that deviate from the standard theory have been developed to analyze various transport regimes. Early investigations into systems with strong advection involved expanding temporal derivatives in an effort to consider dynamics across multiple time scales (Rubinstein & Mauri, 1986; Mei, 1992; Salles et al., 1993; Auriault & Adler, 1995). Other methods handled strong advection by adding *drift* to the pore-scale equations, which involved transforming the large-scale coordinates to a moving coordinate frame (Garnier, 1997; Donato & Piatnitski, 2005; Marušić-Paloka & Piatnitski, 2005). A similar idea of variable transformation was also used to model strong reactive behavior (Mauri, 1991; “Diffusion in Ran-

68 dom Media”, 1995) along with other various mathematical methods (Lewandowska et al., 2002). These  
69 variable transformation methods have since become the standard for homogenizing strongly advective-  
70 reactive systems (Allaire & Raphael, 2007; Allaire, Mikelić, & Piatnitski, 2010; Allaire, Brizzi, et al., 2010)  
71 and more recent homogenization strategies seem to benefit from their influence (Municchi & Icardi, 2020;  
72 Le et al., 2022).

73 As efforts to further generalize and sophisticate upscaling theories persevere, the syntactical, math-  
74 ematical, and procedural complexities employed continue to grow. These come in addition to the com-  
75 plexities inherent to realistic geological reactive systems, which can involve multiple coupled physical pro-  
76 cesses and reaction networks that easily include tens of species or more. The combined complexity is enough  
77 to deter scientists and practitioners away from upscaling techniques and drive them towards alternative,  
78 less rigorous modeling techniques. However, known applicability conditions and error limits bring value  
79 to upscaled models and make them relevant solutions to questions regarding model validity in subsur-  
80 face flow and reactive transport problems (e.g., CO<sub>2</sub> sequestration, H<sub>2</sub> subsurface storage, etc.). In light  
81 of this, it is beneficial to create methods for handling the complexities associated with upscaling tech-  
82 niques, and ultimately democratize upscaling for efficient use in subsurface flow and reactive transport  
83 applications.

84 In this two part series, we propose a general analytical strategy for extending the applicability of  
85 homogenized models with respect to classical homogenization theory (Part 1), and implement the strat-  
86 egy into an automated upscaling framework for rapid use in a wide range of complex systems (Part 2).  
87 The strategy involves generalizing the assumed forms of ordered solutions by constructing them as lin-  
88 ear combinations of closure terms. This leads to the definition of multiple closure problems for a single  
89 ordered solution, whereas in classical homogenization theory, only one closure problem is defined and the  
90 assumed form of the first order solution consists of only one closure term. We then implement the an-  
91 alytical strategy into *Symbolica*, a symbolic computational code for fully automating rigorous analytical  
92 upscaling procedures on problems with realistic complexities. By streamlining the notoriously lengthy  
93 and syntactically complex derivations of upscaling, *Symbolica* enables users with limited mathematical  
94 expertise to rapidly generate and deploy upscaled models for analysis in complex practical systems. As  
95 a result, communal access to upscaling techniques is provided in a similar manner to how computational  
96 physics softwares provide access to numerical methods.

97 Aside from speed, democratization, and the ability to apply upscaling theories in complex practi-  
98 cal systems, *Symbolica* is also capable of quickly, and rigorously, traversing dimensionless parameter spaces  
99 for valid upscaled models. Originally pointed out in previous works (Auriault & Adler, 1995; Battiato  
100 & Tartakovsky, 2011; Boso & Battiato, 2013), the value of this ability has been reemphasized in recent  
101 works that consider homogenization techniques for handling highly advective and reactive systems. These  
102 works highlight that varying the magnitudes of the dimensionless parameters in a system can lead to dif-  
103 ferent macroscopic models:

104 “Namely even starting from the same microscale problem, for different sizes of the characteristic  
105 numbers, the homogenization results in different upscaled (macroscale) model depending on the con-  
106 sidered regime. Different here means that these can be different types of equations, which cannot  
107 be converted to each other by simple fitting of the coefficients.” (Iliev et al., 2020)

108 “Dimensionless parameters are hence obtained explicitly as ratios of characteristic quantities. Con-  
109 sidering these dimensionless parameters, at different orders of magnitude, leads to different macro-  
110 scopic behaviours in the case of homogenisable situations.” (Bloch & Auriault, 2019)

111 As described, the macroscopic model of a system cannot be trivially assumed for general dimensionless  
112 parameter magnitudes; the upscaling procedure must be re-executed for each set of dimensionless param-  
113 eter magnitudes considered. With *Symbolica*, the workload associated with upscaling for each combina-  
114 tion of dimensionless parameter magnitudes is removed, as the code automatically upscales across the  
115 dimensionless parameter space in a short amount of time (Pietrzyk et al., 2021).

116 In Part 1, we present the general analytical strategy for extending applicability by annotating its  
117 implementation in two example reactive mass transport problems and numerically validate the homog-  
118 enized results. Nontrivial homogenized models and effective parameters are found and discussed in de-  
119 tail. The proposed approach has a number of advantages. Firstly, it directly generalizes and extends the  
120 applicability of classically homogenized, reactive mass transport models into moderately reactive regimes,

121 where diffusive and reactive terms are of the same order. Secondly, the presented strategy is compati-  
 122 ble with, and can further generalize, theories for homogenizing highly advective and reactive systems, as  
 123 well as theories for analyzing inhomogeneous boundary conditions (Municchi & Icardi, 2020). Thirdly,  
 124 the strategy can be easily implemented into automated upscaling frameworks in an algorithmic fashion  
 125 for automated closure form and closure problem definition. This capability is explored in Part 2 of this  
 126 series, where we validate the implementation of the strategy in *Symbolica* by analyzing two additional re-  
 127 active mass transport problems. Overall, we find this implementation invaluable, as it enables *Symbol-*  
 128 *ica* to automatically homogenize complex systems with multiple, moderately strong reactions and pro-  
 129 duce nontrivial homogenized models.

130 The manuscript is organized as follows. In Section 2, a general problem of reactive transport in porous  
 131 media is formulated for multiple solutes and reaction interfaces. The governing equations and boundary  
 132 conditions are introduced in Subsection 2.1 with a general scaling, a unit-cell formulation, and expan-  
 133 sions of the temporal derivative and dependent variables presented in Subsections 2.2, 2.3, and 2.4, re-  
 134 spectively. Then, from the previously presented general reactive transport problem, we derive the equa-  
 135 tions and boundary conditions for the first considered transport problem: a single species undergoing a  
 136 linear, heterogeneous reaction (Section 3). While the detailed implementation of the proposed homog-  
 137 enization strategy can be found in Appendix A, the main homogenized results are presented in Subsec-  
 138 tion 3.1 and numerical validation is provided in Subsection 3.2. A second transport problem consisting  
 139 of two solutes undergoing linearly coupled, heterogeneous reactions is then considered in Section 4, where  
 140 the equations and boundary conditions are derived from the general reactive transport problem. Again,  
 141 the detailed implementation can be found in Appendix B while the main homogenized results and nu-  
 142 merical validation are provided in Subsections 4.1 and 4.2, respectively. Finally, concluding remarks for  
 143 Part 1 of this two part series can be found in Section 5.

## 144 2 Problem Formulation

145 Similar to the setup in our previous work (Pietrzyk et al., 2021), we consider a porous medium  $\hat{\Omega}_\epsilon \subset$   
 146  $\mathbb{R}^b$ , where  $b \in \{1, 2, 3\}$ , consisting of a pore-space  $\hat{\mathcal{B}}_\epsilon$  and an impermeable solid matrix  $\hat{\mathcal{G}}_\epsilon$ . A smooth  
 147 interface  $\hat{\Gamma}_\epsilon$  is assumed to exist between the two domains. We also assume the physical gradients within  
 148 this medium are adequately described using two length scales: a larger scale  $\hat{\mathcal{L}}$  and a smaller scale  $\hat{\ell}$ . A  
 149 length scale ratio

$$\epsilon \equiv \frac{\hat{\ell}}{\hat{\mathcal{L}}} \quad (1)$$

150 can then be defined, where  $\hat{\mathcal{L}} \gg \hat{\ell}$  implies  $\epsilon \ll 1$ . Unless otherwise stated, hatted variables are assumed  
 151 to have physical dimension, while variables without hats are assumed to be dimensionless.

### 152 2.1 Governing Equations and Boundary Conditions

153 We assume an incompressible liquid fully saturates the pore-space. The Stokes equation, the incom-  
 154 pressible continuity equation, and a no-slip boundary condition govern the velocity and pressure fields  
 155 of the liquid, such that

$$\hat{\mu} \hat{\nabla}^2 \hat{\mathbf{u}}_\epsilon - \hat{\nabla} \hat{p}_\epsilon = \mathbf{0} \quad \text{in } \hat{\mathcal{B}}_\epsilon, \quad (2a)$$

$$\hat{\nabla} \cdot \hat{\mathbf{u}}_\epsilon = 0 \quad \text{in } \hat{\mathcal{B}}_\epsilon, \quad (2b)$$

156 subject to

$$\hat{\mathbf{u}}_\epsilon = \mathbf{0} \quad \text{on } \hat{\Gamma}_\epsilon, \quad (2c)$$

157 where  $\hat{\mathbf{u}}_\epsilon \equiv \hat{\mathbf{u}}_\epsilon(\hat{\mathbf{x}})$  is the fluid velocity at spatial coordinate  $\hat{\mathbf{x}} \in \hat{\mathcal{B}}_\epsilon$ ,  $\hat{\mu}$  is the dynamic viscosity, and  
 158  $\hat{p}_\epsilon \equiv \hat{p}_\epsilon(\hat{\mathbf{x}})$  is the pressure. Theoretically, we only consider these equations far from the boundaries of  
 159  $\hat{\Omega}_\epsilon$ , such that non-local effects due to macroscale boundary conditions on  $\hat{\Omega}_\epsilon$  are negligible.

160 In addition to the fluid flow, we consider the transport of  $N$  species subject to advection, diffusion,  
 161 and both homogeneous and heterogeneous reactions. For each species  $i$ , where  $i \in \{1, 2, \dots, N\}$ , we con-  
 162 sider bimolecular homogeneous reactions of the type  $A+B \leftrightarrow C+D$  in the liquid phase and heteroge-  
 163 neous reactions of the type  $M_{(l)} \leftrightarrow M_{(s)}$  at the liquid-solid interface. We note that generalizations to  
 164 reactions beyond those described here are straightforward. To accommodate multiple heterogeneous re-  
 165 actions occurring on different sections of the interface  $\hat{\Gamma}_\epsilon$ , we divide the liquid-solid interface into  $N_\Gamma$  parts,  
 166 such that

$$\hat{\Gamma}_\epsilon = \bigcup_{j=1}^{N_\Gamma} \hat{\Gamma}_\epsilon^{(j)}, \quad (3)$$

167 where  $\hat{\Gamma}_\epsilon^{(j)}$  is the interface  $j$ , a subsection of the total interface  $\hat{\Gamma}_\epsilon$ . This allows multiple heterogeneous  
 168 reactions to be defined across the various interface subsections  $\hat{\Gamma}_\epsilon^{(j)}$  for a single solute. Then, the trans-  
 169 port of each reactive species in the pore-space is governed by a system of advective-diffusive-reactive (ADR)  
 170 equations of the form

$$\frac{\partial \hat{c}_\epsilon^{(i)}}{\partial \hat{t}} + \hat{\nabla} \cdot (\hat{\mathbf{u}}_\epsilon \hat{c}_\epsilon^{(i)} - \hat{D}^{(i)} \hat{\nabla} \hat{c}_\epsilon^{(i)}) = \hat{R}_\epsilon^{(i)} \quad \text{in } \hat{\mathcal{B}}_\epsilon, \quad (4a)$$

$$\hat{R}_\epsilon^{(i)} = \sum_{k=1}^N (-1)^{p_L^{(i,k)}} \hat{\mathcal{K}}_L^{(i,k)} \hat{c}_\epsilon^{(k)} + \sum_{k=1}^N \sum_{l=k}^N (-1)^{p_{NL}^{(i,k,l)}} \hat{\mathcal{K}}_{NL}^{(i,k,l)} \hat{c}_\epsilon^{(k)} \hat{c}_\epsilon^{(l)}, \quad (4b)$$

171 subject to

$$-\mathbf{n}^{(j)} \cdot \hat{D}^{(i)} \hat{\nabla} \hat{c}_\epsilon^{(i)} = \hat{T}_\epsilon^{(i,j)} \quad \text{on } \hat{\Gamma}_\epsilon^{(j)}, \quad (4c)$$

$$\begin{aligned} \hat{T}_\epsilon^{(i,j)} &= \sum_{k=1}^N (-1)^{p_{SL}^{(i,j,k)}} \hat{\mathcal{K}}_{SL}^{(i,j,k)} \left( \hat{c}_\epsilon^{(k)} - \hat{C}_{SL}^{(i,j,k)} \right) \\ &+ \sum_{k=1}^N \sum_{l=k}^N (-1)^{p_{SNL}^{(i,j,k,l)}} \hat{\mathcal{K}}_{SNL}^{(i,j,k,l)} \left( \hat{c}_\epsilon^{(k)} \hat{c}_\epsilon^{(l)} - \hat{C}_{SNL}^{(i,j,k,l)^2} \right), \end{aligned} \quad (4d)$$

172 where  $\hat{c}_\epsilon^{(i)} \equiv \hat{c}_\epsilon^{(i)}(\hat{t}, \hat{\mathbf{x}})$  is the concentration of species  $i$  at time  $\hat{t} > 0$  and spatial coordinate  $\hat{\mathbf{x}} \in \hat{\mathcal{B}}_\epsilon$ ,  
 173  $\hat{D}^{(i)}$  is the diffusion coefficient of species  $i$ ,  $\hat{R}_\epsilon^{(i)}$  is the sum of all bulk reaction terms for species  $i$ ,  $p_L^{(i,k)}$   
 174 and  $p_{NL}^{(i,k,l)}$  are either 0 or 1,  $\hat{\mathcal{K}}_L^{(i,k)}$  is the reaction rate constant of the linear bulk reaction correspond-  
 175 ing to species  $k$  in the transport equation for species  $i$ ,  $\hat{\mathcal{K}}_{NL}^{(i,k,l)}$  is the reaction rate constant of the non-  
 176 linear bulk reaction corresponding to species  $k$  and  $l$  in the transport equation for species  $i$ ,  $\mathbf{n}^{(j)} \equiv \mathbf{n}^{(j)}(\hat{\mathbf{x}})$   
 177 is the normal vector to the liquid-solid interface subsection  $j$  pointed towards the solid,  $\hat{T}_\epsilon^{(i,j)}$  is the sum  
 178 of all heterogeneous reaction terms for species  $i$  on the liquid-solid interface subsection  $j$ ,  $p_{SL}^{(i,j,k)}$  and  $p_{SNL}^{(i,j,k,l)}$   
 179 are either 0 or 1,  $\hat{\mathcal{K}}_{SL}^{(i,j,k)}$  is the reaction rate constant of the linear reaction at the liquid-solid interface  
 180 subsection  $j$  corresponding to species  $k$  in the system of equations for species  $i$ ,  $\hat{C}_{SL}^{(i,j,k)}$  is the threshold  
 181 concentration for the linear reaction at the liquid-solid interface subsection  $j$  for species  $k$  in the system  
 182 of equations for species  $i$  (Morse & Arvidson, 2002),  $\hat{\mathcal{K}}_{SNL}^{(i,j,k,l)}$  is the reaction rate constant of the non-linear  
 183 reaction at the liquid-solid interface subsection  $j$  corresponding to species  $k$  and  $l$  in the system of equa-  
 184 tions for species  $i$ , and  $\hat{C}_{SNL}^{(i,j,k,l)}$  is the threshold concentration for the non-linear reaction at the liquid-  
 185 solid interface subsection  $j$  for species  $k$  and  $l$  in the system of equations for species  $i$ . Similar to before,  
 186 we consider these equations far from the boundaries of  $\hat{\Omega}_\epsilon$  to eliminate concern of non-local effects from  
 187 macroscale boundary conditions on  $\hat{\Omega}_\epsilon$ , and do not assume any specific initial conditions.

## 188 2.2 Scaling

189 To scale systems (2) and (4), we consider the following:

$$\begin{aligned}\hat{c}_\epsilon^{(i)} &= \hat{C}^{(i)} c_\epsilon^{(i)}, \quad \hat{\nabla} = \frac{1}{\hat{\mathcal{L}}} \nabla, \quad \hat{D}^{(i)} = \hat{D} D^{(i)}, \quad \hat{\mathbf{u}}_\epsilon = \hat{U} \mathbf{u}_\epsilon, \quad \hat{p}_\epsilon = \hat{P} p_\epsilon, \\ \hat{t} &= \frac{\hat{\mathcal{L}}^2}{\hat{D}} t, \quad \hat{R}_\epsilon^{(i)} = \frac{\hat{D} \hat{C}^{(i)}}{\hat{\mathcal{L}}^2} R_\epsilon^{(i)}, \quad \hat{T}_\epsilon^{(i,j)} = \frac{\hat{D} \hat{C}^{(i)}}{\hat{\mathcal{L}}} T_\epsilon^{(i,j)},\end{aligned}\tag{5}$$

190 where  $\hat{C}^{(i)}$  is the concentration scale for species  $i$ ,  $\hat{D}$  is the diffusion coefficient scale,  $\hat{U}$  is the fluid veloc-  
191 ity scale, and  $\hat{P}$  is the fluid pressure scale. Applying these scales to system (2) yields

$$A_\epsilon \nabla^2 \mathbf{u}_\epsilon - \nabla p_\epsilon = \mathbf{0} \quad \text{in } \mathcal{B}_\epsilon,\tag{6a}$$

$$\nabla \cdot \mathbf{u}_\epsilon = 0 \quad \text{in } \mathcal{B}_\epsilon,\tag{6b}$$

192 subject to

$$\mathbf{u}_\epsilon = \mathbf{0} \quad \text{on } \Gamma_\epsilon.\tag{6c}$$

193 Here, we note that the ratio  $A_\epsilon = \hat{\mu} \hat{U} / (\hat{P} \hat{\mathcal{L}})$  in equation (6a) is assumed to have a magnitude of  $\mathcal{O}(\epsilon^2)$   
194 in the classical homogenization of the Stokes equation (Auriault & Adler, 1995). After applying the de-  
195 fined scales to system (4), we obtain

$$\frac{\partial c_\epsilon^{(i)}}{\partial t} + \nabla \cdot \left( \text{Pe} \mathbf{u}_\epsilon c_\epsilon^{(i)} - D^{(i)} \nabla c_\epsilon^{(i)} \right) = R_\epsilon^{(i)} \quad \text{in } \mathcal{B}_\epsilon,\tag{7a}$$

$$R_\epsilon^{(i)} = \sum_{k=1}^N (-1)^{p_L^{(i,k)}} \text{Da}_L^{(i,k)} c_\epsilon^{(k)} + \sum_{k=1}^N \sum_{l=k}^N (-1)^{p_{NL}^{(i,k,l)}} \text{Da}_{NL}^{(i,k,l)} c_\epsilon^{(k)} c_\epsilon^{(l)},\tag{7b}$$

196 subject to

$$-\mathbf{n}^{(j)} \cdot D^{(i)} \nabla c_\epsilon^{(i)} = T_\epsilon^{(i,j)} \quad \text{on } \Gamma_\epsilon^{(j)},\tag{7c}$$

$$\begin{aligned}T_\epsilon^{(i,j)} &= \sum_{k=1}^N (-1)^{p_{SL}^{(i,j,k)}} \text{Da}_{SL}^{(i,j,k)} \left( c_\epsilon^{(k)} - \theta_{SL}^{(i,j,k)} \right) \\ &+ \sum_{k=1}^N \sum_{l=k}^N (-1)^{p_{SNL}^{(i,j,k,l)}} \text{Da}_{SNL}^{(i,j,k,l)} \left( c_\epsilon^{(k)} c_\epsilon^{(l)} - \theta_{SNL}^{(i,j,k,l)} \right),\end{aligned}\tag{7d}$$

197 where the dimensionless numbers are defined as

$$\begin{aligned}\text{Pe} &= \frac{\hat{U} \hat{\mathcal{L}}}{\hat{D}}, \quad \text{Da}_L^{(i,k)} = \frac{\hat{\mathcal{K}}_L^{(i,k)} \hat{\mathcal{L}}^2 \hat{C}^{(k)}}{\hat{D} \hat{C}^{(i)}}, \quad \text{Da}_{NL}^{(i,k,l)} = \frac{\hat{\mathcal{K}}_{NL}^{(i,k,l)} \hat{\mathcal{L}}^2 \hat{C}^{(k)} \hat{C}^{(l)}}{\hat{D} \hat{C}^{(i)}}, \quad \text{Da}_{SL}^{(i,j,k)} = \frac{\hat{\mathcal{K}}_{SL}^{(i,j,k)} \hat{\mathcal{L}} \hat{C}^{(k)}}{\hat{D} \hat{C}^{(i)}}, \\ \theta_{SL}^{(i,j,k)} &= \frac{\hat{C}_{SL}^{(i,j,k)}}{\hat{C}^{(k)}}, \quad \text{Da}_{SNL}^{(i,j,k,l)} = \frac{\hat{\mathcal{K}}_{SNL}^{(i,j,k,l)} \hat{\mathcal{L}} \hat{C}^{(k)} \hat{C}^{(l)}}{\hat{D} \hat{C}^{(i)}}, \quad \theta_{SNL}^{(i,j,k,l)} = \frac{\hat{C}_{SNL}^{(i,j,k,l)^2}}{\hat{C}^{(k)} \hat{C}^{(l)}}.\end{aligned}\tag{8}$$

198 Here,  $\text{Pe}$  is the Péclet number,  $\text{Da}_L^{(i,k)}$ ,  $\text{Da}_{NL}^{(i,k,l)}$ ,  $\text{Da}_{SL}^{(i,j,k)}$ , and  $\text{Da}_{SNL}^{(i,j,k,l)}$  are Damköhler numbers, and  $\theta_{SL}^{(i,j,k)}$   
199 and  $\theta_{SNL}^{(i,j,k,l)}$  are concentration ratios.

### 2.3 Unit-Cell Domain Formulation

We define the unit-cell in a similar manner as our previous work (Pietrzyk et al., 2021), and provide the formulation here for completeness. By introducing a spatially-dependent variable  $\hat{\boldsymbol{\xi}}(\hat{\mathbf{x}}) \equiv \hat{\mathbf{x}}$ , and scaling  $\hat{\boldsymbol{\xi}}(\hat{\mathbf{x}})$  by  $\hat{\ell}$  and  $\hat{\mathbf{x}}$  by  $\hat{\mathcal{L}}$ , we obtain

$$\boldsymbol{\xi}(\mathbf{x}) = \epsilon^{-1}\mathbf{x}, \quad (9)$$

where  $\boldsymbol{\xi}(\mathbf{x})$  and  $\mathbf{x}$  are referred to as “fast” and “slow” variables, respectively (Hornung, 1997). Any spatially-dependent function  $f_\epsilon(\mathbf{x})$  is then written as  $f_\epsilon(\mathbf{x}) = f(\mathbf{x}, \boldsymbol{\xi}(\mathbf{x}))$ , and the chain rule is applied when considering  $\nabla$ , the total differential operator in space, to write

$$\nabla f_\epsilon \equiv \nabla_{\mathbf{x}} f + \frac{1}{\epsilon} \nabla_{\boldsymbol{\xi}} f. \quad (10)$$

Here,  $\nabla$  is shown to be a sum of two differential operators in space:  $\nabla_{\mathbf{x}}$  and  $\nabla_{\boldsymbol{\xi}}$ , which scale with  $1/\hat{\mathcal{L}}$  and  $1/\hat{\ell}$ , respectively.

We now assume  $\epsilon \ll 1$  and consider systems with spatial periodicity on the length scale  $\hat{\ell}$ . Under these constraints, we treat  $\boldsymbol{\xi}(\mathbf{x})$  as an independent variable  $\boldsymbol{\xi}$ , uncoupled from  $\mathbf{x}$ , that traverses a spatially periodic “unit-cell” domain  $Y$ . This domain consists of a pore-space region  $\mathcal{B}$  and an impermeable solid region  $\mathcal{G}$ . A smooth interface  $\Gamma = \cup_{j=1}^{N_\Gamma} \Gamma^{(j)}$  consisting of  $N_\Gamma$  subsections  $\Gamma^{(j)}$  exists within  $Y$  between  $\mathcal{B}$  and  $\mathcal{G}$ . Finally, we note that regions  $\mathcal{B}$  and  $\mathcal{G}$  should be arranged within  $Y$  such that a collection of contiguously placed unit-cell domains  $Y$  is representative of how  $\hat{\mathcal{B}}_\epsilon$  and  $\hat{\mathcal{G}}_\epsilon$  are arranged within  $\hat{\Omega}_\epsilon$ .

With the provided unit-cell formulation, our intention is to average the reactive transport and fluid flow over the unit-cell domain (Bachmat & Bear, 1986). To do this, we reconsider  $\mathbf{x}$  as an element of  $\Omega \equiv \Omega_\epsilon = \hat{\Omega}_\epsilon/\hat{\mathcal{L}}^b$ , a fictitious model domain treated as an “ $\hat{\ell}$ -averaged” continuum, and define averaging operators over the unit-cell  $Y$ , its pore-space  $\mathcal{B}$ , the total liquid-solid interface  $\Gamma$ , and the liquid-solid interface subsections  $\Gamma^{(j)}$  as

$$\begin{aligned} \langle \cdot \rangle_Y &\equiv \frac{1}{|Y|} \int_{\mathcal{B}} (\cdot) d\boldsymbol{\xi}, & \langle \cdot \rangle_{\mathcal{B}} &\equiv \frac{1}{|\mathcal{B}|} \int_{\mathcal{B}} (\cdot) d\boldsymbol{\xi}, & \langle \cdot \rangle_{\Gamma} &\equiv \frac{1}{|\Gamma|} \int_{\Gamma} (\cdot) d\boldsymbol{\xi}, \\ \text{and } \langle \cdot \rangle_{\Gamma^{(j)}} &\equiv \frac{1}{|\Gamma^{(j)}|} \int_{\Gamma^{(j)}} (\cdot) d\boldsymbol{\xi}, \end{aligned} \quad (11)$$

respectively. Depending on  $b$ ,  $|Y|$ ,  $|\mathcal{B}|$ ,  $|\Gamma|$ , and  $|\Gamma^{(j)}|$  are the volumes, areas, segments, or points of the unit-cell, the pore-space in the unit-cell, the liquid-solid interface in the unit-cell, and the liquid-solid interface subsections in the unit-cell, respectively. Here, we also define  $\phi = |\mathcal{B}|/|Y|$  as the porosity of the unit-cell and note that  $\langle \cdot \rangle_{\mathcal{B}} = \phi^{-1} \langle \cdot \rangle_Y$ .

### 2.4 Expansions of the Temporal Derivative and Dependent Variables

Similar to the handling of multiple spatial scales, we introduce additional time variables to account for the dynamics occurring on small time scales. Typically, these time variables are introduced based on the dimensionless numbers related to advective and reactive time scales (i.e., Péclet and Damköhler numbers) (Rubinstein & Mauri, 1986; Mei, 1992; Salles et al., 1993; Auriault & Adler, 1995; Battiato & Tartakovsky, 2011; Boso & Battiato, 2013), as these are often the only physical mechanisms appearing in the governing equations besides diffusion. Here, however, we explicitly define the time variables  $\tau_m(t) = \epsilon^{-m}t$ , where  $m \in \{1, 2\}$ , to introduce a temporal derivative at each equation order considered during our homogenization procedure. This allows us to clarify the assumptions implied when not considering additional time scales, and ultimately remove ambiguity in the role of additional time scales in the homogenization procedure. We note that while further time variables may be defined in this manner, the time variables introduced here are sufficient for analyzing all small time scale dynamics in our analysis. Any temporally-dependent function  $f_\epsilon(t)$  is then written as  $f_\epsilon(t) = f(t, \boldsymbol{\tau}(t))$ , where  $\boldsymbol{\tau}(t)$  is a tuple with components  $[\boldsymbol{\tau}(t)]_m = \tau_m(t)$ , and the total differential operator in time takes the form

$$\frac{\partial f_\epsilon}{\partial t} \equiv \frac{\partial f}{\partial t} + \epsilon^{-1} \frac{\partial f}{\partial \tau_1} + \epsilon^{-2} \frac{\partial f}{\partial \tau_2}. \quad (12)$$

239 While simultaneously considering the independent variables in space, dependent variables  $c_\epsilon^{(i)}(t, \mathbf{x})$   
 240 and  $\mathbf{u}_\epsilon(\mathbf{x})$  are now redefined as functions of  $\boldsymbol{\xi}$  and  $\boldsymbol{\tau}(t)$ , and expanded as power series in terms of  $\epsilon$  such  
 241 that

$$c_\epsilon^{(i)}(t, \mathbf{x}) \equiv c^{(i)}(t, \mathbf{x}, \boldsymbol{\tau}(t), \boldsymbol{\xi}) = \sum_{k=0}^{\infty} \epsilon^k c_k^{(i)}(t, \mathbf{x}, \boldsymbol{\tau}(t), \boldsymbol{\xi}), \quad (13a)$$

$$\mathbf{u}_\epsilon(\mathbf{x}) \equiv \mathbf{u}(\mathbf{x}, \boldsymbol{\xi}) = \sum_{k=0}^{\infty} \epsilon^k \mathbf{u}_k(\mathbf{x}, \boldsymbol{\xi}), \quad (13b)$$

242 where  $c_k^{(i)}(t, \mathbf{x}, \boldsymbol{\tau}(t), \boldsymbol{\xi})$  and  $\mathbf{u}_k(\mathbf{x}, \boldsymbol{\xi})$  are assumed to be periodic in  $\boldsymbol{\xi}$ .

### 243 3 Linear Heterogeneous Reaction: One Species

We now demonstrate our strategy for generalizing the closure form by homogenizing the mass transport of a single species undergoing a linear heterogeneous reaction. We note that a similar problem setup may be found in previous analyses (Pietrzyk et al., 2021; Battiato & Tartakovsky, 2011). While a detailed outline of the applied strategy can be found in Appendix A, we provide a brief description of the problem and homogenized results here. We consider the reactive transport of a single species, whose concentration  $c_\epsilon$  is governed by

$$\frac{\partial c_\epsilon}{\partial t} + \nabla \cdot (\text{Pe} \mathbf{u}_\epsilon c_\epsilon - D \nabla c_\epsilon) = 0 \quad \text{in } \mathcal{B}_\epsilon, \quad (14a)$$

244 subject to

$$-\mathbf{n} \cdot D \nabla c_\epsilon = \text{Da} (c_\epsilon - \theta) \quad \text{on } \Gamma_\epsilon, \quad (14b)$$

245 where the Péclet number  $\text{Pe}$ , Damköhler number  $\text{Da}$ , and concentration ratio  $\theta$  are defined as

$$\text{Pe} = \frac{\hat{U} \hat{\mathcal{L}}}{\hat{D}}, \quad \text{Da} = \frac{\hat{\mathcal{K}} \hat{\mathcal{L}}}{\hat{D}}, \quad \theta = \frac{\hat{C}}{\hat{C}}. \quad (15)$$

246 System (14) can be obtained from the general mass transport problem in system (7) by letting  $N = 1$ ,  
 247  $N_\Gamma = 1$ ,  $i \in \{1\}$ ,  $j \in \{1\}$ ,  $R_\epsilon^{(i)} = 0$ ,  $p_{SL}^{(i,j,k)} = 0$ , and  $\text{Da}_{SNL}^{(i,j,k,l)} = 0$ , and simplifying the notation  
 248 of the remaining variables to  $\{c_\epsilon^{(1)}, \hat{C}^{(1)}, D^{(1)}, \Gamma_\epsilon^{(1)}, \mathbf{n}^{(1)}, \text{Da}_{SL}^{(1,1,1)}, \hat{\mathcal{K}}_{SL}^{(1,1,1)}, \theta_{SL}^{(1,1,1)}, \hat{C}_{SL}^{(1,1,1)}\} =$   
 249  $\{c_\epsilon, \hat{C}, D, \Gamma_\epsilon, \mathbf{n}, \text{Da}, \hat{\mathcal{K}}, \theta, \hat{C}\}$ .

We homogenize the system for a moderately reactive case, where diffusive and reactive terms are of similar order, i.e.,

$$\text{Pe} \sim \mathcal{O}(\epsilon^{-1}), \quad \text{Da} \sim \mathcal{O}(\epsilon^0), \quad \theta \sim \mathcal{O}(\epsilon^0). \quad (16)$$

250 As highlighted in the work of Municchi and Icardi (Municchi & Icardi, 2020), the classical treatment for  
 251 systems involving heterogeneous reactions is limited to slow reaction rates (i.e.,  $\text{Da} \leq \mathcal{O}(\epsilon)$ ), and there-  
 252 fore, cannot be used to homogenize this physical scenario. We also note that a large advective term is  
 253 considered, but we recover the diffusion-reaction model studied in Bourbatache *et al.* (Bourbatache et  
 254 al., 2020) by letting  $\text{Pe} = 0$  and  $\theta = 0$ .

#### 255 3.1 Homogenized Results

256 With the provided formulation, we show in Appendix A that a homogenized system for  $\langle c \rangle_Y = \langle c_0 \rangle_Y +$   
 257  $\epsilon \langle c_1 \rangle_Y + \mathcal{O}(\epsilon^2)$  can be derived for the moderately reactive case with  $\mathcal{O}(\epsilon)$  error using the closure form

$$c_1 = \boldsymbol{\chi}^{[1]} \cdot \nabla_{\mathbf{x}} c_0 + (c_0 - \theta) \boldsymbol{\chi}^{[2]} + \bar{c}_1, \quad (17)$$

$$c_1 = \boldsymbol{\chi} \cdot \nabla_{\mathbf{x}} c_0 + \bar{c}_1, \quad (18)$$

259 where  $\bar{c}_1 \equiv \bar{c}_1(t, \mathbf{x}, \boldsymbol{\tau}(t)) = \phi^{-1} \langle c_1 \rangle_Y$ , and  $\boldsymbol{\chi}^{[1]}$  and  $\chi^{[2]}$  are the closure variables. The resulting homogenized equation is written as

$$\phi \frac{\partial \langle c \rangle_Y}{\partial t} + \mathbf{U} \cdot \nabla_{\mathbf{x}} \langle c \rangle_Y - \nabla_{\mathbf{x}} \cdot (\mathbf{D} \cdot \nabla_{\mathbf{x}} \langle c \rangle_Y) + \mathcal{R} (\phi \langle c \rangle_Y - \phi^2 \theta) = \mathcal{O}(\epsilon) \quad \text{for } \mathbf{x} \in \Omega, \quad (19a)$$

261 where the effective parameters are defined as

$$\mathbf{U} = \text{Pe} \langle \mathbf{u} \rangle_Y + \phi \text{Da} \frac{|\Gamma|}{|\mathcal{B}|} \langle \boldsymbol{\chi}^{[1]} \rangle_{\Gamma} - D \langle \nabla_{\boldsymbol{\xi}} \chi^{[2]} \rangle_Y + \text{Pe} \epsilon \langle \mathbf{u} \chi^{[2]} \rangle_Y, \quad (19b)$$

$$\mathbf{D} = \phi D \mathbf{I} + D \langle \nabla_{\boldsymbol{\xi}} \boldsymbol{\chi}^{[1]} \rangle_Y - \text{Pe} \epsilon \langle \mathbf{u} \otimes \boldsymbol{\chi}^{[1]} \rangle_Y, \quad (19c)$$

$$\mathcal{R} = \text{Da} \frac{|\Gamma|}{|\mathcal{B}|} \left[ \epsilon^{-1} + \langle \chi^{[2]} \rangle_{\Gamma} \right]. \quad (19d)$$

262 In system (19), the closure variables are found by solving the closure problems

$$\text{Pe} \epsilon (\mathbf{u}_0 - \langle \mathbf{u}_0 \rangle_{\mathcal{B}}) + \text{Pe} \epsilon \mathbf{u}_0 \cdot \nabla_{\boldsymbol{\xi}} \chi^{[1]} - D \nabla_{\boldsymbol{\xi}} \cdot (\mathbf{I} + \nabla_{\boldsymbol{\xi}} \boldsymbol{\chi}^{[1]}) = \mathbf{0} \quad \text{for } \boldsymbol{\xi} \in \mathcal{B}, \quad (20a)$$

263 subject to

$$-\mathbf{n} \cdot D (\mathbf{I} + \nabla_{\boldsymbol{\xi}} \boldsymbol{\chi}^{[1]}) = \mathbf{0} \quad \text{for } \boldsymbol{\xi} \in \Gamma, \quad (20b)$$

264 and

$$-\text{Da} \frac{|\Gamma|}{|\mathcal{B}|} + \text{Pe} \epsilon \mathbf{u}_0 \cdot \nabla_{\boldsymbol{\xi}} \chi^{[2]} - D \nabla_{\boldsymbol{\xi}}^2 \chi^{[2]} = 0 \quad \text{for } \boldsymbol{\xi} \in \mathcal{B}, \quad (21a)$$

265 subject to

$$-\mathbf{n} \cdot D \nabla_{\boldsymbol{\xi}} \chi^{[2]} = \text{Da} \quad \text{for } \boldsymbol{\xi} \in \Gamma. \quad (21b)$$

266 Here,  $\langle \boldsymbol{\chi}^{[1]} \rangle_{\mathcal{B}} = \mathbf{0}$  and  $\langle \chi^{[2]} \rangle_{\mathcal{B}} = 0$ . As shown, by generalizing the assumed closure form of  $c_1$ , valid closure problems can be created in scenarios where the traditionally assumed closure form (equation (18)) fails. While an additional closure problem needs to be solved, virtually no mathematical complexity is added to the classical homogenization theory through this strategy.

270 Upon analyzing the homogenized equation and effective parameters, we find contributions due to the moderate reaction rate in both the effective reaction rate  $\mathcal{R}$  and effective velocity  $\mathbf{U}$ . We notice the product between  $\phi$  and the first term in  $\mathcal{R}$  exactly matches the effective reaction rate previously derived for slow heterogeneous reactions (i.e.,  $\text{Da} \sim \mathcal{O}(\epsilon)$ ) (Battiato & Tartakovsky, 2011; Boso & Battiato, 2013). As detailed in Appendix A, the second term in  $\mathcal{R}$ , which contains  $\langle \chi^{[2]} \rangle_{\Gamma}$ , acts as the first correction to the effective reaction rate. In light of closure problem in system (21), this correction modifies the effective reaction rate based on the microscopic geometry and high advective flux. Regarding the effective velocity  $\mathbf{U}$ , three contributions are made due to the moderate reaction rate. This coincides with the results of previous analyses showing reaction-dependent effective velocities (Mikelić et al., 2006). We note that contributions  $-D \langle \nabla_{\boldsymbol{\xi}} \chi^{[2]} \rangle_Y$  and  $\text{Pe} \epsilon \langle \mathbf{u} \chi^{[2]} \rangle_Y$  are similar to the contributions in the dispersion tensor involving  $\boldsymbol{\chi}^{[1]}$  (i.e.,  $D \langle \nabla_{\boldsymbol{\xi}} \boldsymbol{\chi}^{[1]} \rangle_Y$  and  $-\text{Pe} \epsilon \langle \mathbf{u} \otimes \boldsymbol{\chi}^{[1]} \rangle_Y$ ). Therefore,  $-D \langle \nabla_{\boldsymbol{\xi}} \chi^{[2]} \rangle_Y$  and  $\text{Pe} \epsilon \langle \mathbf{u} \chi^{[2]} \rangle_Y$  are interpreted analogously as contributions that account for the interactions between (i) the effective reaction

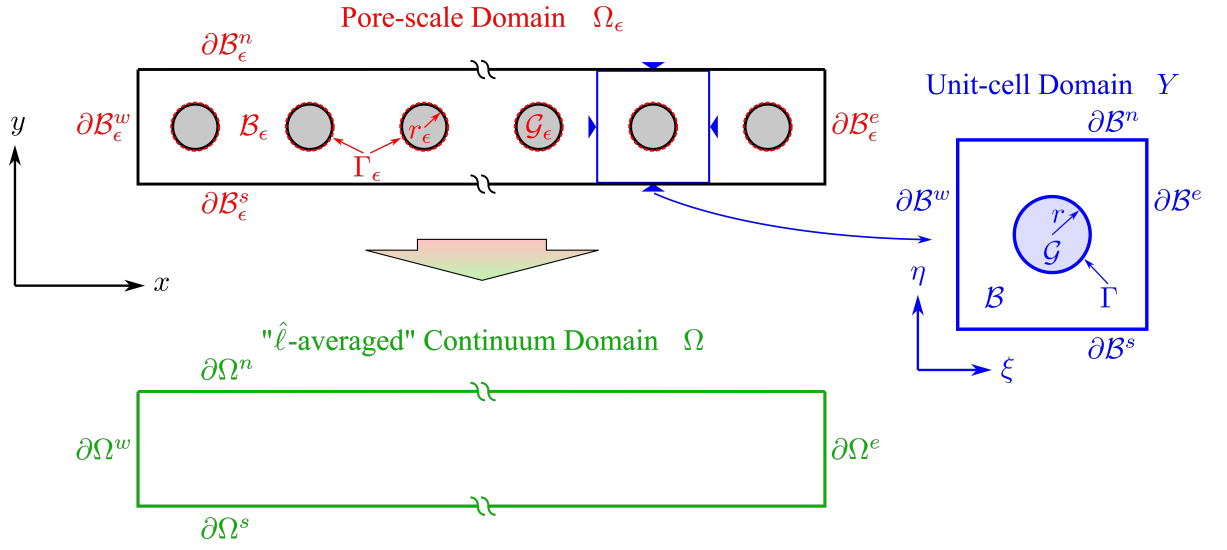


**Figure 1.** A schematic of the 2D pore-scale, unit-cell, and continuum domains considered for the array of cylinders geometry. Details of the labeled geometric aspects are found in Table 1.

282 rate correction and the diffusive flux, and (ii) the effective reaction rate correction and the advective flux,  
 283 respectively. Finally, the third contribution to the effective velocity,  $\phi\text{Da}\frac{|\Gamma|}{|\mathcal{B}|}\langle\chi^{[1]}\rangle_\Gamma$ , represents the addi-  
 284 tional reactive flux due to the diffusion flux correction.

285 We emphasize that the effective velocity remains in the homogenized equation, even if  $\text{Pe} = 0$  and  
 286  $\theta = 0$ . Further, the remaining terms in the effective velocity (i.e.,  $\phi\text{Da}\frac{|\Gamma|}{|\mathcal{B}|}\langle\chi^{[1]}\rangle_\Gamma$  and  $-D\langle\nabla_\xi\chi^{[2]}\rangle_Y$ ) rep-  
 287 resent a coupling between diffusion and reaction, even though the effective reaction rate does not depend  
 288 on diffusion, and the dispersion tensor does not depend on reaction. This early onset of coupling between  
 289 diffusion and reaction causes the macroscopic equations to not simply consist of terms similar to those  
 290 in the microscopic equations, a case warned about in the work of Iliev *et al.* (Iliev *et al.*, 2020). These  
 291 results advise caution when assuming the form of macroscopic equations to be similar to their microscopic  
 292 counterparts.

## 293 3.2 Numerical Validation

### 294 3.2.1 Problem Setup

295 We now provide validation for the homogenized model derived using the generalized closure form  
 296 strategy by numerically resolving and comparing the averaged solutions from the pore-scale (system (14))  
 297 and homogenized (systems (19), (20), and (21)) models.

298 To conduct the validation, we consider a 2D array of cylinders geometry in a Cartesian plane (i.e.,  
 299  $\mathbf{x} \equiv [x, y]$  and  $\boldsymbol{\xi} \equiv [\xi, \eta]$ ). Schematics of the considered pore-scale, unit-cell, and continuum domains  
 300 can be found in Figure 1 with relevant geometric labels, which are detailed in Table 1. We also consider  
 301 an initial discontinuous concentration profile in the pore-scale simulation, where the concentration is al-  
 302 ternatively equal to 0 and 1 in the two halves of the domain. To obtain the corresponding initial condi-  
 303 tion for the homogenized model, we average the pore-scale initial condition using the averaging opera-  
 304 tor

$$\langle \cdot \rangle_{\mathcal{W}_\epsilon(\mathbf{x})} \equiv \epsilon^{-2} \frac{1}{|Y|} \int_{\mathcal{W}_\epsilon(\mathbf{x})} (\cdot) d\mathbf{y}, \quad (22a)$$

305 where

$$\mathcal{W}_\epsilon(\mathbf{x}) = \{(x', y') : x - 0.5\epsilon < x' < x + 0.5\epsilon, y + 0.5\epsilon < y' < y - 0.5\epsilon, \mathbf{x}' \in \mathcal{B}_\epsilon\} \quad \text{for } \mathbf{x} \in \Omega. \quad (22b)$$

**Table 1.** Specifications for the geometric aspects in the pore-scale, unit-cell, and continuum domains considering the 2D array of cylinders geometry.

Variable	Definition for the 2D Array of Cylinders Geometry
	<u>Dimensional Parameters</u>
$\hat{\ell}$	Unit-cell domain length
$\hat{\mathcal{L}}$	Pore-scale domain length
$\hat{r}_\epsilon$	Cylinder radius
	<u>Pore-scale Domain</u>
$r_\epsilon$	$\hat{r}_\epsilon / \hat{\mathcal{L}}$
$\Omega_\epsilon$	$\{(x, y) : -0.5 < x < 0.5, -0.5\epsilon < y < 0.5\epsilon\}$
$\mathcal{G}_\epsilon$	$\{(x, y) : (x + 0.5(1 + \epsilon) - m\epsilon)^2 + y^2 < r_\epsilon^2, m \in \mathbb{Z}^+, m \leq \epsilon^{-1}\}$
$\Gamma_\epsilon$	$\{(x, y) : (x + 0.5(1 + \epsilon) - m\epsilon)^2 + y^2 = r_\epsilon^2, m \in \mathbb{Z}^+, m \leq \epsilon^{-1}\}$
$\mathcal{B}_\epsilon$	$\Omega_\epsilon \setminus (\mathcal{G}_\epsilon \cup \Gamma_\epsilon)$
$\partial\mathcal{B}_\epsilon^w$	$\{(x, y) : x = -0.5, -0.5\epsilon < y < 0.5\epsilon\}$
$\partial\mathcal{B}_\epsilon^e$	$\{(x, y) : x = 0.5, -0.5\epsilon < y < 0.5\epsilon\}$
$\partial\mathcal{B}_\epsilon^s$	$\{(x, y) : -0.5 < x < 0.5, y = -0.5\epsilon\}$
$\partial\mathcal{B}_\epsilon^n$	$\{(x, y) : -0.5 < x < 0.5, y = 0.5\epsilon\}$
	<u>Unit-cell Domain</u>
$r$	$\hat{r}_\epsilon / \hat{\ell}$
$Y$	$\{(\xi, \eta) : -0.5 < \xi < 0.5, -0.5 < \eta < 0.5\}$
$\mathcal{G}$	$\{(\xi, \eta) : \xi^2 + \eta^2 < r^2\}$
$\Gamma$	$\{(\xi, \eta) : \xi^2 + \eta^2 = r^2\}$
$\mathcal{B}$	$\Omega \setminus (\mathcal{G} \cup \Gamma)$
$\partial\mathcal{B}^w$	$\{(\xi, \eta) : \xi = -0.5, -0.5 < \eta < 0.5\}$
$\partial\mathcal{B}^e$	$\{(\xi, \eta) : \xi = 0.5, -0.5 < \eta < 0.5\}$
$\partial\mathcal{B}^s$	$\{(\xi, \eta) : -0.5 < \xi < 0.5, \eta = -0.5\}$
$\partial\mathcal{B}^n$	$\{(\xi, \eta) : -0.5 < \xi < 0.5, \eta = 0.5\}$
$ Y $	1
$ \mathcal{G} $	$\pi r^2$
$ \Gamma $	$2\pi r$
$ \mathcal{B} $	$ Y  -  \mathcal{G} $
$\phi$	$ \mathcal{B}  /  Y $
	<u>"<math>\hat{\ell}</math>-averaged" Continuum Domain</u>
$\Omega$	$\{(x, y) : -0.5 < x < 0.5, -0.5\epsilon < y < 0.5\epsilon\}$
$\partial\Omega^w$	$\{(x, y) : x = -0.5, -0.5\epsilon < y < 0.5\epsilon\}$
$\partial\Omega^e$	$\{(x, y) : x = 0.5, -0.5\epsilon < y < 0.5\epsilon\}$
$\partial\Omega^s$	$\{(x, y) : -0.5 < x < 0.5, y = -0.5\epsilon\}$
$\partial\Omega^n$	$\{(x, y) : -0.5 < x < 0.5, y = 0.5\epsilon\}$

**Table 2.** The simulation and mesh parameters used to solve the various models and problems defined on the pore-scale, unit-cell, and continuum domains for the single species system undergoing a linear heterogeneous reaction. Here,  $\mathbf{e}_x$  and  $\mathbf{e}_\xi$  are the unit vectors in the  $x$ -direction and  $\xi$ -direction, respectively.

Simulation and Mesh Parameters
<u>General Parameters</u>
$\epsilon = 0.1, \quad D = 1, \quad \text{Pe} = \epsilon^{-1}, \quad \text{Da} = \epsilon^0, \quad \theta = \epsilon^0, \quad \Delta t = 10^{-4}$
<u>Pore-scale Fluid Flow and Mass Transport</u>
$r_\epsilon = 0.02, \quad A_\epsilon = \epsilon^2, \quad \Phi_\epsilon = 8\mathbf{e}_x, \quad N_{elem} = 38287, \quad \max(\Delta x) = 0.0036$
<u>Homogenized Mass Transport</u>
$\phi = 0.8744, \quad N_{elem} = 4006, \quad \max(\Delta x) = 0.0113$
<u>Unit-cell Fluid Flow and Closure Problems</u>
$r = 0.2, \quad A = 1, \quad \Phi = 8\mathbf{e}_\xi, \quad N_{elem} = 44413, \quad \max(\Delta \xi) = 0.0099$

306 This averaging operator can be considered a “moving-average” that brings pore-scale concentration fields  
 307 into the continuum domain. We note that the extension of this operator at points near the edges of the  
 308 continuum domain is trivial when using periodic boundary conditions, as will be considered here. Fur-  
 309 ther details regarding the simulation parameters are provided in Table 2, while details regarding the bound-  
 310 ary conditions and initial conditions are provided in Table 3. All numerical calculations are completed  
 311 using FEniCS, an open-source finite element software (Logg et al., 2012; Alnaes et al., 2015). To min-  
 312 imize the potential for under-resolved results, the spatial and temporal discretizations are refined to show  
 313 converged solutions to plotting accuracy, and second-order elements are used. Further details regarding  
 314 the discretizations of each mesh, including the number of elements  $N_{elem}$  and maximum spacing between  
 315 vertices  $[\max(\Delta x), \max(\Delta \xi)]$ , are presented with the other simulation parameters in Table 2.

316 To obtain fluid velocity and pressure fields for the pore-scale model, system (6) is resolved for  $A_\epsilon =$   
 317  $\epsilon^2$ , the same value considered in the classical homogenization of the Stokes equation (Auriault & Adler,  
 318 1995). To drive the flow, we allow the pressure gradient to be represented as  $\nabla p_\epsilon = \Phi_\epsilon + \nabla \tilde{p}_\epsilon$ , where  
 319  $\Phi_\epsilon$  is physically interpreted as a known, large-scale pressure gradient across the pore-scale domain and  
 320  $\nabla \tilde{p}_\epsilon$  is interpreted as the gradient of an unknown local pressure field. By choosing an appropriate value  
 321 for  $\Phi_\epsilon$ , the flow fields  $\mathbf{u}_\epsilon$  and  $\tilde{p}_\epsilon$  can be solved for such that  $|\mathbf{u}_\epsilon| \sim \mathcal{O}(1)$ . This ultimately verifies that  
 322 the value of  $\hat{U}$  calculated using the definition of the Péclet number in equation (15) is consistent with the  
 323 magnitude of the flow driven by  $\Phi_\epsilon$ .

324 For the homogenized model, the equations governing fluid flow are directly taken from the classi-  
 325 cal homogenization of the Stokes equation (equation (20) in (Auriault & Adler, 1995)) and written as

$$A \nabla_\xi^2 \mathbf{u} - \nabla_\xi \tilde{p} - \Phi = \mathbf{0} \quad \text{for } \boldsymbol{\xi} \in \mathcal{B}, \quad (23a)$$

$$\nabla_\xi \cdot \mathbf{u} = 0 \quad \text{for } \boldsymbol{\xi} \in \mathcal{B}, \quad (23b)$$

326 subject to

$$\mathbf{u} = \mathbf{0} \quad \text{for } \boldsymbol{\xi} \in \Gamma, \quad (23c)$$

327 where we let  $A = 1$  and  $\Phi$  is physically interpreted as a known, large-scale pressure gradient across the  
 328 unit-cell domain. We note that the flow driven in the unit-cell domain by  $\Phi$  should be reflective of that  
 329 driven in the pore-scale domain by  $\Phi_\epsilon$ , i.e.,  $\Phi = \Phi_\epsilon$ . Upon solving system (23) in the unit-cell domain,  
 330 the velocity field  $\mathbf{u}$  can be averaged over the unit-cell and used to calculate the effective parameters (equa-  
 331 tions (19b)-(19d)).

**Table 3.** The simulation boundary conditions and initial conditions used to solve the various problems on the pore-scale, unit-cell, and continuum domains for the single species system undergoing a linear heterogeneous reaction. Here,  $H(x)$  is the Heaviside function.

Simulation Boundary Conditions	
<u>Pore-scale Mass Transport</u>	
$c_\epsilon _{\partial\mathcal{B}_\epsilon^w} = c_\epsilon _{\partial\mathcal{B}_\epsilon^e}$	$\mathbf{n} \cdot \nabla c_\epsilon _{\partial\mathcal{B}_\epsilon^w} = -\mathbf{n} \cdot \nabla c_\epsilon _{\partial\mathcal{B}_\epsilon^e}$
$c_\epsilon _{\partial\mathcal{B}_\epsilon^s} = c_\epsilon _{\partial\mathcal{B}_\epsilon^n}$	$\mathbf{n} \cdot \nabla c_\epsilon _{\partial\mathcal{B}_\epsilon^s} = -\mathbf{n} \cdot \nabla c_\epsilon _{\partial\mathcal{B}_\epsilon^n}$
<u>Pore-scale Fluid Flow</u>	
$\mathbf{u}_\epsilon _{\partial\mathcal{B}_\epsilon^w} = \mathbf{u}_\epsilon _{\partial\mathcal{B}_\epsilon^e}$	$\mathbf{n} \cdot \nabla \mathbf{u}_\epsilon _{\partial\mathcal{B}_\epsilon^w} = -\mathbf{n} \cdot \nabla \mathbf{u}_\epsilon _{\partial\mathcal{B}_\epsilon^e}$
$\mathbf{u}_\epsilon _{\partial\mathcal{B}_\epsilon^s} = \mathbf{u}_\epsilon _{\partial\mathcal{B}_\epsilon^n}$	$\mathbf{n} \cdot \nabla \mathbf{u}_\epsilon _{\partial\mathcal{B}_\epsilon^s} = -\mathbf{n} \cdot \nabla \mathbf{u}_\epsilon _{\partial\mathcal{B}_\epsilon^n}$
$\tilde{p}_\epsilon _{\partial\mathcal{B}_\epsilon^w} = \tilde{p}_\epsilon _{\partial\mathcal{B}_\epsilon^e}$	$\mathbf{n} \cdot \nabla \tilde{p}_\epsilon _{\partial\mathcal{B}_\epsilon^w} = -\mathbf{n} \cdot \nabla \tilde{p}_\epsilon _{\partial\mathcal{B}_\epsilon^e}$
$\tilde{p}_\epsilon _{\partial\mathcal{B}_\epsilon^s} = \tilde{p}_\epsilon _{\partial\mathcal{B}_\epsilon^n}$	$\mathbf{n} \cdot \nabla \tilde{p}_\epsilon _{\partial\mathcal{B}_\epsilon^s} = -\mathbf{n} \cdot \nabla \tilde{p}_\epsilon _{\partial\mathcal{B}_\epsilon^n}$
<u>Homogenized Mass Transport</u>	
$\langle c \rangle_Y _{\partial\Omega^w} = \langle c \rangle_Y _{\partial\Omega^e}$	$\mathbf{n} \cdot \nabla_{\mathbf{x}} \langle c \rangle_Y _{\partial\Omega^w} = -\mathbf{n} \cdot \nabla_{\mathbf{x}} \langle c \rangle_Y _{\partial\Omega^e}$
$\langle c \rangle_Y _{\partial\Omega^s} = \langle c \rangle_Y _{\partial\Omega^n}$	$\mathbf{n} \cdot \nabla_{\mathbf{x}} \langle c \rangle_Y _{\partial\Omega^s} = -\mathbf{n} \cdot \nabla_{\mathbf{x}} \langle c \rangle_Y _{\partial\Omega^n}$
<u>Closure Problems</u>	
$\chi^{[1]} _{\partial\mathcal{B}^w} = \chi^{[1]} _{\partial\mathcal{B}^e}$	$\mathbf{n} \cdot \nabla_{\xi} \chi^{[1]} _{\partial\mathcal{B}^w} = -\mathbf{n} \cdot \nabla_{\xi} \chi^{[1]} _{\partial\mathcal{B}^e}$
$\chi^{[1]} _{\partial\mathcal{B}^s} = \chi^{[1]} _{\partial\mathcal{B}^n}$	$\mathbf{n} \cdot \nabla_{\xi} \chi^{[1]} _{\partial\mathcal{B}^s} = -\mathbf{n} \cdot \nabla_{\xi} \chi^{[1]} _{\partial\mathcal{B}^n}$
$\chi^{[2]} _{\partial\mathcal{B}^w} = \chi^{[2]} _{\partial\mathcal{B}^e}$	$\mathbf{n} \cdot \nabla_{\xi} \chi^{[2]} _{\partial\mathcal{B}^w} = -\mathbf{n} \cdot \nabla_{\xi} \chi^{[2]} _{\partial\mathcal{B}^e}$
$\chi^{[2]} _{\partial\mathcal{B}^s} = \chi^{[2]} _{\partial\mathcal{B}^n}$	$\mathbf{n} \cdot \nabla_{\xi} \chi^{[2]} _{\partial\mathcal{B}^s} = -\mathbf{n} \cdot \nabla_{\xi} \chi^{[2]} _{\partial\mathcal{B}^n}$
<u>Unit-cell Fluid Flow</u>	
$\mathbf{u} _{\partial\mathcal{B}^w} = \mathbf{u} _{\partial\mathcal{B}^e}$	$\mathbf{n} \cdot \nabla_{\xi} \mathbf{u} _{\partial\mathcal{B}^w} = -\mathbf{n} \cdot \nabla_{\xi} \mathbf{u} _{\partial\mathcal{B}^e}$
$\mathbf{u} _{\partial\mathcal{B}^s} = \mathbf{u} _{\partial\mathcal{B}^n}$	$\mathbf{n} \cdot \nabla_{\xi} \mathbf{u} _{\partial\mathcal{B}^s} = -\mathbf{n} \cdot \nabla_{\xi} \mathbf{u} _{\partial\mathcal{B}^n}$
$\tilde{p} _{\partial\mathcal{B}^w} = \tilde{p} _{\partial\mathcal{B}^e}$	$\mathbf{n} \cdot \nabla_{\xi} \tilde{p} _{\partial\mathcal{B}^w} = -\mathbf{n} \cdot \nabla_{\xi} \tilde{p} _{\partial\mathcal{B}^e}$
$\tilde{p} _{\partial\mathcal{B}^s} = \tilde{p} _{\partial\mathcal{B}^n}$	$\mathbf{n} \cdot \nabla_{\xi} \tilde{p} _{\partial\mathcal{B}^s} = -\mathbf{n} \cdot \nabla_{\xi} \tilde{p} _{\partial\mathcal{B}^n}$
Simulation Initial Conditions	
<u>Pore-scale Mass Transport</u>	<u>Homogenized Mass Transport</u>
$c_\epsilon = H(-x) \quad \text{for } (x, y) \in \mathcal{B}_\epsilon, t = 0$	$\langle c \rangle_Y = \langle c_\epsilon \rangle_{\mathcal{W}_\epsilon(\mathbf{x})} \quad \text{for } (x, y) \in \Omega, t = 0$

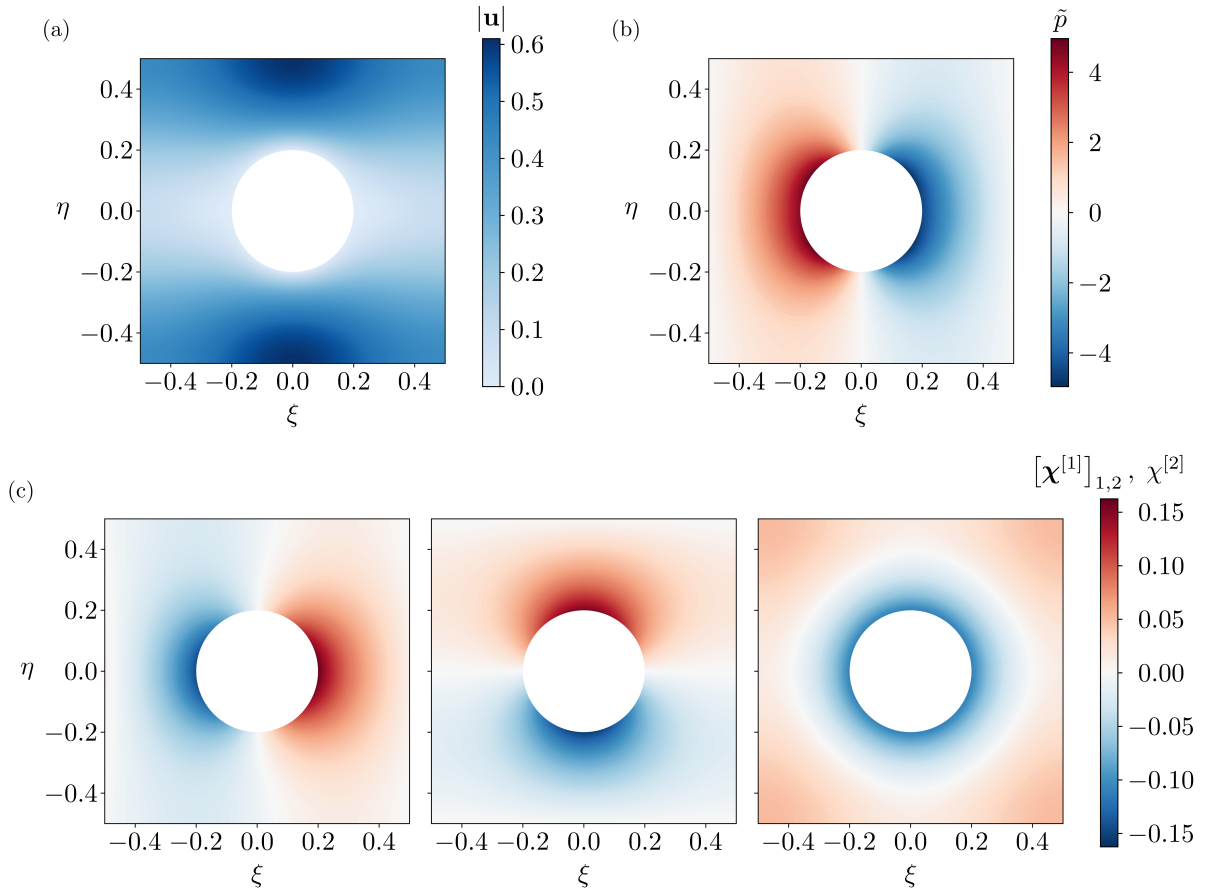


**Figure 2.** The numerical results of the flow and closure problems in the unit-cell for the single species system undergoing a linear heterogeneous reaction. (a) The magnitude of the resulting flow velocity in the unit-cell. (b) The local pressure of the resulting flow in the unit-cell. (c) The resulting closure solutions  $\chi^{[1]}$  and  $\chi^{[2]}$ . From left to right:  $[\chi^{[1]}]_1$  the  $\xi$ -component of  $\chi^{[1]}$ ,  $[\chi^{[1]}]_2$  the  $\eta$ -component of  $\chi^{[1]}$ , and  $\chi^{[2]}$ .

### 3.2.2 Flow and Closure Problem Results

Prior to solving the homogenized model, solutions to the flow and closure problems must be obtained. The flow problem described in system (6) is solved on the pore-scale domain, and system (23) on the unit-cell domain. The resulting flow velocity magnitude  $|\mathbf{u}|$  and local pressure  $\tilde{p}$  contours are found in Figures 2(a) and 2(b), respectively. As shown in Figure 2(a), the choice of  $\Phi = 8\mathbf{e}_\xi$  (Table 2) is suitable for the current problem due to  $|\mathbf{u}| \sim \mathcal{O}(1)$ . We also note that only the flow fields in the unit-cell domain are presented, as the pore-scale flow fields result in contiguously placed unit-cell flow fields due to the periodicity of the pore-scale domain. Therefore, no new information is provided by the pore-scale flow fields. Regarding the closure problems, systems (20) and (21) are solved on the unit-cell domain, and the resulting components of  $\chi^{[1]}$ ,  $[\chi^{[1]}]_1$  and  $[\chi^{[1]}]_2$ , are plotted alongside  $\chi^{[2]}$  in Figure 2(c). As shown, the contour of  $\chi^{[2]}$  has a different appearance than  $[\chi^{[1]}]_1$  and  $[\chi^{[1]}]_2$ , but maintains a similar magnitude for the considered geometry.

### 3.2.3 Pore-scale and Homogenized Model Results

With the solutions to the closure and flow problems, the pore-scale (system (14)) and homogenized (systems (19), (20), and (21)) models are solved using the simulation parameters, boundary conditions, and initial conditions provided in Tables 2 and 3. Then, the pore-scale solution  $c_\epsilon$  is averaged using the averaging operator in equation (22a) to obtain the averaged pore-scale solution  $\langle c_\epsilon \rangle_{\mathcal{W}_\epsilon(\mathbf{x})}$ . To quantitatively compare  $\langle c_\epsilon \rangle_{\mathcal{W}_\epsilon(\mathbf{x})}$  to the homogenized solution  $\langle c \rangle_Y$ , we define the absolute error function

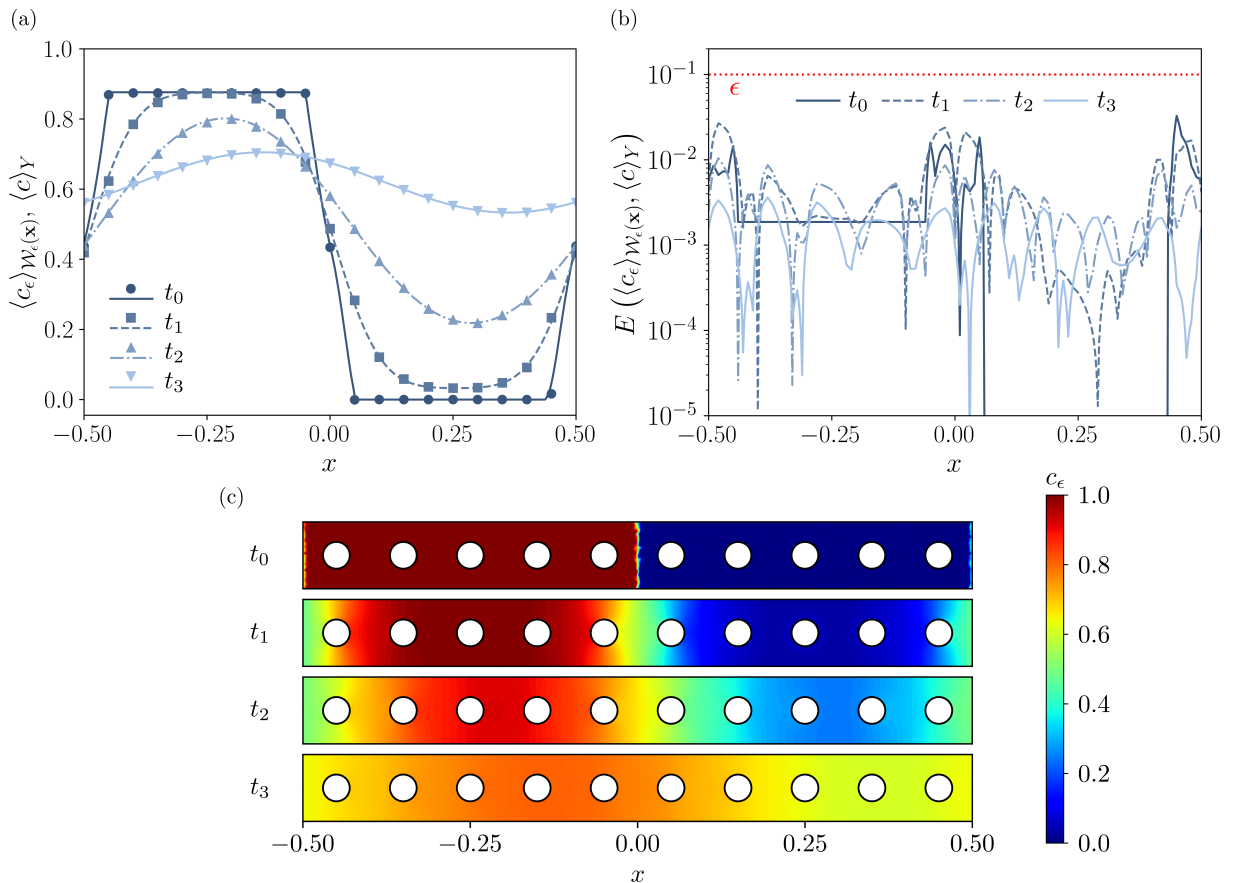


**Figure 3.** The numerical results for the system involving a single species undergoing a linear heterogeneous reaction. (a) The  $\mathcal{W}_\epsilon(\mathbf{x})$ -averaged and  $Y$ -averaged concentration profiles from the pore-scale (symbols) and homogenized (lines) models, respectively, at various times along the  $x$ -direction. (b) The absolute error between the averaged concentration profiles of  $\langle c_\epsilon \rangle_{\mathcal{W}_\epsilon(\mathbf{x})}$  and  $\langle c \rangle_Y$  at various times along the  $x$ -direction. The upper error limit predicted by the homogenized model is displayed by the red dotted line. (c) Contour plots of the pore-scale concentration field  $c_\epsilon$  at various times. Here,  $t_0 = 0$ ,  $t_1 = 0.25 \times 10^{-2}$ ,  $t_2 = 1.25 \times 10^{-2}$ , and  $t_3 = 3.75 \times 10^{-2}$ .

$$E(\langle \Psi_\epsilon \rangle_{\mathcal{W}_\epsilon(\mathbf{x})}, \langle \Psi \rangle_Y) = |\langle \Psi_\epsilon \rangle_{\mathcal{W}_\epsilon(\mathbf{x})} - \langle \Psi \rangle_Y|, \quad (24)$$

350 where  $\langle \Psi_\epsilon \rangle_{\mathcal{W}_\epsilon(\mathbf{x})}$  and  $\langle \Psi \rangle_Y$  are dummy averaged pore-scale and homogenized solutions, respectively.

351 In Figure 3, we present the pore-scale, averaged pore-scale, and homogenized model results. The  
352 qualitative comparison between  $\langle c_\epsilon \rangle_{\mathcal{W}_\epsilon(\mathbf{x})}$  and  $\langle c \rangle_Y$  in Figure 3(a) shows the homogenized model is capable of capturing the averaged behavior of the pore-scale model along the  $x$ -direction at the recorded  
353 times. We note that in conjunction with the periodicity, the prescribed initial condition in this problem  
354 causes the evolution of  $\langle c_\epsilon \rangle_{\mathcal{W}_\epsilon(\mathbf{x})}$  and  $\langle c \rangle_Y$  to be 1D, and therefore, the results in Figure 3(a) are independent of  $y$ . We also note that while the prescribed initial condition in the pore-scale simulation is discontinuous at  $x = 0$  (as recorded in Table 3 and shown in Figure 3(c) at  $t = t_0$ ), the initial condition  
355 of the homogenized model shown at  $t = t_0$  in Figure 3(a) displays a sharp slope around  $x = 0$ . This  
356 is due to the averaging of the pore-scale initial condition using equation (22a) that was completed to obtain the appropriate corresponding initial condition for the homogenized model.  
357  
358  
359  
360

361 In addition to the qualitative comparison, a quantitative comparison between  $\langle c_\epsilon \rangle_{\mathcal{W}_\epsilon(\mathbf{x})}$  and  $\langle c \rangle_Y$   
362 at the recorded times is provided in Figure 3(b), where the absolute error between the solutions along  
363 the  $x$ -direction is calculated using equation (24). As shown, the absolute error remains below the upper  
364 error limit predicted by the homogenized model ( $\sim \mathcal{O}(\epsilon)$ ; denoted by the red dotted line) for all times.  
365 This provides confidence in the validity of the generalized closure form strategy used to derive the ho-  
366 mogenized model.

367 Finally, contours of the pore-scale solution at the recorded times are provided in Figure 3(c). As  
 368 previously noted, the initial discontinuous concentration profile can be seen in the contour at  $t = t_0$ .  
 369 With the progression of time, the solute diffuses to eliminate the discontinuity at  $t = t_1$  and  $t = t_2$ ,  
 370 and advection translates the solute in the positive  $x$ -direction. We note that the concentration gradients  
 371 above and below the cylinders are observed to be slightly  $y$ -dependent due to the transport around the  
 372 cylindrical obstacles. Lastly, in the contour at  $t = t_3$ , the system is observed to evolve toward a homo-  
 373 geneous state.

374 With the qualitative and quantitative evidence in Figure 3, we deem the generalized closure form  
 375 strategy valid for problems involving moderately reactive physics, where diffusive and reactive terms are  
 376 of similar order. In the next section, this strategy is applied to develop a homogenized model for a more  
 377 complex case involving two species.

#### 378 4 Linear Heterogeneous Reaction: Two Species

379 We now apply the generalized closure form strategy to a system of two species undergoing linear  
 380 heterogeneous reactions. In particular, we investigate the system presented in the work of Bourbatache  
 381 *et al.* (Bourbatache *et al.*, 2021) with advection, which is written as

$$\frac{\partial \hat{c}_\epsilon^{(1)}}{\partial \hat{t}} + \hat{\nabla} \cdot \left( \hat{\mathbf{u}}_\epsilon \hat{c}_\epsilon^{(1)} - \hat{D}^{(1)} \hat{\nabla} \hat{c}_\epsilon^{(1)} \right) = 0 \quad \text{in } \hat{\mathcal{B}}_\epsilon, \quad (25a)$$

$$\frac{\partial \hat{c}_\epsilon^{(2)}}{\partial \hat{t}} + \hat{\nabla} \cdot \left( \hat{\mathbf{u}}_\epsilon \hat{c}_\epsilon^{(2)} - \hat{D}^{(2)} \hat{\nabla} \hat{c}_\epsilon^{(2)} \right) = 0 \quad \text{in } \hat{\mathcal{B}}_\epsilon, \quad (25b)$$

382 subject to

$$-\mathbf{n} \cdot \hat{D}^{(1)} \hat{\nabla} \hat{c}_\epsilon^{(1)} = \hat{\mathcal{K}}_{SL}^{(1)} \hat{c}_\epsilon^{(1)} - \hat{\mathcal{K}}_{SL}^{(2)} \hat{c}_\epsilon^{(2)} \quad \text{on } \hat{\Gamma}_\epsilon, \quad (25c)$$

$$-\mathbf{n} \cdot \hat{D}^{(2)} \hat{\nabla} \hat{c}_\epsilon^{(2)} = \hat{\mathcal{K}}_{SL}^{(2)} \hat{c}_\epsilon^{(2)} - \hat{\mathcal{K}}_{SL}^{(1)} \hat{c}_\epsilon^{(1)} \quad \text{on } \hat{\Gamma}_\epsilon. \quad (25d)$$

383 These equations can be described using system (4) by letting  $N = 2$ ,  $N_\Gamma = 1$ ,  $i \in \{1, 2\}$ ,  $j \in \{1\}$ ,  
 384  $\hat{R}_\epsilon^{(i)} = 0$ ,  $\hat{C}_{SL}^{(i,j,k)} = 0$ ,  $\hat{\mathcal{K}}_{SNL}^{(i,j,k,l)} = 0$ ,  $\hat{C}_{SNL}^{(i,j,k,l)} = 0$ ,  $p_{SL}^{(1,1,1)} = p_{SL}^{(2,1,2)} = 0$ ,  $p_{SL}^{(1,1,2)} = p_{SL}^{(2,1,1)} = 1$ ,  $\mathbf{n}^{(1)} = \mathbf{n}$ ,  
 385  $\hat{\Gamma}_\epsilon^{(1)} = \hat{\Gamma}_\epsilon$ ,  $\hat{\mathcal{K}}_{SL}^{(n,1,1)} = \hat{\mathcal{K}}_{SL}^{(1)}$  for  $n \in \{1, 2\}$ , and  $\hat{\mathcal{K}}_{SL}^{(n,1,2)} = \hat{\mathcal{K}}_{SL}^{(2)}$  for  $n \in \{1, 2\}$ . To scale the system, we  
 386 use the relevant nondimensionalizations in equation (5) to gain

$$\frac{\partial c_\epsilon^{(1)}}{\partial t} + \nabla \cdot \left( \text{Pe} \mathbf{u}_\epsilon c_\epsilon^{(1)} - D^{(1)} \nabla c_\epsilon^{(1)} \right) = 0 \quad \text{in } \mathcal{B}_\epsilon, \quad (26a)$$

$$\frac{\partial c_\epsilon^{(2)}}{\partial t} + \nabla \cdot \left( \text{Pe} \mathbf{u}_\epsilon c_\epsilon^{(2)} - D^{(2)} \nabla c_\epsilon^{(2)} \right) = 0 \quad \text{in } \mathcal{B}_\epsilon, \quad (26b)$$

387 subject to

$$-\mathbf{n} \cdot D^{(1)} \nabla c_\epsilon^{(1)} = \text{Da}_{SL}^{(1)} c_\epsilon^{(1)} - \text{Da}_{SL}^{(2)} c_\epsilon^{(2)} \quad \text{on } \Gamma_\epsilon, \quad (26c)$$

$$-\mathbf{n} \cdot D^{(2)} \nabla c_\epsilon^{(2)} = \text{Da}_{SL}^{(2)} c_\epsilon^{(2)} - \text{Da}_{SL}^{(1)} c_\epsilon^{(1)} \quad \text{on } \Gamma_\epsilon, \quad (26d)$$

388 where

$$\text{Pe} = \frac{\hat{\mathcal{U}} \hat{\mathcal{L}}}{\hat{\mathcal{D}}}, \quad \text{Da}_{SL}^{(1)} = \frac{\hat{\mathcal{K}}_{SL}^{(1)} \hat{\mathcal{L}}}{\hat{\mathcal{D}}}, \quad \text{Da}_{SL}^{(2)} = \frac{\hat{\mathcal{K}}_{SL}^{(2)} \hat{\mathcal{L}}}{\hat{\mathcal{D}}}. \quad (27)$$

389 In addition to the previous syntactic simplifications, we have let  $\text{Da}_{SL}^{(n,1,1)} = \text{Da}_{SL}^{(1)}$  and  $\text{Da}_{SL}^{(n,1,2)} = \text{Da}_{SL}^{(2)}$   
 390 for  $n \in \{1, 2\}$  with respect to the notation used in system (7) and equation (8).

391 In their previous work, Bourbatache *et al.* found that their homogenized models for moderate to  
 392 high values of Damköhler numbers (i.e.,  $\text{Da}_{SL}^{(1)} \geq \mathcal{O}(\epsilon^0)$  and  $\text{Da}_{SL}^{(2)} \geq \mathcal{O}(\epsilon^0)$ ) were unable to capture  
 393 the system dynamics at early times (Bourbatache et al., 2021). Here, we study the case where diffusive  
 394 and reactive terms are of similar order, namely the moderately reactive regime where

$$\text{Pe} \sim \mathcal{O}(\epsilon^{-1}), \quad \text{Da}_{SL}^{(1)} \sim \mathcal{O}(\epsilon^0), \quad \text{Da}_{SL}^{(2)} \sim \mathcal{O}(\epsilon^0), \quad (28)$$

395 and show that the generalized closure form strategy can be used to derive a homogenized model for the  
 396 system that remains accurate at early times.

#### 397 4.1 Homogenized Results

398 With the provided formulation, we show in Appendix B that a homogenized system for  $\langle c^{(i)} \rangle_Y =$   
 399  $\langle c_0^{(i)} \rangle_Y + \epsilon \langle c_1^{(i)} \rangle_Y + \mathcal{O}(\epsilon^2)$ , where  $i = \{1, 2\}$ , can be derived for the moderately reactive case with  $\mathcal{O}(\epsilon)$   
 400 error using the closure forms

$$c_1^{(1)} = \boldsymbol{\chi}^{(1)[1]} \cdot \nabla_{\mathbf{x}} c_0^{(1)} + \left( \text{Da}_{SL}^{(1)} c_0^{(1)} - \text{Da}_{SL}^{(2)} c_0^{(2)} \right) \chi^{(1)[2]} + \bar{c}_1^{(1)}, \quad (29a)$$

$$c_1^{(2)} = \boldsymbol{\chi}^{(2)[1]} \cdot \nabla_{\mathbf{x}} c_0^{(2)} + \left( \text{Da}_{SL}^{(2)} c_0^{(2)} - \text{Da}_{SL}^{(1)} c_0^{(1)} \right) \chi^{(2)[2]} + \bar{c}_1^{(2)}, \quad (29b)$$

401 where  $\bar{c}_1^{(i)} \equiv \bar{c}_1^{(i)}(t, \mathbf{x}, \boldsymbol{\tau}(t)) = \phi^{-1} \langle c_1^{(i)} \rangle_Y$ , and  $\boldsymbol{\chi}^{(i)[1]}$  and  $\chi^{(i)[1]}$  are closure variables. The resulting ho-  
 402 mogenized system is written as

$$\begin{aligned} \phi \frac{\partial \langle c^{(1)} \rangle_Y}{\partial t} + \mathbf{U}^{(1)} \cdot \nabla_{\mathbf{x}} \langle c^{(1)} \rangle_Y - \mathbf{V}^{(1)} \cdot \nabla_{\mathbf{x}} \langle c^{(2)} \rangle_Y - \nabla_{\mathbf{x}} \cdot \left( \mathbf{D}^{(1)} \cdot \nabla_{\mathbf{x}} \langle c^{(1)} \rangle_Y \right) \\ = \mathcal{R}^{(2)} \langle c^{(2)} \rangle_Y - \mathcal{R}^{(1)} \langle c^{(1)} \rangle_Y + \mathcal{O}(\epsilon) \quad \text{for } \mathbf{x} \in \Omega, \end{aligned} \quad (30a)$$

$$\begin{aligned} \phi \frac{\partial \langle c^{(2)} \rangle_Y}{\partial t} + \mathbf{U}^{(2)} \cdot \nabla_{\mathbf{x}} \langle c^{(2)} \rangle_Y - \mathbf{V}^{(2)} \cdot \nabla_{\mathbf{x}} \langle c^{(1)} \rangle_Y - \nabla_{\mathbf{x}} \cdot \left( \mathbf{D}^{(2)} \cdot \nabla_{\mathbf{x}} \langle c^{(2)} \rangle_Y \right) \\ = \mathcal{R}^{(1)} \langle c^{(1)} \rangle_Y - \mathcal{R}^{(2)} \langle c^{(2)} \rangle_Y + \mathcal{O}(\epsilon) \quad \text{for } \mathbf{x} \in \Omega, \end{aligned} \quad (30b)$$

403 where the effective parameters are defined as

$$\mathbf{U}^{(i)} = \text{Pe} \langle \mathbf{u} \rangle_Y + \text{Da}_{SL}^{(i)} \left[ \phi \frac{|\Gamma|}{|\mathcal{B}|} \langle \boldsymbol{\chi}^{(i)[1]} \rangle_{\Gamma} - D^{(i)} \langle \nabla_{\boldsymbol{\xi}} \chi^{(i)[2]} \rangle_Y + \text{Pe} \epsilon \langle \mathbf{u} \chi^{(i)[2]} \rangle_Y \right], \quad (30c)$$

$$\mathbf{V}^{(1)} = \text{Da}_{SL}^{(2)} \left[ \phi \frac{|\Gamma|}{|\mathcal{B}|} \langle \boldsymbol{\chi}^{(2)[1]} \rangle_{\Gamma} - D^{(1)} \langle \nabla_{\boldsymbol{\xi}} \chi^{(1)[2]} \rangle_Y + \text{Pe} \epsilon \langle \mathbf{u} \chi^{(1)[2]} \rangle_Y \right], \quad (30d)$$

$$\mathbf{V}^{(2)} = \text{Da}_{SL}^{(1)} \left[ \phi \frac{|\Gamma|}{|\mathcal{B}|} \langle \boldsymbol{\chi}^{(1)[1]} \rangle_{\Gamma} - D^{(2)} \langle \nabla_{\boldsymbol{\xi}} \chi^{(2)[2]} \rangle_Y + \text{Pe} \epsilon \langle \mathbf{u} \chi^{(2)[2]} \rangle_Y \right], \quad (30e)$$

$$\mathbf{D}^{(i)} = \phi D^{(i)} \mathbf{I} + D^{(i)} \langle \nabla_{\boldsymbol{\xi}} \boldsymbol{\chi}^{(i)[1]} \rangle_Y - \text{Pe} \epsilon \langle \mathbf{u} \otimes \boldsymbol{\chi}^{(i)[1]} \rangle_Y, \quad (30f)$$

$$\mathcal{R}^{(i)} = \text{Da}_{SL}^{(i)} \mathcal{R}, \quad (30g)$$

$$\mathcal{R} = \phi \frac{|\Gamma|}{|\mathcal{B}|} \left[ \epsilon^{-1} + \text{Da}_{SL}^{(1)} \langle \chi^{(1)[2]} \rangle_{\Gamma} + \text{Da}_{SL}^{(2)} \langle \chi^{(2)[2]} \rangle_{\Gamma} \right], \quad (30h)$$

404 for  $i \in \{1, 2\}$ . In system (30), the four closure variables are found by solving the closure problems

$$\text{Pe}\epsilon(\mathbf{u}_0 - \langle \mathbf{u}_0 \rangle_{\mathcal{B}}) + \text{Pe}\epsilon \mathbf{u}_0 \cdot \nabla_{\xi} \chi^{(i)[1]} - D^{(i)} \nabla_{\xi} \cdot (\mathbf{I} + \nabla_{\xi} \chi^{(i)[1]}) = \mathbf{0} \quad \text{for } \xi \in \mathcal{B}, \quad (31a)$$

subject to

$$-\mathbf{n} \cdot D^{(i)} (\mathbf{I} + \nabla_{\xi} \chi^{(i)[1]}) = \mathbf{0} \quad \text{for } \xi \in \Gamma, \quad (31b)$$

and

$$-\frac{|\Gamma|}{|\mathcal{B}|} + \text{Pe}\epsilon \mathbf{u}_0 \cdot \nabla_{\xi} \chi^{(i)[2]} - D^{(i)} \nabla_{\xi}^2 \chi^{(i)[2]} = 0 \quad \text{for } \xi \in \mathcal{B}, \quad (32a)$$

subject to

$$-\mathbf{n} \cdot D^{(i)} \nabla_{\xi} \chi^{(i)[2]} = 1 \quad \text{for } \xi \in \Gamma. \quad (32b)$$

We note that even for  $\text{Pe} = 0$ , the homogenized equations differ from those derived in the work of Bourbatache *et al.* (Bourbatache et al., 2020). In comparison to the previous problem, similar contributions to the effective velocities  $\mathbf{U}^{(i)}$  are found; however, the effective reaction rates  $\mathcal{R}^{(i)}$  contain additional contributions that account for the heterogeneous reactions involving the opposing solute (i.e.,  $\mathcal{R}^{(1)}$  contains  $\text{Da}_{SL}^{(2)} \langle \chi^{(2)[2]} \rangle_{\Gamma}$  and  $\mathcal{R}^{(2)}$  contains  $\text{Da}_{SL}^{(1)} \langle \chi^{(1)[2]} \rangle_{\Gamma}$ ). As a result, not only do the terms  $\mathcal{R}^{(1)} \langle c^{(1)} \rangle_Y$  and  $\mathcal{R}^{(2)} \langle c^{(2)} \rangle_Y$  couple the homogenized equations, but the effective reaction rates  $\mathcal{R}^{(i)}$  induce a coupling between the averaged reactive mass transport behavior of the solutes through the closure variables.

In addition to the coupling induced by the reaction terms,  $\mathbf{V}^{(1)} \cdot \nabla_{\mathbf{x}} \langle c^{(2)} \rangle_Y$  and  $\mathbf{V}^{(2)} \cdot \nabla_{\mathbf{x}} \langle c^{(1)} \rangle_Y$  appear in the homogenized equations for  $\langle c^{(1)} \rangle_Y$  and  $\langle c^{(2)} \rangle_Y$ , respectively, due to the moderate reaction rates. These terms induce emergent behaviors in the system through nontrivial couplings within their corresponding homogenized equations, as they consider the gradient of the opposing solute in an advective-like fashion. While  $\mathbf{V}^{(1)}$  and  $\mathbf{V}^{(2)}$  have similar forms to the reaction induced contributions in the effective velocities  $\mathbf{U}^{(i)}$ , they each contain contributions that consider the scalar closure variable of the corresponding species (i.e.,  $\mathbf{V}^{(1)}$  contains  $-\text{Da}_{SL}^{(2)} D^{(1)} \langle \nabla_{\xi} \chi^{(1)[2]} \rangle_Y + \text{Da}_{SL}^{(2)} \text{Pe}\epsilon \langle \mathbf{u}\chi^{(1)[2]} \rangle_Y$  and  $\mathbf{V}^{(2)}$  contains  $-\text{Da}_{SL}^{(1)} D^{(2)} \langle \nabla_{\xi} \chi^{(2)[2]} \rangle_Y + \text{Da}_{SL}^{(1)} \text{Pe}\epsilon \langle \mathbf{u}\chi^{(2)[2]} \rangle_Y$ ), and a contribution that considers the vector closure variable of the opposing species (i.e.,  $\mathbf{V}^{(1)}$  contains  $\phi \text{Da}_{SL}^{(2)} \frac{|\Gamma|}{|\mathcal{B}|} \langle \chi^{(2)[1]} \rangle_{\Gamma}$  and  $\mathbf{V}^{(2)}$  contains  $\phi \text{Da}_{SL}^{(1)} \frac{|\Gamma|}{|\mathcal{B}|} \langle \chi^{(1)[1]} \rangle_{\Gamma}$ ). As in the case of the effective reaction rate, these contributions induce a coupling between the averaged reactive mass transport behavior of the solutes through the closure variables in the effective parameters  $\mathbf{V}^{(i)}$ . Because the contributions have similar forms to those in the previous problem, we interpret them in an analogous manner, and again note that they also demonstrate the early onset of a coupling between advective, diffusive, and reactive physics.

Upon analyzing the homogenized model obtained through the generalized closure form strategy, we reemphasize and add to the point made by Iliev *et al.* (Iliev et al., 2020). The macroscopic equations derived for this problem are considerably different than their microscopic counterparts (system (26)) due to the emergent terms. These terms induce nontrivial couplings between the equations and disallow homogenized models derived for slow reaction rates to accurately model systems with moderate reaction rates by simply fitting effective parameters. Furthermore, we highlight that new effective parameters  $\mathbf{V}^{(i)}$  appeared with the emergent terms, and the contributions to  $\mathcal{R}^{(i)}$  and  $\mathbf{V}^{(i)}$  involve closure variables (i.e., information about the advective, diffusive, and reactive physics) of the opposing solute, as previously noted in our analysis. Therefore, not only can macroscopic equations vastly differ from their microscopic counterparts due to emergent terms, but new effective parameters that inherently couple the macroscopic behavior through the closure variables can appear with the emergent terms. As a result, predicting macroscopic equations from their microscopic counterparts is nontrivial on multiple accounts: the equation forms can differ, the ratio of effective parameters to microscopic coefficients may not be one-to-one, and the effective parameters can be inherently coupled to different physical transport mechanisms in the system through the closure variables (e.g.,  $\mathbf{V}^{(1)}$ , an effective parameter of  $\langle c^{(1)} \rangle_Y$ , depends on  $\chi^{(2)[1]}$ , a closure variable of  $\langle c^{(2)} \rangle_Y$ ). Overall, these intricacies greatly support and push the boundary of the point made by Iliev *et al.* (Iliev et al., 2020), and for this reason, we again advise caution when assuming the form of macroscopic equations from the microscopic counterparts.

**Table 4.** The simulation and mesh parameters used to solve the various models and problems defined on the pore-scale, unit-cell, and continuum domains for the two species system undergoing linear heterogeneous reactions.

---

Simulation and Mesh Parameters
<u>General Parameters</u>
$\epsilon = 0.05, \quad D^{(1)} = 1, \quad D^{(2)} = 2, \quad \text{Pe} = 0,$ $\text{Da}_{SL}^{(1)} = \epsilon^{-1}/2, \quad \text{Da}_{SL}^{(2)} = \epsilon^{-1}/2, \quad \Delta t = 10^{-4}$
<u>Pore-scale Fluid Flow and Mass Transport</u>
$r_\epsilon = 0.01, \quad N_{elem} = 38617, \quad \max(\Delta x) = 0.0026$
<u>Homogenized Mass Transport</u>
$\phi = 0.8744, \quad N_{elem} = 4054, \quad \max(\Delta x) = 0.0078$
<u>Closure Problems and Unit-cell Fluid Flow</u>
$r = 0.2, \quad N_{elem} = 44413, \quad \max(\Delta \xi) = 0.0099$

---

## 4.2 Numerical Validation

### 4.2.1 Problem Setup

We now provide validation for the derived homogenized model (systems (30), (31), and (32)) by numerically resolving and comparing its solutions to the averaged solutions from the pore-scale model (system (26)). To provide a direct comparison with the work of Bourbatache *et al.*, we consider  $\text{Pe} = 0$  for the validation (Bourbatache et al., 2021). Similar to before, we use FEniCS to fully resolve the models on the pore-scale, unit-cell, and continuum domains found in Figure 1, which consider the 2D array of cylinders geometry. The discretization details for each mesh are presented in Table 4 with other simulation parameters. Again, the geometric specifications of each domain are outlined in Table 1; however, we note that  $\epsilon = 0.05$  in this validation, which differs from the previous problem.

Regarding initial conditions, we consider discontinuous concentration profiles for each solute in the pore-scale simulation, where the concentrations are alternatively equal to 0 and 1 in the two halves of the domain. The corresponding initial conditions for the homogenized model are then obtained by averaging the pore-scale initial condition using the equation (22a). Further details regarding the simulation parameters, boundary conditions, and initial conditions can be found in Tables 4 and 5.

### 4.2.2 Closure Problem Results

Similar to before, the four closure problems described in systems (31) and (32) must be solved on the unit-cell domain prior to resolving the homogenized model. As shown in Figure 4, the components of  $\chi^{(1)[1]}$ ,  $[\chi^{(1)[1]}]_1$  and  $[\chi^{(1)[1]}]_2$ , are plotted alongside  $\chi^{(1)[2]}$  in Figure 4(a), and the components of  $\chi^{(2)[1]}$ ,  $[\chi^{(2)[1]}]_1$  and  $[\chi^{(2)[1]}]_2$ , are plotted alongside  $\chi^{(2)[2]}$  in Figure 4(b). The contours of  $[\chi^{(i)[1]}]_1$ ,  $[\chi^{(i)[1]}]_2$ , and  $\chi^{(i)[2]}$  for  $i \in \{1, 2\}$  have similar appearance to those of  $[\chi^{[1]}]_1$ ,  $[\chi^{[1]}]_2$ , and  $\chi^{[2]}$  from the first problem (Figure 2(c)), but the presence of advection in the first problem slightly alters  $[\chi^{[1]}]_1$  from  $[\chi^{(1)[1]}]_1$  and  $[\chi^{(2)[1]}]_1$ . Additionally, we note that the magnitudes displayed by  $\chi^{(2)[2]}$  are less than those of  $\chi^{(1)[2]}$  and  $\chi^{[2]}$ . We attribute this difference to the high diffusive constant  $D^{(2)}$  (Table 4), which is the only difference between the closure problems for  $\chi^{(1)[2]}$  and  $\chi^{(2)[2]}$  (system (32)).

### 4.2.3 Pore-scale and Homogenized Model Results

With the closure solutions, the pore-scale (system (26)) and homogenized (systems (30), (31), and (32)) models are solved. Upon doing so, the pore-scale solutions  $c_\epsilon^{(1)}$  and  $c_\epsilon^{(2)}$  are averaged using the averaging operator in equation (22a) to obtain the averaged pore-scale solutions  $\langle c_\epsilon^{(1)} \rangle_{\mathcal{W}_\epsilon(\mathbf{x})}$  and  $\langle c_\epsilon^{(2)} \rangle_{\mathcal{W}_\epsilon(\mathbf{x})}$ . The absolute errors between the averaged pore-scale solutions and the respective homogenized solutions  $\langle c^{(1)} \rangle_Y$  and  $\langle c^{(2)} \rangle_Y$  are then calculated using equation (24).

**Table 5.** The simulation boundary conditions and initial conditions used to solve the various problems on the pore-scale, unit-cell, and continuum domains for the two species system undergoing linear heterogeneous reactions. Here,  $H(x)$  is the Heaviside function and  $i \in \{1, 2\}$ .

Simulation Boundary Conditions	
<u>Pore-scale Mass Transport</u>	
$c_\epsilon^{(i)} \Big _{\partial \mathcal{B}_\epsilon^w} = c_\epsilon^{(i)} \Big _{\partial \mathcal{B}_\epsilon^e}$	$\mathbf{n} \cdot \nabla c_\epsilon^{(i)} \Big _{\partial \mathcal{B}_\epsilon^w} = -\mathbf{n} \cdot \nabla c_\epsilon^{(i)} \Big _{\partial \mathcal{B}_\epsilon^e}$
$c_\epsilon^{(i)} \Big _{\partial \mathcal{B}_\epsilon^s} = c_\epsilon^{(i)} \Big _{\partial \mathcal{B}_\epsilon^n}$	$\mathbf{n} \cdot \nabla c_\epsilon^{(i)} \Big _{\partial \mathcal{B}_\epsilon^s} = -\mathbf{n} \cdot \nabla c_\epsilon^{(i)} \Big _{\partial \mathcal{B}_\epsilon^n}$
<u>Homogenized Mass Transport</u>	
$\langle c^{(i)} \rangle_Y \Big _{\partial \Omega^w} = \langle c^{(i)} \rangle_Y \Big _{\partial \Omega^e}$	$\mathbf{n} \cdot \nabla_{\mathbf{x}} \langle c^{(i)} \rangle_Y \Big _{\partial \Omega^w} = -\mathbf{n} \cdot \nabla_{\mathbf{x}} \langle c^{(i)} \rangle_Y \Big _{\partial \Omega^e}$
$\langle c^{(i)} \rangle_Y \Big _{\partial \Omega^s} = \langle c^{(i)} \rangle_Y \Big _{\partial \Omega^n}$	$\mathbf{n} \cdot \nabla_{\mathbf{x}} \langle c^{(i)} \rangle_Y \Big _{\partial \Omega^s} = -\mathbf{n} \cdot \nabla_{\mathbf{x}} \langle c^{(i)} \rangle_Y \Big _{\partial \Omega^n}$
<u>Closure Problems</u>	
$\chi^{(i)[1]} \Big _{\partial \mathcal{B}^w} = \chi^{(i)[1]} \Big _{\partial \mathcal{B}^e}$	$\mathbf{n} \cdot \nabla_{\xi} \chi^{(i)[1]} \Big _{\partial \mathcal{B}^w} = -\mathbf{n} \cdot \nabla_{\xi} \chi^{(i)[1]} \Big _{\partial \mathcal{B}^e}$
$\chi^{(i)[1]} \Big _{\partial \mathcal{B}^s} = \chi^{(i)[1]} \Big _{\partial \mathcal{B}^n}$	$\mathbf{n} \cdot \nabla_{\xi} \chi^{(i)[1]} \Big _{\partial \mathcal{B}^s} = -\mathbf{n} \cdot \nabla_{\xi} \chi^{(i)[1]} \Big _{\partial \mathcal{B}^n}$
$\chi^{(i)[2]} \Big _{\partial \mathcal{B}^w} = \chi^{(i)[2]} \Big _{\partial \mathcal{B}^e}$	$\mathbf{n} \cdot \nabla_{\xi} \chi^{(i)[2]} \Big _{\partial \mathcal{B}^w} = -\mathbf{n} \cdot \nabla_{\xi} \chi^{(i)[2]} \Big _{\partial \mathcal{B}^e}$
$\chi^{(i)[2]} \Big _{\partial \mathcal{B}^s} = \chi^{(i)[2]} \Big _{\partial \mathcal{B}^n}$	$\mathbf{n} \cdot \nabla_{\xi} \chi^{(i)[2]} \Big _{\partial \mathcal{B}^s} = -\mathbf{n} \cdot \nabla_{\xi} \chi^{(i)[2]} \Big _{\partial \mathcal{B}^n}$
Simulation Initial Conditions	
<u>Pore-scale Mass Transport</u>	
$c_\epsilon^{(1)} = H(-x)$ for $(x, y) \in \mathcal{B}_\epsilon, t = 0$	<u>Homogenized Mass Transport</u>
$c_\epsilon^{(2)} = H(x)$ for $(x, y) \in \mathcal{B}_\epsilon, t = 0$	$\langle c^{(i)} \rangle_Y = \langle c_\epsilon^{(i)} \rangle_{\mathcal{W}_\epsilon(\mathbf{x})}$ for $(x, y) \in \Omega, t = 0$

478 In a similar manner as before, the pore-scale, averaged pore-scale, and homogenized model results  
479 for the first and second solutes are presented in Figures 5 and 6, respectively. The qualitative compar-  
480 isons found in Figures 5(a) and 6(a) between averaged pore-scale and homogenized solutions show match-  
481 ing profiles along the  $x$ -direction, even at simulation times as early as  $t = t_1 = 0.625 \times 10^{-4}$ . For simi-  
482 lar reasons as before, we note that the results in Figures 5(a) and 6(a) are independent of  $y$ , and the ini-  
483 tial conditions of the homogenized model (displayed at  $t = t_0$ ) show a sharp slope around  $x = 0$  due  
484 to the averaging of the discontinuous pore-scale initial conditions using equation (22a).

485 To provide quantitative comparisons, Figures 5(b) and 6(b) show the absolute errors between the  
486 averaged pore-scale and homogenized solutions along the  $x$ -direction calculated using equation (24). De-  
487 spite considering early times, the absolute errors remain below the upper error limits denoted by the red  
488 dotted lines for all times. In this regard, we compare our results with those of Bourbatache *et al.* (Bourbatache  
489 *et al.*, 2021), who reported discrepancies between their macroscopic and microscopic models for the same  
490 problem at early simulation times, and offer the generalized closure form strategy as a solution to deriv-  
491 ing homogenized models in the moderately reactive regime. Ultimately, finding the absolute errors within  
492 the error limits predicted by homogenization theory provides confidence in the validity of the general-  
493 ized closure form strategy.

494 Finally, contours of the pore-scale solutions at various times are presented in Figures 5(c) and 6(c).  
495 While the initial discontinuous concentration profiles are seen at  $t = t_0$ , the reactive and diffusive mech-  
496 anisms of the problem can be seen at  $t = t_1$  through small gradients around the cylinders in the satu-  
497 rated regions and through the diffusion of the discontinuity in the initial concentration profiles, respec-  
498 tively. These mechanisms continue to act into  $t = t_2$  until the concentration profiles evolve towards uni-  
499 form steady-states, as in  $t = t_3$ .

500 With the numerical results presented in Figures 5 and 6, we again find that the generalized closure  
501 form strategy provides valid homogenized models for moderately reactive systems where diffusive and re-

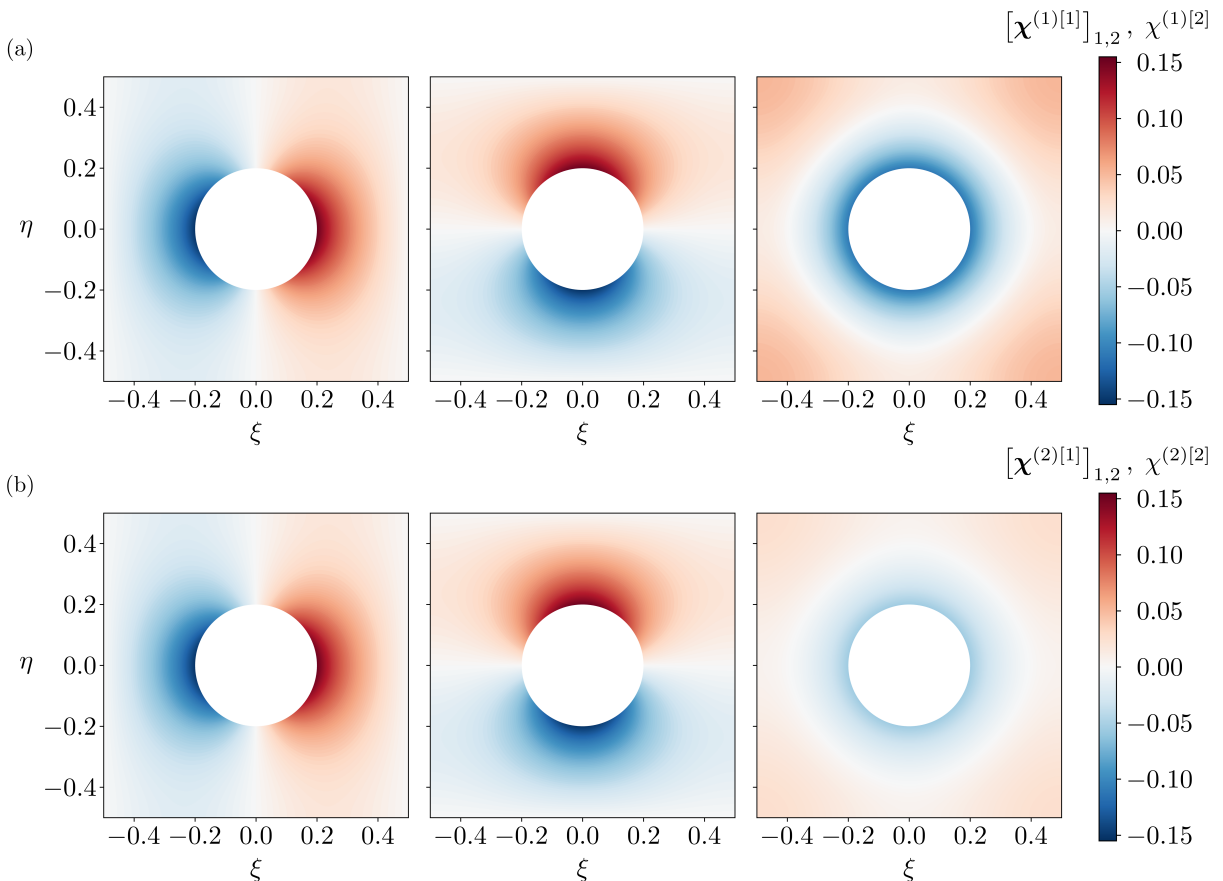


**Figure 4.** The numerical results of the closure problems for each solute in the system of two species undergoing linear heterogeneous reactions. (a) The resulting closure solutions  $\chi^{(1)[1]}$  and  $\chi^{(1)[2]}$ . From left to right:  $[\chi^{(1)[1]}]_1$  the  $\xi$ -component of  $\chi^{(1)[1]}$ ,  $[\chi^{(1)[1]}]_2$  the  $\eta$ -component of  $\chi^{(1)[1]}$ , and  $\chi^{(1)[2]}$ . (b) The resulting closure solutions  $\chi^{(2)[1]}$  and  $\chi^{(2)[2]}$ . From left to right:  $[\chi^{(2)[1]}]_1$  the  $\xi$ -component of  $\chi^{(2)[1]}$ ,  $[\chi^{(2)[1]}]_2$  the  $\eta$ -component of  $\chi^{(2)[1]}$ , and  $\chi^{(2)[2]}$ .

502 active terms are of similar orders, even at early times. Therefore, we offer this method as a more gen-  
 503 eral approach to the classical homogenization procedure.

## 504 5 Conclusion

505 To summarize Part 1 of this series, we introduced a strategy for generalizing the closure form that  
 506 increases the applicability of classical homogenization theory with only slight deviation from the tradi-  
 507 tional procedure. As detailed in Appendix A and Appendix B, this strategy involves considering ordered  
 508 solution forms as linear combinations of closure terms, which are chosen based on the equation for which  
 509 closure is sought. As a result, multiple closure problems can be defined for a single homogenized equa-  
 510 tion, whereas classical homogenization theory typically consist of only one closure problem per homog-  
 511 enized equation. In our first problem, we considered a linear heterogeneous reaction with a moderate rea-  
 512 ction rate, which cannot be handled by classical homogenization theory, and provided a demonstration  
 513 for how our strategy can be implemented to homogenize the system. An analysis of the homogenized model  
 514 then followed, where we emphasized that additional contributions to the effective velocity were found due  
 515 to interactions between diffusive and reactive fluxes. These contributions do not vanish for  $Pe = 0$  and  
 516 indicate an early onset of coupling between diffusion and reaction, despite the effective reaction rate be-  
 517 ing independent of diffusion and the effective dispersion tensor being independent of reaction. We then  
 518 validated our homogenized model, and ultimately the generalized closure form strategy, by numerically  
 519 solving the model and comparing the solution to the averaged pore-scale solution. Upon finding the ab-  
 520 solute error within the upper error limit predicted by homogenization theory, we deemed the strategy and  
 521 our homogenized model valid.

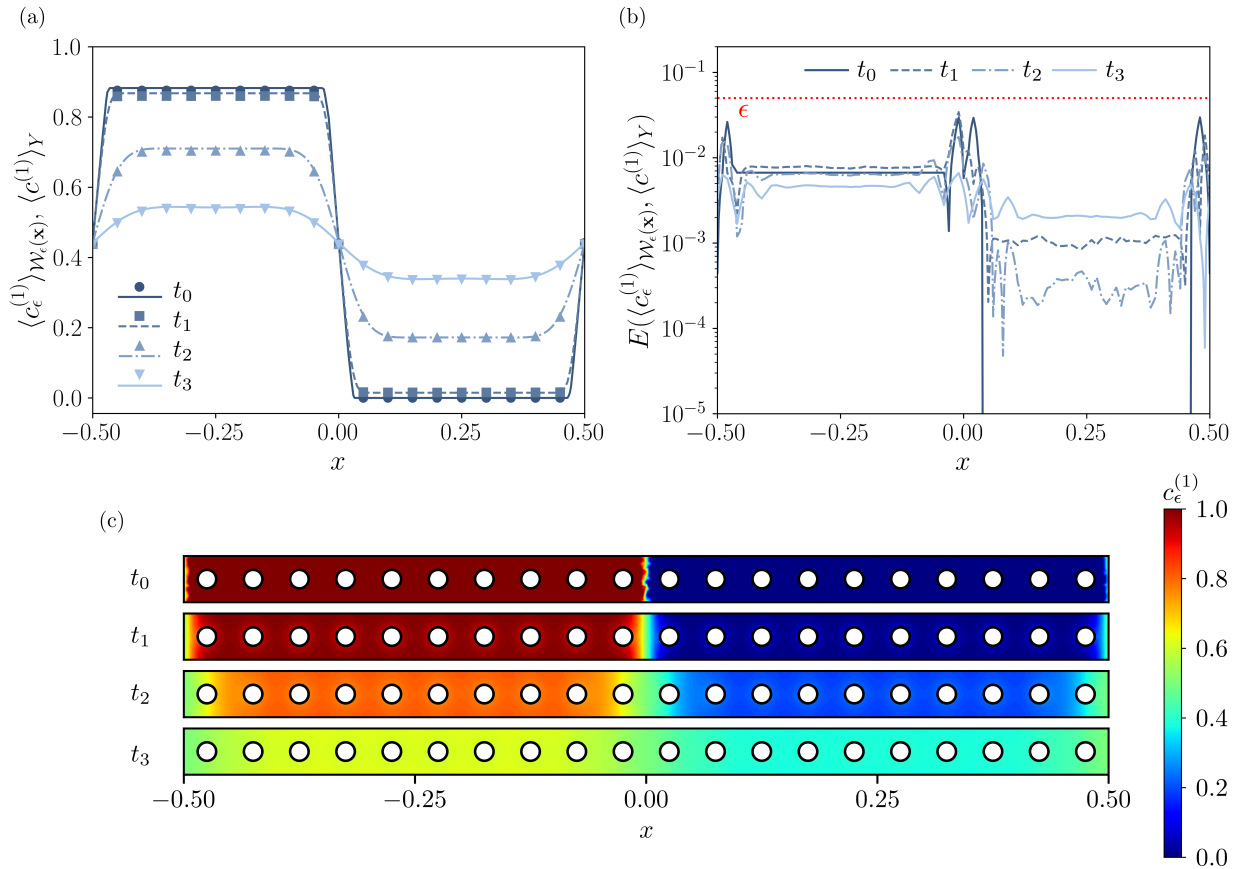


**Figure 5.** The numerical results of the first concentration in the system involving two species undergoing linear heterogeneous reactions. (a) The  $\mathcal{W}_\epsilon(\mathbf{x})$ -averaged and  $Y$ -averaged concentration profiles from the pore-scale (symbols) and homogenized (lines) models, respectively, at various times along the  $x$ -direction. (b) The absolute error between the averaged concentration profiles of  $\langle c_\epsilon^{(1)} \rangle_{\mathcal{W}_\epsilon(\mathbf{x})}$  and  $\langle c^{(1)} \rangle_Y$  at various times along the  $x$ -direction. The upper error limit predicted by the homogenized model is displayed by the red dotted line. (c) Contour plots of the pore-scale concentration field  $c_\epsilon^{(1)}$  at various times. Here,  $t_0 = 0$ ,  $t_1 = 0.625 \times 10^{-4}$ ,  $t_2 = 9.375 \times 10^{-4}$ , and  $t_3 = 28.125 \times 10^{-4}$ .

522 In the second problem, we applied the generalized closure form strategy to a system previously in-  
523 vestigated by Bourbatache *et al.* (Bourbatache et al., 2021) with advection, which consisted of two species  
524 undergoing linear heterogeneous reactions in the moderately reactive regime. After detailing the homogen-  
525 ization procedure using the generalized closure form strategy in Appendix B, we obtained a homogen-  
526 ized model consisting of terms that induce emergent behaviors through nontrivial couplings. The new  
527 effective parameters that appeared with these emergent terms rely on the closure variables of both sol-  
528 utes, which indicates an inherent coupling between the new effective parameters and the behavior of the  
529 different system components. Ultimately, this furthers the argument that macroscopic equations do not  
530 always take the form of their microscopic counterpart and can be nontrivial. Upon numerically solving  
531 the homogenized model and comparing its solution to the averaged pore-scale solution, we again found  
532 qualitative and quantitative evidence that the homogenized model captures the behavior of the averaged  
533 pore-scale solution within the upper error limit predicted by homogenization theory, even for early times.  
534 This further validates the presented generalized closure form strategy.

535 In light of the numerical evidence validating the nontrivial homogenized models and their effective  
536 parameters, we deem the generalized closure form strategy valid and offer it as a standard homogeniza-  
537 tion method that generalizes the classical approach. As we will demonstrate in Part 2 of this series, an  
538 algorithmic procedure can be developed for efficient implementation of the strategy using automated (sym-  
539 bolic) upscaling frameworks like Symbolica. By encoding this procedure, automated frameworks will be  
540 capable of automatically defining closure forms and closure problems based on the provided equations,  
541 with no *a priori* postulations of closure forms and no human interference. We believe this ability will be

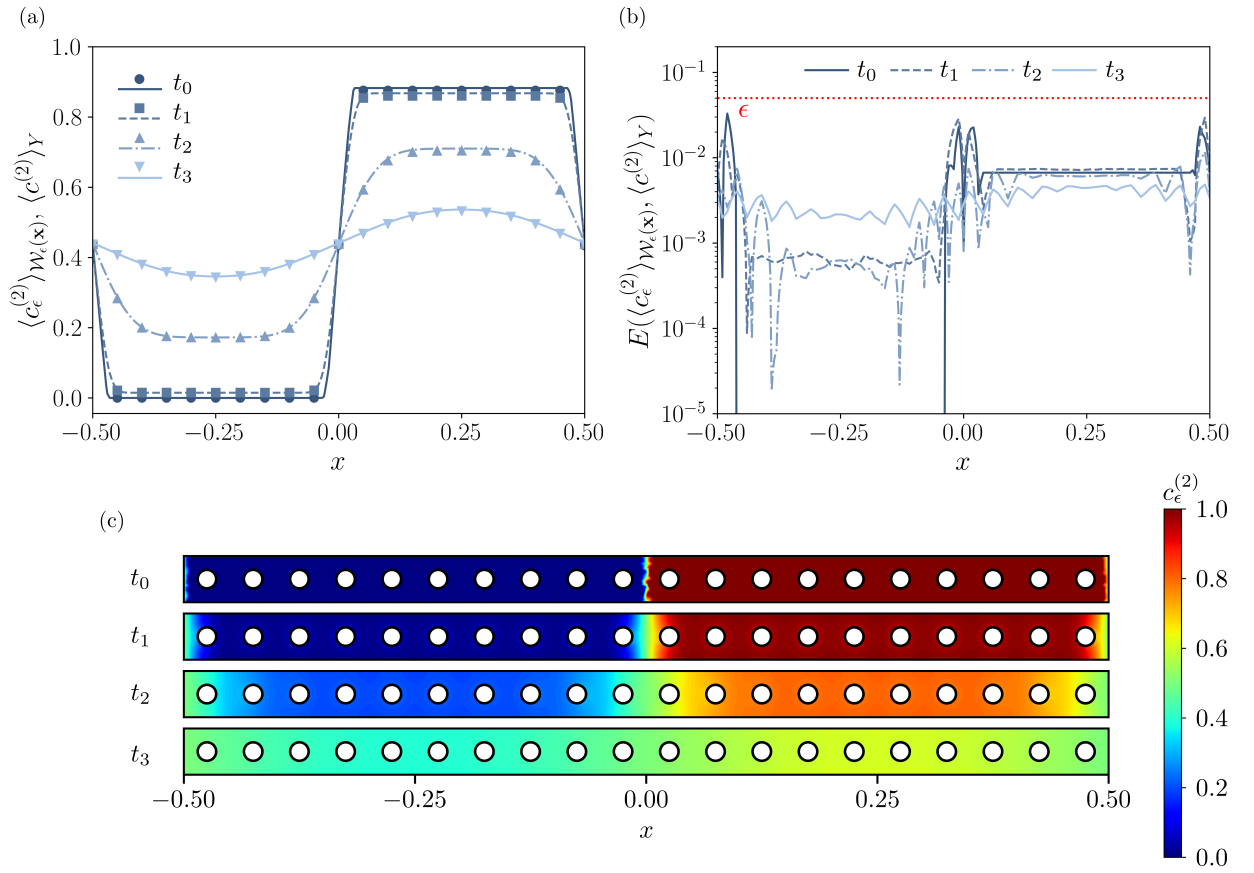


**Figure 6.** The numerical results of the second concentration in the system involving two species undergoing linear heterogeneous reactions. (a) The  $\mathcal{W}_\epsilon(\mathbf{x})$ -averaged and  $Y$ -averaged concentration profiles from the pore-scale (symbols) and homogenized (lines) models, respectively, at various times along the  $x$ -direction. (b) The absolute error between the averaged concentration profiles of  $\langle c_\epsilon^{(2)} \rangle_{\mathcal{W}_\epsilon(\mathbf{x})}$  and  $\langle c^{(2)} \rangle_Y$  at various times along the  $x$ -direction. The upper error limit predicted by the homogenized model is displayed by the red dotted line. (c) Contour plots of the pore-scale concentration field  $c_\epsilon^{(2)}$  at various times. Here,  $t_0 = 0$ ,  $t_1 = 0.625 \times 10^{-4}$ ,  $t_2 = 9.375 \times 10^{-4}$ , and  $t_3 = 28.125 \times 10^{-4}$ .

542  
543

invaluable for further development, generalization, and utilization of automated upscaling frameworks that utilize symbolic computing.

544  
545  
546  
547

### Acknowledgments

Support by the Department of Energy under the Early Career award DE-SC0019075 ‘Multiscale dynamics of reactive fronts in the subsurface’ is gratefully acknowledged. KP was also supported by the Stanford Graduate Fellowship in Science and Engineering.

## Appendix A Homogenization of a Linear Heterogeneous Reaction: One-Species

In this Appendix, we provide the detailed derivation of the homogenized system (19) from the pore-scale system (14). The strategy to construct a more general closure form for  $c_1$  (equation (17)) is also explicitly discussed.

### A1 Homogenization

Upon expanding the spatial operators, temporal operators, and dependent variables using equations (10), (12), and system (13), we simplify system (14) to

$$\begin{aligned}
& \epsilon^{-2} \left[ \frac{\partial c_0}{\partial \tau_2} + \nabla_{\boldsymbol{\xi}} \cdot \left( \text{Pe}^{(s)} \mathbf{u}_0 c_0 - D \nabla_{\boldsymbol{\xi}} c_0 \right) \right] \\
& + \epsilon^{-1} \left[ \frac{\partial c_0}{\partial \tau_1} + \frac{\partial c_1}{\partial \tau_2} + \nabla_{\mathbf{x}} \cdot \left( \text{Pe}^{(s)} \mathbf{u}_0 c_0 - D \nabla_{\boldsymbol{\xi}} c_0 \right) \right. \\
& \quad \left. + \nabla_{\boldsymbol{\xi}} \cdot \left( \text{Pe}^{(s)} \mathbf{u}_1 c_0 + \text{Pe}^{(s)} \mathbf{u}_0 c_1 - D \nabla_{\mathbf{x}} c_0 - D \nabla_{\boldsymbol{\xi}} c_1 \right) \right] \\
& + \epsilon^0 \left[ \frac{\partial c_0}{\partial t} + \frac{\partial c_1}{\partial \tau_1} + \frac{\partial c_2}{\partial \tau_2} + \nabla_{\mathbf{x}} \cdot \left( \text{Pe}^{(s)} \mathbf{u}_1 c_0 + \text{Pe}^{(s)} \mathbf{u}_0 c_1 - D \nabla_{\mathbf{x}} c_0 - D \nabla_{\boldsymbol{\xi}} c_1 \right) \right. \\
& \quad \left. + \nabla_{\boldsymbol{\xi}} \cdot \left( \text{Pe}^{(s)} \mathbf{u}_2 c_0 + \text{Pe}^{(s)} \mathbf{u}_1 c_1 + \text{Pe}^{(s)} \mathbf{u}_0 c_2 - D \nabla_{\mathbf{x}} c_1 - D \nabla_{\boldsymbol{\xi}} c_2 \right) \right] \\
& = \mathcal{O}(\epsilon) \quad \text{for } \mathbf{x} \in \Omega, \boldsymbol{\xi} \in \mathcal{B},
\end{aligned} \tag{A1a}$$

subject to

$$\begin{aligned}
& \epsilon^{-1} [-\mathbf{n} \cdot D \nabla_{\boldsymbol{\xi}} c_0] + \epsilon^0 [-\mathbf{n} \cdot D (\nabla_{\mathbf{x}} c_0 + \nabla_{\boldsymbol{\xi}} c_1)] + \epsilon [-\mathbf{n} \cdot D (\nabla_{\mathbf{x}} c_1 + \nabla_{\boldsymbol{\xi}} c_2)] \\
& = \epsilon^0 [\text{Da}^{(s)} (c_0 - \theta^{(s)})] + \epsilon [\text{Da}^{(s)} c_1] + \mathcal{O}(\epsilon^2) \quad \text{for } \mathbf{x} \in \Omega, \boldsymbol{\xi} \in \Gamma,
\end{aligned} \tag{A1b}$$

where  $\text{Pe}^{(s)} \equiv \text{Pe} \epsilon \sim \mathcal{O}(\epsilon^0)$ ,  $\text{Da}^{(s)} \equiv \text{Da} \sim \mathcal{O}(\epsilon^0)$ , and  $\theta^{(s)} \equiv \theta \sim \mathcal{O}(\epsilon^0)$  are used to track where the dimensionless numbers appear in the final homogenized model. In addition to the mass transport equation, we find it useful to simplify equation (6b) using equations (10) and (13b), such that

$$\epsilon^{-1} [\nabla_{\boldsymbol{\xi}} \cdot \mathbf{u}_0] + \epsilon^0 [\nabla_{\mathbf{x}} \cdot \mathbf{u}_0 + \nabla_{\boldsymbol{\xi}} \cdot \mathbf{u}_1] + \epsilon [\nabla_{\mathbf{x}} \cdot \mathbf{u}_1 + \nabla_{\boldsymbol{\xi}} \cdot \mathbf{u}_2] = \mathcal{O}(\epsilon^2) \quad \text{for } \mathbf{x} \in \Omega, \boldsymbol{\xi} \in \mathcal{B}. \tag{A2}$$

We now create a system of differential equations from system (A1) by considering the terms at each order of  $\epsilon$  independently.

#### A11 Terms of Order $\mathcal{O}(\epsilon^{-2})$

After collecting the leading order terms in system (A1), we gain

$$\frac{\partial c_0}{\partial \tau_2} + \nabla_{\boldsymbol{\xi}} \cdot \left( \text{Pe}^{(s)} \mathbf{u}_0 c_0 - D \nabla_{\boldsymbol{\xi}} c_0 \right) = 0 \quad \text{for } \mathbf{x} \in \Omega, \boldsymbol{\xi} \in \mathcal{B}, \tag{A3a}$$

subject to the leading order boundary condition (i.e., at  $\mathcal{O}(\epsilon^{-1})$ )

$$-\mathbf{n} \cdot D \nabla_{\boldsymbol{\xi}} c_0 = 0 \quad \text{for } \mathbf{x} \in \Omega, \boldsymbol{\xi} \in \Gamma. \tag{A3b}$$

By applying the averaging operator  $\langle \cdot \rangle_{\mathcal{B}}$  (equation (11)) to equation (A3a), we implement the divergence theorem on both the diffusive and advective flux terms. While the boundary condition (equation (A3b)) is applied through the diffusive flux, we enforce the no-slip condition and consider that  $\mathbf{u}_0$  and  $c_0$  are periodic in  $\boldsymbol{\xi}$  to simplify the advective flux and gain

$$\frac{\partial \langle c_0 \rangle_{\mathcal{B}}}{\partial \tau_2} = 0 \quad \text{for } \mathbf{x} \in \Omega. \tag{A4}$$

568 As shown in equation (A4), if our hypotheses regarding the magnitudes of the dimensionless parameters  
 569 and periodicity of the system are correct, we find that the zeroth order average concentration should not  
 570 vary on the smallest time scale according to homogenization theory (i.e., vary with  $\tau_2(t)$ ). We empha-  
 571 size that this is not a limitation of homogenization theory, but rather a result of upholding our initial hy-  
 572 potheses and remaining within the applicability conditions considered. This highlights the importance  
 573 of ensuring that the dynamics of a system do not violate the underlying hypotheses at any time; other-  
 574 wise, the homogenized model will be invalid for analyzing the system.

575 After briefly analyzing equation (A2) to obtain  $\nabla_{\boldsymbol{\xi}} \cdot \mathbf{u}_0 = 0$  from the  $\mathcal{O}(\epsilon^{-1})$  terms, we rewrite  
 576 system (A3) as

$$\frac{\partial c_0}{\partial \tau_2} + \text{Pe}^{(s)} \mathbf{u}_0 \cdot \nabla_{\boldsymbol{\xi}} c_0 - \nabla_{\boldsymbol{\xi}} \cdot (D \nabla_{\boldsymbol{\xi}} c_0) = 0 \quad \text{for } \mathbf{x} \in \Omega, \boldsymbol{\xi} \in \mathcal{B}, \quad (\text{A5a})$$

577 subject to

$$-\mathbf{n} \cdot D \nabla_{\boldsymbol{\xi}} c_0 = 0 \quad \text{for } \mathbf{x} \in \Omega, \boldsymbol{\xi} \in \Gamma. \quad (\text{A5b})$$

578 Considering initial conditions for  $c_0$  that are independent of  $\boldsymbol{\xi}$ , we find  $c_0$  to be independent of  $\tau_2$ . It then  
 579 follows from the homogeneity of the system that  $c_0$  is independent of  $\boldsymbol{\xi}$ , and therefore  $c_0 \equiv c_0(t, \mathbf{x}, \tau_1(t))$ .  
 580 This coincides with the familiar leading order result of classical homogenization theory, where the fastest  
 581 time variable (i.e.,  $\tau_2(t)$ ) is typically not introduced for the sake of brevity.

## 582 **A12 Terms of Order $\mathcal{O}(\epsilon^{-1})$**

583 At the following order, we collect terms from system (A1) to write

$$\begin{aligned} & \frac{\partial c_0}{\partial \tau_1} + \frac{\partial c_1}{\partial \tau_2} + \nabla_{\mathbf{x}} \cdot \left( \text{Pe}^{(s)} \mathbf{u}_0 c_0 - D \nabla_{\boldsymbol{\xi}} c_0 \right) \\ & + \nabla_{\boldsymbol{\xi}} \cdot \left( \text{Pe}^{(s)} \mathbf{u}_1 c_0 + \text{Pe}^{(s)} \mathbf{u}_0 c_1 - D \nabla_{\mathbf{x}} c_0 - D \nabla_{\boldsymbol{\xi}} c_1 \right) = 0 \quad \text{for } \mathbf{x} \in \Omega, \boldsymbol{\xi} \in \mathcal{B}, \end{aligned} \quad (\text{A6a})$$

584 subject to the boundary condition (i.e., at  $\mathcal{O}(\epsilon^0)$ )

$$-\mathbf{n} \cdot D (\nabla_{\mathbf{x}} c_0 + \nabla_{\boldsymbol{\xi}} c_1) = \text{Da}^{(s)} \left( c_0 - \theta^{(s)} \right) \quad \text{for } \mathbf{x} \in \Omega, \boldsymbol{\xi} \in \Gamma. \quad (\text{A6b})$$

585 Again, we apply the averaging operator  $\langle \cdot \rangle_{\mathcal{B}}$  (equation (11)) to equation (A6a), implement the divergence  
 586 theorem, and apply the boundary condition (equation (A6b)) and no-slip condition to the equation. We  
 587 also consider that  $\mathbf{u}_0$ ,  $\mathbf{u}_1$ , and  $c_1$  are periodic in  $\boldsymbol{\xi}$  to simplify the equation to

$$\frac{\partial c_0}{\partial \tau_1} + \frac{\partial \langle c_1 \rangle_{\mathcal{B}}}{\partial \tau_2} + \text{Pe}^{(s)} \langle \mathbf{u}_0 \rangle_{\mathcal{B}} \cdot \nabla_{\mathbf{x}} c_0 + \text{Da}^{(s)} \frac{|\Gamma|}{|\mathcal{B}|} \left( c_0 - \theta^{(s)} \right) = 0 \quad \text{for } \mathbf{x} \in \Omega. \quad (\text{A7})$$

588 As shown, equation (A7) describes how  $c_0$  and  $\langle c_1 \rangle_{\mathcal{B}}$  vary with fast time variables  $\tau_1(t)$  and  $\tau_2(t)$ , respec-  
 589 tively.

590 Now, we return to equation (A2) and conclude that  $\nabla_{\mathbf{x}} \cdot \mathbf{u}_0 = 0$  from the  $\mathcal{O}(\epsilon^0)$  terms after ap-  
 591 plying the averaging operator  $\langle \cdot \rangle_{\mathcal{B}}$ , the divergence theorem, and assuming  $\mathbf{u}_1$  is periodic in  $\boldsymbol{\xi}$  with the  
 592 no-slip condition. Ultimately, this leads to  $\nabla_{\boldsymbol{\xi}} \cdot \mathbf{u}_1 = 0$  as well. After subtracting equation (A7) from  
 593 equation (A6a), we gain

$$\begin{aligned} & \frac{\partial c_1}{\partial \tau_2} - \frac{\partial \langle c_1 \rangle_{\mathcal{B}}}{\partial \tau_2} + \text{Pe}^{(s)} (\mathbf{u}_0 - \langle \mathbf{u}_0 \rangle_{\mathcal{B}}) \cdot \nabla_{\mathbf{x}} c_0 - \text{Da}^{(s)} \frac{|\Gamma|}{|\mathcal{B}|} \left( c_0 - \theta^{(s)} \right) \\ & + \text{Pe}^{(s)} \mathbf{u}_0 \cdot \nabla_{\boldsymbol{\xi}} c_1 - D \nabla_{\boldsymbol{\xi}} \cdot (\nabla_{\mathbf{x}} c_0 + \nabla_{\boldsymbol{\xi}} c_1) = 0 \quad \text{for } \mathbf{x} \in \Omega, \boldsymbol{\xi} \in \mathcal{B}, \end{aligned} \quad (\text{A8})$$

594 subject to the boundary condition previously presented in equation (A6b). Here, we note that through  
 595 brief analysis of equations (A8) and (A6b), the traditionally used closure form  $c_1 = \boldsymbol{\chi} \cdot \nabla_{\mathbf{x}} c_0 + \bar{c}_1$ , where

596  $\chi \equiv \chi(\xi)$  is the *closure variable* and  $\bar{c}_1 \equiv \bar{c}_1(t, \mathbf{x}, \boldsymbol{\tau}(t)) = \langle c_1 \rangle_{\mathcal{B}}$  is the average of the first-order con-  
 597 centration over  $\mathcal{B}$  (which implies  $\langle \chi \rangle_{\mathcal{B}} = \mathbf{0}$ ), cannot be used to separate scales and create a valid clo-  
 598 sure problem, i.e., a problem where the only independent variable is  $\xi$ . This is due to the reaction terms  
 599 that exist in both the equation and boundary condition, which are not dotted with  $\nabla_{\mathbf{x}}c_0$ . However, due  
 600 to the linearity of equations (A8) and (A6b), we can simply assume a solution of the form  $c_1 = c_1^{[1]} +$   
 601  $c_1^{[2]}$  and linearly separate the system to consider the terms multiplied by  $(c_0 - \theta^{(s)})$  and the terms dot-  
 602 ted with  $\nabla_{\mathbf{x}}c_0$  independently. In doing so, we obtain

$$\begin{aligned} \frac{\partial c_1^{[1]}}{\partial \tau_2} - \frac{\partial \langle c_1^{[1]} \rangle_{\mathcal{B}}}{\partial \tau_2} + \text{Pe}^{(s)}(\mathbf{u}_0 - \langle \mathbf{u}_0 \rangle_{\mathcal{B}}) \cdot \nabla_{\mathbf{x}}c_0 + \text{Pe}^{(s)}\mathbf{u}_0 \cdot \nabla_{\xi}c_1^{[1]} \\ - D\nabla_{\xi} \cdot (\nabla_{\mathbf{x}}c_0 + \nabla_{\xi}c_1^{[1]}) = 0 \quad \text{for } \mathbf{x} \in \Omega, \xi \in \mathcal{B}, \end{aligned} \quad (\text{A9a})$$

603 subject to

$$-\mathbf{n} \cdot D(\nabla_{\mathbf{x}}c_0 + \nabla_{\xi}c_1^{[1]}) = 0 \quad \text{for } \mathbf{x} \in \Omega, \xi \in \Gamma, \quad (\text{A9b})$$

604 which considers the terms dotted by  $\nabla_{\mathbf{x}}c_0$ , and

$$\frac{\partial c_1^{[2]}}{\partial \tau_2} - \frac{\partial \langle c_1^{[2]} \rangle_{\mathcal{B}}}{\partial \tau_2} - \text{Da}^{(s)} \frac{|\Gamma|}{|\mathcal{B}|} (c_0 - \theta^{(s)}) + \text{Pe}^{(s)}\mathbf{u}_0 \cdot \nabla_{\xi}c_1^{[2]} - D\nabla_{\xi}^2c_1^{[2]} = 0 \quad \text{for } \mathbf{x} \in \Omega, \xi \in \mathcal{B}, \quad (\text{A10a})$$

605 subject to

$$-\mathbf{n} \cdot D\nabla_{\xi}c_1^{[2]} = \text{Da}^{(s)}(c_0 - \theta^{(s)}) \quad \text{for } \mathbf{x} \in \Omega, \xi \in \Gamma, \quad (\text{A10b})$$

606 which considers the terms multiplied by  $(c_0 - \theta^{(s)})$ . By assuming different closure forms for  $c_1^{[1]}$  and  $c_1^{[2]}$ ,  
 607 two closure problems can be created (i.e., one from system (A9) and one from system (A10)) to accom-  
 608 modate all terms in equations (A8) and (A6b). Here, we let

$$c_1^{[1]} = \boldsymbol{\chi}^{[1]} \cdot \nabla_{\mathbf{x}}c_0 + \bar{c}_1^{[1]}, \quad (\text{A11a})$$

$$c_1^{[2]} = (c_0 - \theta^{(s)})\chi^{[2]} + \bar{c}_1^{[2]}, \quad (\text{A11b})$$

609 where  $\boldsymbol{\chi}^{[1]} \equiv \boldsymbol{\chi}^{[1]}(\xi)$  is the vector closure variable for  $c_1^{[1]}$ ,  $\chi^{[2]} \equiv \chi^{[2]}(\xi)$  is the scalar closure variable  
 610 for  $c_1^{[2]}$ ,  $\bar{c}_1^{[1]} \equiv \bar{c}_1^{[1]}(t, \mathbf{x}, \boldsymbol{\tau}(t)) = \langle c_1^{[1]} \rangle_{\mathcal{B}}$  is the average of the first component to the first-order concen-  
 611 tration over  $\mathcal{B}$ , and  $\bar{c}_1^{[2]} \equiv \bar{c}_1^{[2]}(t, \mathbf{x}, \boldsymbol{\tau}(t)) = \langle c_1^{[2]} \rangle_{\mathcal{B}}$  is the average of the second component to the first-  
 612 order concentration over  $\mathcal{B}$ . Similar to before, we note that  $\langle \boldsymbol{\chi}^{[1]} \rangle_{\mathcal{B}} = \mathbf{0}$  and  $\langle \chi^{[2]} \rangle_{\mathcal{B}} = 0$ . We also note  
 613 that due to the lack of dependency on  $\tau_2$  in the equations, we find it suitable to assume  $\bar{c}_1^{[1]}$  and  $\bar{c}_1^{[2]}$  are  
 614 the only parts of  $c_1^{[1]}$  and  $c_1^{[2]}$  that depend on  $\tau_2$ . Upon substituting equation (A11a) into system (A9)  
 615 and equation (A11b) into system (A10), we can write the closure problems as

$$\text{Pe}^{(s)}(\mathbf{u}_0 - \langle \mathbf{u}_0 \rangle_{\mathcal{B}}) + \text{Pe}^{(s)}\mathbf{u}_0 \cdot \nabla_{\xi}\boldsymbol{\chi}^{[1]} - D\nabla_{\xi} \cdot (\mathbf{I} + \nabla_{\xi}\boldsymbol{\chi}^{[1]}) = \mathbf{0} \quad \text{for } \xi \in \mathcal{B}, \quad (\text{A12a})$$

616 subject to

$$-\mathbf{n} \cdot D(\mathbf{I} + \nabla_{\xi}\boldsymbol{\chi}^{[1]}) = \mathbf{0} \quad \text{for } \xi \in \Gamma, \quad (\text{A12b})$$

617 and

$$-\text{Da}^{(s)} \frac{|\Gamma|}{|\mathcal{B}|} + \text{Pe}^{(s)}\mathbf{u}_0 \cdot \nabla_{\xi}\chi^{[2]} - D\nabla_{\xi}^2\chi^{[2]} = 0 \quad \text{for } \xi \in \mathcal{B}, \quad (\text{A13a})$$

$$-\mathbf{n} \cdot D\nabla_{\boldsymbol{\xi}}\chi^{[2]} = \text{Da}^{(s)} \quad \text{for } \boldsymbol{\xi} \in \Gamma. \quad (\text{A13b})$$

619 From the derived closure problems, we physically interpret  $\chi^{[2]}$  as a function that provides correction to  
 620 the reactive flux due to the presence of microscopic geometry and high advection, similar to how  $\chi^{[1]}$  pro-  
 621 vides correction to the diffusive flux. Finally, we note that the full closure form of  $c_1$  to be used through-  
 622 out the rest of the homogenization procedure is written as

$$c_1 = \boldsymbol{\chi}^{[1]} \cdot \nabla_{\mathbf{x}}c_0 + \left(c_0 - \theta^{(s)}\right)\chi^{[2]} + \bar{c}_1, \quad (\text{A14})$$

623 where  $\bar{c}_1 \equiv \bar{c}_1^{[1]} + \bar{c}_1^{[2]}$ . As demonstrated, linearly separating equations (A8) and (A6b) and generalizing  
 624 the assumed closure form of  $c_1$  as a linear combination of closure terms allows for valid closure problems  
 625 to be created in scenarios where the traditionally assumed closure form fails.

### 626 **A13 Terms of Order $\mathcal{O}(\epsilon^0)$**

627 Finally, we collect terms of  $\mathcal{O}(\epsilon^0)$  from system (A1) to write

$$\begin{aligned} & \frac{\partial c_0}{\partial t} + \frac{\partial c_1}{\partial \tau_1} + \frac{\partial c_2}{\partial \tau_2} + \nabla_{\mathbf{x}} \cdot \left( \text{Pe}^{(s)}\mathbf{u}_1c_0 + \text{Pe}^{(s)}\mathbf{u}_0c_1 - D\nabla_{\mathbf{x}}c_0 - D\nabla_{\boldsymbol{\xi}}c_1 \right) \\ & + \nabla_{\boldsymbol{\xi}} \cdot \left( \text{Pe}^{(s)}\mathbf{u}_2c_0 + \text{Pe}^{(s)}\mathbf{u}_1c_1 + \text{Pe}^{(s)}\mathbf{u}_0c_2 - D\nabla_{\mathbf{x}}c_1 - D\nabla_{\boldsymbol{\xi}}c_2 \right) = 0 \quad \text{for } \mathbf{x} \in \Omega, \boldsymbol{\xi} \in \mathcal{B}, \end{aligned} \quad (\text{A15a})$$

628 subject to the boundary condition (i.e., at  $\mathcal{O}(\epsilon)$ )

$$-\mathbf{n} \cdot D \left( \nabla_{\mathbf{x}}c_1 + \nabla_{\boldsymbol{\xi}}c_2 \right) = \text{Da}^{(s)}c_1 \quad \text{for } \mathbf{x} \in \Omega, \boldsymbol{\xi} \in \Gamma. \quad (\text{A15b})$$

629 After substituting in the solution for  $c_1$  (equation (A14)), we again apply the averaging operator  $\langle \cdot \rangle_{\mathcal{B}}$  (equa-  
 630 tion (11)) to equation (A15a) and implement the divergence theorem to incorporate the boundary con-  
 631 dition (equation (A15b)) and apply the no-slip condition. Further simplifications regarding the period-  
 632 icity of the dependent variables in  $\boldsymbol{\xi}$  are also made to write equation (A15a) as

$$\begin{aligned} & \frac{\partial c_0}{\partial t} + \frac{\partial \bar{c}_1}{\partial \tau_1} + \frac{\partial \langle c_2 \rangle_{\mathcal{B}}}{\partial \tau_2} \\ & + \left[ \text{Pe}^{(s)} \left( \langle \mathbf{u}_1 \rangle_{\mathcal{B}} + \langle \mathbf{u}_0\chi^{[2]} \rangle_{\mathcal{B}} \right) + \text{Da}^{(s)} \frac{|\Gamma|}{|\mathcal{B}|} \langle \chi^{[1]} \rangle_{\Gamma} - D \langle \nabla_{\boldsymbol{\xi}}\chi^{[2]} \rangle_{\mathcal{B}} \right] \cdot \nabla_{\mathbf{x}}c_0 \\ & + \text{Pe}^{(s)} \langle \mathbf{u}_0 \rangle_{\mathcal{B}} \cdot \nabla_{\mathbf{x}}\bar{c}_1 \\ & - \nabla_{\mathbf{x}} \cdot \left[ \left( D\mathbf{I} + D \langle \nabla_{\boldsymbol{\xi}}\chi^{[1]} \rangle_{\mathcal{B}} - \text{Pe}^{(s)} \langle \mathbf{u}_0 \otimes \chi^{[1]} \rangle_{\mathcal{B}} \right) \cdot \nabla_{\mathbf{x}}c_0 \right] \\ & + \text{Da}^{(s)} \frac{|\Gamma|}{|\mathcal{B}|} \left[ \left( c_0 - \theta^{(s)} \right) \langle \chi^{[2]} \rangle_{\Gamma} + \bar{c}_1 \right] = 0 \quad \text{for } \mathbf{x} \in \Omega. \end{aligned} \quad (\text{A16})$$

633 We now add equations (A4), (A7), and (A16), and make the substitutions  $\text{Pe}^{(s)} = \text{Pe}\epsilon$ ,  $\text{Da}^{(s)} = \text{Da}$ ,  
 634 and  $\theta^{(s)} = \theta$ , to obtain

$$\begin{aligned} & \epsilon^{-2} \frac{\partial c_0}{\partial \tau_2} + \epsilon^{-1} \left( \frac{\partial c_0}{\partial \tau_1} + \frac{\partial \bar{c}_1}{\partial \tau_2} \right) + \frac{\partial c_0}{\partial t} + \frac{\partial \bar{c}_1}{\partial \tau_1} + \frac{\partial \langle c_2 \rangle_{\mathcal{B}}}{\partial \tau_2} \\ & + \text{Pe} \left[ \langle \mathbf{u}_0 \rangle_{\mathcal{B}} \cdot \nabla_{\mathbf{x}}c_0 + \epsilon \left( \langle \mathbf{u}_1 \rangle_{\mathcal{B}} \cdot \nabla_{\mathbf{x}}c_0 + \langle \mathbf{u}_0 \rangle_{\mathcal{B}} \cdot \nabla_{\mathbf{x}}\bar{c}_1 \right) \right] \\ & + \left[ \text{Da} \frac{|\Gamma|}{|\mathcal{B}|} \langle \chi^{[1]} \rangle_{\Gamma} - D \langle \nabla_{\boldsymbol{\xi}}\chi^{[2]} \rangle_{\mathcal{B}} + \text{Pe}\epsilon \langle \mathbf{u}_0\chi^{[2]} \rangle_{\mathcal{B}} \right] \cdot \nabla_{\mathbf{x}}c_0 \\ & - \nabla_{\mathbf{x}} \cdot \left[ \left( D\mathbf{I} + D \langle \nabla_{\boldsymbol{\xi}}\chi^{[1]} \rangle_{\mathcal{B}} - \text{Pe}\epsilon \langle \mathbf{u}_0 \otimes \chi^{[1]} \rangle_{\mathcal{B}} \right) \cdot \nabla_{\mathbf{x}}c_0 \right] \\ & + \text{Da} \frac{|\Gamma|}{|\mathcal{B}|} \left[ \left( c_0 - \theta \right) \langle \chi^{[2]} \rangle_{\Gamma} + \left( \frac{1}{\epsilon}c_0 + \bar{c}_1 \right) - \frac{1}{\epsilon}\theta \right] = 0 \quad \text{for } \mathbf{x} \in \Omega. \end{aligned} \quad (\text{A17})$$

$$\frac{\partial \langle c \rangle_{\mathcal{B}}}{\partial t} = \epsilon^{-2} \frac{\partial c_0}{\partial \tau_2} + \epsilon^{-1} \left( \frac{\partial c_0}{\partial \tau_1} + \frac{\partial \bar{c}_1}{\partial \tau_2} \right) + \frac{\partial c_0}{\partial t} + \frac{\partial \bar{c}_1}{\partial \tau_1} + \frac{\partial \langle c_2 \rangle_{\mathcal{B}}}{\partial \tau_2} + \mathcal{O}(\epsilon), \quad (\text{A18a})$$

$$\text{Pe} \langle \mathbf{u} \rangle_{\mathcal{B}} \cdot \nabla_{\mathbf{x}} \langle c \rangle_{\mathcal{B}} = \text{Pe} [\langle \mathbf{u}_0 \rangle_{\mathcal{B}} \cdot \nabla_{\mathbf{x}} c_0 + \epsilon (\langle \mathbf{u}_1 \rangle_{\mathcal{B}} \cdot \nabla_{\mathbf{x}} c_0 + \langle \mathbf{u}_0 \rangle_{\mathcal{B}} \cdot \nabla_{\mathbf{x}} \bar{c}_1)] + \mathcal{O}(\epsilon), \quad (\text{A18b})$$

$$\langle c \rangle_{\mathcal{B}} = c_0 + \epsilon \bar{c}_1 + \mathcal{O}(\epsilon^2), \quad (\text{A18c})$$

$$\langle \mathbf{u} \rangle_{\mathcal{B}} = \mathbf{u}_0 + \mathcal{O}(\epsilon), \quad (\text{A18d})$$

636 obtained using equations (10), (12), and system (13), we can simplify equation (A17) to write the homog-  
637 enized model in system (19) as

$$\phi \frac{\partial \langle c \rangle_Y}{\partial t} + \mathbf{U} \cdot \nabla_{\mathbf{x}} \langle c \rangle_Y - \nabla_{\mathbf{x}} \cdot (\mathbf{D} \cdot \nabla_{\mathbf{x}} \langle c \rangle_Y) + \mathcal{R} (\phi \langle c \rangle_Y - \phi^2 \theta) = \mathcal{O}(\epsilon) \quad \text{for } \mathbf{x} \in \Omega, \quad (\text{A19a})$$

$$\mathbf{U} = \text{Pe} \langle \mathbf{u} \rangle_Y + \phi \text{Da} \frac{|\Gamma|}{|\mathcal{B}|} \langle \chi^{[1]} \rangle_{\Gamma} - D \langle \nabla_{\xi} \chi^{[2]} \rangle_Y + \text{Pe} \epsilon \langle \mathbf{u} \chi^{[2]} \rangle_Y, \quad (\text{A19b})$$

$$\mathbf{D} = \phi D \mathbf{I} + D \langle \nabla_{\xi} \chi^{[1]} \rangle_Y - \text{Pe} \epsilon \langle \mathbf{u} \otimes \chi^{[1]} \rangle_Y, \quad (\text{A19c})$$

$$\mathcal{R} = \text{Da} \frac{|\Gamma|}{|\mathcal{B}|} \left[ \epsilon^{-1} + \langle \chi^{[2]} \rangle_{\Gamma} \right], \quad (\text{A19d})$$

638 where  $\chi^{[1]}$  is found by solving system (A12),  $\chi^{[2]}$  is found by solving system (A13), and we have used  $\langle \cdot \rangle_{\mathcal{B}} =$   
639  $\phi^{-1} \langle \cdot \rangle_Y$  to convert the averaging operators. We emphasize that these equations are valid when  $\text{Pe} \sim \mathcal{O}(\epsilon^{-1})$ ,  
640  $\text{Da} \sim \mathcal{O}(\epsilon^0)$ , and  $\theta \sim \mathcal{O}(\epsilon^0)$ .

641 With the homogenized model, we reiterate that generalizing the closure form as a linear combina-  
642 tion of closure terms allowed the moderately reactive case considered to be homogenized. While the clas-  
643 sical treatment of heterogeneous reactions is limited to slow reaction rates (i.e.,  $\text{Da} \leq \mathcal{O}(\epsilon)$ ) (Municchi  
644 & Icardi, 2020), we were able to linearly separate the inhomogeneous terms of equations (A8) and (A6b)  
645 such that two valid closure problems could be defined with an appropriate closure form for  $c_1$ . The ho-  
646 mogenization procedure could then be completed with little deviation from the classical treatment.

## 647 Appendix B Homogenization of a Linear Heterogeneous Reaction: Two-Species

648 In this Appendix, we provide the detailed derivation of the homogenized system (30) from the pore-  
649 scale system (26). Again, the strategy to construct general closure forms for  $c_1^{(1)}$  and  $c_1^{(2)}$  (system (29))  
650 is explicitly discussed in detail.

### 651 B1 Homogenization

652 Upon expanding the spatial operators, temporal operators, and dependent variables using equations  
653 (10), (12), and system (13), we simplify system (26) to

$$\begin{aligned}
& \epsilon^{-2} \left[ \frac{\partial c_0^{(1)}}{\partial \tau_2} + \nabla_{\boldsymbol{\xi}} \cdot \left( \text{Pe}^{(s)} \mathbf{u}_0 c_0^{(1)} - D^{(1)} \nabla_{\boldsymbol{\xi}} c_0^{(1)} \right) \right] \\
& + \epsilon^{-1} \left[ \frac{\partial c_0^{(1)}}{\partial \tau_1} + \frac{\partial c_1^{(1)}}{\partial \tau_2} + \nabla_{\mathbf{x}} \cdot \left( \text{Pe}^{(s)} \mathbf{u}_0 c_0^{(1)} - D^{(1)} \nabla_{\boldsymbol{\xi}} c_0^{(1)} \right) \right. \\
& \quad \left. + \nabla_{\boldsymbol{\xi}} \cdot \left( \text{Pe}^{(s)} \mathbf{u}_1 c_0^{(1)} + \text{Pe}^{(s)} \mathbf{u}_0 c_1^{(1)} - D^{(1)} \nabla_{\mathbf{x}} c_0^{(1)} - D^{(1)} \nabla_{\boldsymbol{\xi}} c_1^{(1)} \right) \right] \tag{B1a} \\
& + \epsilon^0 \left[ \frac{\partial c_0^{(1)}}{\partial t} + \frac{\partial c_1^{(1)}}{\partial \tau_1} + \frac{\partial c_2^{(1)}}{\partial \tau_2} + \nabla_{\mathbf{x}} \cdot \left( \text{Pe}^{(s)} \mathbf{u}_1 c_0^{(1)} + \text{Pe}^{(s)} \mathbf{u}_0 c_1^{(1)} - D^{(1)} \nabla_{\mathbf{x}} c_0^{(1)} - D^{(1)} \nabla_{\boldsymbol{\xi}} c_1^{(1)} \right) \right. \\
& \quad \left. + \nabla_{\boldsymbol{\xi}} \cdot \left( \text{Pe}^{(s)} \mathbf{u}_2 c_0^{(1)} + \text{Pe}^{(s)} \mathbf{u}_1 c_1^{(1)} + \text{Pe}^{(s)} \mathbf{u}_0 c_2^{(1)} - D^{(1)} \nabla_{\mathbf{x}} c_1^{(1)} - D^{(1)} \nabla_{\boldsymbol{\xi}} c_2^{(1)} \right) \right] \\
& \quad = \mathcal{O}(\epsilon) \quad \text{for } \mathbf{x} \in \Omega, \boldsymbol{\xi} \in \mathcal{B},
\end{aligned}$$

$$\begin{aligned}
& \epsilon^{-2} \left[ \frac{\partial c_0^{(2)}}{\partial \tau_2} + \nabla_{\boldsymbol{\xi}} \cdot \left( \text{Pe}^{(s)} \mathbf{u}_0 c_0^{(2)} - D^{(2)} \nabla_{\boldsymbol{\xi}} c_0^{(2)} \right) \right] \\
& + \epsilon^{-1} \left[ \frac{\partial c_0^{(2)}}{\partial \tau_1} + \frac{\partial c_1^{(2)}}{\partial \tau_2} + \nabla_{\mathbf{x}} \cdot \left( \text{Pe}^{(s)} \mathbf{u}_0 c_0^{(2)} - D^{(2)} \nabla_{\boldsymbol{\xi}} c_0^{(2)} \right) \right. \\
& \quad \left. + \nabla_{\boldsymbol{\xi}} \cdot \left( \text{Pe}^{(s)} \mathbf{u}_1 c_0^{(2)} + \text{Pe}^{(s)} \mathbf{u}_0 c_1^{(2)} - D^{(2)} \nabla_{\mathbf{x}} c_0^{(2)} - D^{(2)} \nabla_{\boldsymbol{\xi}} c_1^{(2)} \right) \right] \tag{B1b} \\
& + \epsilon^0 \left[ \frac{\partial c_0^{(2)}}{\partial t} + \frac{\partial c_1^{(2)}}{\partial \tau_1} + \frac{\partial c_2^{(2)}}{\partial \tau_2} + \nabla_{\mathbf{x}} \cdot \left( \text{Pe}^{(s)} \mathbf{u}_1 c_0^{(2)} + \text{Pe}^{(s)} \mathbf{u}_0 c_1^{(2)} - D^{(2)} \nabla_{\mathbf{x}} c_0^{(2)} - D^{(2)} \nabla_{\boldsymbol{\xi}} c_1^{(2)} \right) \right. \\
& \quad \left. + \nabla_{\boldsymbol{\xi}} \cdot \left( \text{Pe}^{(s)} \mathbf{u}_2 c_0^{(2)} + \text{Pe}^{(s)} \mathbf{u}_1 c_1^{(2)} + \text{Pe}^{(s)} \mathbf{u}_0 c_2^{(2)} - D^{(2)} \nabla_{\mathbf{x}} c_1^{(2)} - D^{(2)} \nabla_{\boldsymbol{\xi}} c_2^{(2)} \right) \right] \\
& \quad = \mathcal{O}(\epsilon) \quad \text{for } \mathbf{x} \in \Omega, \boldsymbol{\xi} \in \mathcal{B},
\end{aligned}$$

654 subject to

$$\begin{aligned}
& \epsilon^{-1} \left[ -\mathbf{n} \cdot D^{(1)} \nabla_{\boldsymbol{\xi}} c_0^{(1)} \right] + \epsilon^0 \left[ -\mathbf{n} \cdot D^{(1)} \left( \nabla_{\mathbf{x}} c_0^{(1)} + \nabla_{\boldsymbol{\xi}} c_1^{(1)} \right) \right] + \epsilon \left[ -\mathbf{n} \cdot D^{(1)} \left( \nabla_{\mathbf{x}} c_1^{(1)} + \nabla_{\boldsymbol{\xi}} c_2^{(1)} \right) \right] \\
& = \epsilon^0 \left[ \text{Da}_{SL}^{(1,s)} c_0^{(1)} - \text{Da}_{SL}^{(2,s)} c_0^{(2)} \right] + \epsilon \left[ \text{Da}_{SL}^{(1,s)} c_1^{(1)} - \text{Da}_{SL}^{(2,s)} c_1^{(2)} \right] + \mathcal{O}(\epsilon^2) \quad \text{for } \mathbf{x} \in \Omega, \boldsymbol{\xi} \in \Gamma, \tag{B1c}
\end{aligned}$$

$$\begin{aligned}
& \epsilon^{-1} \left[ -\mathbf{n} \cdot D^{(2)} \nabla_{\boldsymbol{\xi}} c_0^{(2)} \right] + \epsilon^0 \left[ -\mathbf{n} \cdot D^{(2)} \left( \nabla_{\mathbf{x}} c_0^{(2)} + \nabla_{\boldsymbol{\xi}} c_1^{(2)} \right) \right] + \epsilon \left[ -\mathbf{n} \cdot D^{(2)} \left( \nabla_{\mathbf{x}} c_1^{(2)} + \nabla_{\boldsymbol{\xi}} c_2^{(2)} \right) \right] \\
& = \epsilon^0 \left[ \text{Da}_{SL}^{(2,s)} c_0^{(2)} - \text{Da}_{SL}^{(1,s)} c_0^{(1)} \right] + \epsilon \left[ \text{Da}_{SL}^{(2,s)} c_1^{(2)} - \text{Da}_{SL}^{(1,s)} c_1^{(1)} \right] + \mathcal{O}(\epsilon^2) \quad \text{for } \mathbf{x} \in \Omega, \boldsymbol{\xi} \in \Gamma, \tag{B1d}
\end{aligned}$$

655 where  $\text{Pe}^{(s)} \equiv \text{Pe} \epsilon \sim \mathcal{O}(\epsilon^0)$ ,  $\text{Da}_{SL}^{(1,s)} \equiv \text{Da}_{SL}^{(1)} \sim \mathcal{O}(\epsilon^0)$ , and  $\text{Da}_{SL}^{(2,s)} \equiv \text{Da}_{SL}^{(2)} \sim \mathcal{O}(\epsilon^0)$  are used to track  
656 where the dimensionless numbers appear in the final homogenized model. Similar to before, we simplify  
657 equation (6b) using equations (10) and (13b), such that

$$\epsilon^{-1} [\nabla_{\boldsymbol{\xi}} \cdot \mathbf{u}_0] + \epsilon^0 [\nabla_{\mathbf{x}} \cdot \mathbf{u}_0 + \nabla_{\boldsymbol{\xi}} \cdot \mathbf{u}_1] + \epsilon [\nabla_{\mathbf{x}} \cdot \mathbf{u}_1 + \nabla_{\boldsymbol{\xi}} \cdot \mathbf{u}_2] = \mathcal{O}(\epsilon^2) \quad \text{for } \mathbf{x} \in \Omega, \boldsymbol{\xi} \in \mathcal{B}. \tag{B2}$$

658 We now create a system of differential equations from system (B1) by considering the terms at each or-  
659 der of  $\epsilon$  independently.

### 660 **B11 Terms of Order $\mathcal{O}(\epsilon^{-2})$**

661 After collecting the leading order terms in system (B1), we gain

$$\frac{\partial c_0^{(1)}}{\partial \tau_2} + \nabla_{\boldsymbol{\xi}} \cdot \left( \text{Pe}^{(s)} \mathbf{u}_0 c_0^{(1)} - D^{(1)} \nabla_{\boldsymbol{\xi}} c_0^{(1)} \right) = 0 \quad \text{for } \mathbf{x} \in \Omega, \boldsymbol{\xi} \in \mathcal{B}, \tag{B3a}$$

$$\frac{\partial c_0^{(2)}}{\partial \tau_2} + \nabla_{\boldsymbol{\xi}} \cdot \left( \text{Pe}^{(s)} \mathbf{u}_0 c_0^{(2)} - D^{(2)} \nabla_{\boldsymbol{\xi}} c_0^{(2)} \right) = 0 \quad \text{for } \mathbf{x} \in \Omega, \boldsymbol{\xi} \in \mathcal{B}, \quad (\text{B3b})$$

662 subject to the leading order boundary conditions (i.e., at  $\mathcal{O}(\epsilon^{-1})$ )

$$-\mathbf{n} \cdot D^{(1)} \nabla_{\boldsymbol{\xi}} c_0^{(1)} = 0 \quad \text{for } \mathbf{x} \in \Omega, \boldsymbol{\xi} \in \Gamma, \quad (\text{B3c})$$

$$-\mathbf{n} \cdot D^{(2)} \nabla_{\boldsymbol{\xi}} c_0^{(2)} = 0 \quad \text{for } \mathbf{x} \in \Omega, \boldsymbol{\xi} \in \Gamma. \quad (\text{B3d})$$

663 Similar to before, we apply the averaging operator  $\langle \cdot \rangle_{\mathcal{B}}$  (equation (11)) to equations (B3a)-(B3b) and im-  
 664 plement the divergence theorem on both the diffusive and advective flux terms. While the boundary con-  
 665 ditions (equations (B3c)-(B3d)) are applied through the diffusive flux, we enforce the no-slip condition  
 666 and consider that  $\mathbf{u}_0$  and  $c_0$  are periodic in  $\boldsymbol{\xi}$  to simplify the advective flux and gain

$$\frac{\partial \langle c_0^{(1)} \rangle_{\mathcal{B}}}{\partial \tau_2} = 0 \quad \text{for } \mathbf{x} \in \Omega, \quad (\text{B4a})$$

$$\frac{\partial \langle c_0^{(2)} \rangle_{\mathcal{B}}}{\partial \tau_2} = 0 \quad \text{for } \mathbf{x} \in \Omega. \quad (\text{B4b})$$

667 Again, we find these equations to be results of upholding the initial hypotheses regarding the magnitudes  
 668 of the dimensionless parameters and the periodicity of the system. Then, considering  $\nabla_{\boldsymbol{\xi}} \cdot \mathbf{u}_0 = 0$  from  
 669 the  $\mathcal{O}(\epsilon^{-1})$  terms of equation (B2), initial conditions that are independent of  $\boldsymbol{\xi}$ , and the homogeneity of  
 670 the system, we find  $c_0^{(1)} = c_0^{(1)}(t, \mathbf{x}, \tau_1(t))$  and  $c_0^{(2)} = c_0^{(2)}(t, \mathbf{x}, \tau_1(t))$ .

### 671 *B12 Terms of Order $\mathcal{O}(\epsilon^{-1})$*

672 At the following order, we collect terms from system (B1) to write

$$\begin{aligned} & \frac{\partial c_0^{(1)}}{\partial \tau_1} + \frac{\partial c_1^{(1)}}{\partial \tau_2} + \nabla_{\mathbf{x}} \cdot \left( \text{Pe}^{(s)} \mathbf{u}_0 c_0^{(1)} - D^{(1)} \nabla_{\boldsymbol{\xi}} c_0^{(1)} \right) \\ & + \nabla_{\boldsymbol{\xi}} \cdot \left( \text{Pe}^{(s)} \mathbf{u}_1 c_0^{(1)} + \text{Pe}^{(s)} \mathbf{u}_0 c_1^{(1)} - D^{(1)} \nabla_{\mathbf{x}} c_0^{(1)} - D^{(1)} \nabla_{\boldsymbol{\xi}} c_1^{(1)} \right) = 0 \quad \text{for } \mathbf{x} \in \Omega, \boldsymbol{\xi} \in \mathcal{B}, \end{aligned} \quad (\text{B5a})$$

$$\begin{aligned} & \frac{\partial c_0^{(2)}}{\partial \tau_1} + \frac{\partial c_1^{(2)}}{\partial \tau_2} + \nabla_{\mathbf{x}} \cdot \left( \text{Pe}^{(s)} \mathbf{u}_0 c_0^{(2)} - D^{(2)} \nabla_{\boldsymbol{\xi}} c_0^{(2)} \right) \\ & + \nabla_{\boldsymbol{\xi}} \cdot \left( \text{Pe}^{(s)} \mathbf{u}_1 c_0^{(2)} + \text{Pe}^{(s)} \mathbf{u}_0 c_1^{(2)} - D^{(2)} \nabla_{\mathbf{x}} c_0^{(2)} - D^{(2)} \nabla_{\boldsymbol{\xi}} c_1^{(2)} \right) = 0 \quad \text{for } \mathbf{x} \in \Omega, \boldsymbol{\xi} \in \mathcal{B}, \end{aligned} \quad (\text{B5b})$$

673 subject to the boundary conditions (i.e., at  $\mathcal{O}(\epsilon^0)$ )

$$-\mathbf{n} \cdot D^{(1)} \left( \nabla_{\mathbf{x}} c_0^{(1)} + \nabla_{\boldsymbol{\xi}} c_1^{(1)} \right) = \text{Da}_{SL}^{(1,s)} c_0^{(1)} - \text{Da}_{SL}^{(2,s)} c_0^{(2)} \quad \text{for } \mathbf{x} \in \Omega, \boldsymbol{\xi} \in \Gamma, \quad (\text{B5c})$$

$$-\mathbf{n} \cdot D^{(2)} \left( \nabla_{\mathbf{x}} c_0^{(2)} + \nabla_{\boldsymbol{\xi}} c_1^{(2)} \right) = \text{Da}_{SL}^{(2,s)} c_0^{(2)} - \text{Da}_{SL}^{(1,s)} c_0^{(1)} \quad \text{for } \mathbf{x} \in \Omega, \boldsymbol{\xi} \in \Gamma. \quad (\text{B5d})$$

674 Again, we apply the averaging operator  $\langle \cdot \rangle_{\mathcal{B}}$  (equation (11)) to equations (B5a)-(B5b), implement the  
 675 divergence theorem, and apply the boundary conditions (equations (B5c)-(B5d)) and no-slip condition  
 676 to the equations. In doing so, we consider  $\mathbf{u}_0$ ,  $\mathbf{u}_1$ , and  $c_1$  as periodic in  $\boldsymbol{\xi}$  to simplify the system to

$$\frac{\partial c_0^{(1)}}{\partial \tau_1} + \frac{\partial \langle c_1^{(1)} \rangle_{\mathcal{B}}}{\partial \tau_2} + \text{Pe}^{(s)} \langle \mathbf{u}_0 \rangle_{\mathcal{B}} \cdot \nabla_{\mathbf{x}} c_0^{(1)} + \frac{|\Gamma|}{|\mathcal{B}|} \left( \text{Da}_{SL}^{(1,s)} c_0^{(1)} - \text{Da}_{SL}^{(2,s)} c_0^{(2)} \right) = 0 \quad \text{for } \mathbf{x} \in \Omega, \quad (\text{B6a})$$

$$\frac{\partial c_0^{(2)}}{\partial \tau_1} + \frac{\partial \langle c_1^{(2)} \rangle_{\mathcal{B}}}{\partial \tau_2} + \text{Pe}^{(s)} \langle \mathbf{u}_0 \rangle_{\mathcal{B}} \cdot \nabla_{\mathbf{x}} c_0^{(2)} + \frac{|\Gamma|}{|\mathcal{B}|} \left( \text{Da}_{SL}^{(2,s)} c_0^{(2)} - \text{Da}_{SL}^{(1,s)} c_0^{(1)} \right) = 0 \quad \text{for } \mathbf{x} \in \Omega. \quad (\text{B6b})$$

677 Similar to before, system (B6) describes how the zeroth and averaged first order concentrations vary with  
 678 fast time variables  $\tau_1(t)$  and  $\tau_2(t)$ , respectively. It is worth noting that a steady state can exist (i.e., when  
 679  $\partial c_0^{(i)}/\partial \tau_1 = 0$  and  $\partial \langle c_1^{(i)} \rangle_{\mathcal{B}}/\partial \tau_2 = 0$  for  $i \in \{1, 2\}$ ), but is not required for all times, as implied by equa-  
 680 tion (30) in the work of Bourbatache *et al.* (Bourbatache et al., 2020). This difference is a result of con-  
 681 sidering additional time scales in the derivation.

682 Returning to equation (B2), we apply the averaging operator  $\langle \cdot \rangle_{\mathcal{B}}$  and the divergence theorem to  
 683 the  $\mathcal{O}(\epsilon^0)$  terms, and assume  $\mathbf{u}_1$  is periodic in  $\boldsymbol{\xi}$  with the no-slip condition to conclude that  $\nabla_{\mathbf{x}} \cdot \mathbf{u}_0 =$   
 684  $0$ . Ultimately, this lead to  $\nabla_{\boldsymbol{\xi}} \cdot \mathbf{u}_1 = 0$  as well. Then, we subtract equation (B6a) from equation (B5a),  
 685 and equation (B6b) from equation (B5b) to gain

$$\begin{aligned} \frac{\partial c_1^{(1)}}{\partial \tau_2} - \frac{\partial \langle c_1^{(1)} \rangle_{\mathcal{B}}}{\partial \tau_2} + \text{Pe}^{(s)} (\mathbf{u}_0 - \langle \mathbf{u}_0 \rangle_{\mathcal{B}}) \cdot \nabla_{\mathbf{x}} c_0^{(1)} - \frac{|\Gamma|}{|\mathcal{B}|} \left( \text{Da}_{SL}^{(1,s)} c_0^{(1)} - \text{Da}_{SL}^{(2,s)} c_0^{(2)} \right) \\ + \text{Pe}^{(s)} \mathbf{u}_0 \cdot \nabla_{\boldsymbol{\xi}} c_1^{(1)} - \nabla_{\boldsymbol{\xi}} \cdot \left( D^{(1)} \nabla_{\mathbf{x}} c_0^{(1)} + D^{(1)} \nabla_{\boldsymbol{\xi}} c_1^{(1)} \right) = 0 \quad \text{for } \mathbf{x} \in \Omega, \boldsymbol{\xi} \in \mathcal{B}, \end{aligned} \quad (\text{B7a})$$

$$\begin{aligned} \frac{\partial c_1^{(2)}}{\partial \tau_2} - \frac{\partial \langle c_1^{(2)} \rangle_{\mathcal{B}}}{\partial \tau_2} + \text{Pe}^{(s)} (\mathbf{u}_0 - \langle \mathbf{u}_0 \rangle_{\mathcal{B}}) \cdot \nabla_{\mathbf{x}} c_0^{(2)} - \frac{|\Gamma|}{|\mathcal{B}|} \left( \text{Da}_{SL}^{(2,s)} c_0^{(2)} - \text{Da}_{SL}^{(1,s)} c_0^{(1)} \right) \\ + \text{Pe}^{(s)} \mathbf{u}_0 \cdot \nabla_{\boldsymbol{\xi}} c_1^{(2)} - \nabla_{\boldsymbol{\xi}} \cdot \left( D^{(2)} \nabla_{\mathbf{x}} c_0^{(2)} + D^{(2)} \nabla_{\boldsymbol{\xi}} c_1^{(2)} \right) = 0 \quad \text{for } \mathbf{x} \in \Omega, \boldsymbol{\xi} \in \mathcal{B}, \end{aligned} \quad (\text{B7b})$$

686 subject to the boundary conditions in equations (B5c)-(B5d). Due to the linearity of the system, we again  
 687 assume solutions of the form  $c_1^{(i)} = c_1^{(i)[1]} + c_1^{(i)[2]}$ , for  $i \in \{1, 2\}$ , and linearly separate the systems.  
 688 While the separated equations for  $c_1^{(i)[1]}$  and  $c_1^{(i)[2]}$  may be found in Appendix C, we provide the assumed  
 689 solution forms as

$$c_1^{(1)} = \boldsymbol{\chi}^{(1)[1]} \cdot \nabla_{\mathbf{x}} c_0^{(1)} + \left( \text{Da}_{SL}^{(1,s)} c_0^{(1)} - \text{Da}_{SL}^{(2,s)} c_0^{(2)} \right) \boldsymbol{\chi}^{(1)[2]} + \bar{c}_1^{(1)}, \quad (\text{B8a})$$

$$c_1^{(2)} = \boldsymbol{\chi}^{(2)[1]} \cdot \nabla_{\mathbf{x}} c_0^{(2)} + \left( \text{Da}_{SL}^{(2,s)} c_0^{(2)} - \text{Da}_{SL}^{(1,s)} c_0^{(1)} \right) \boldsymbol{\chi}^{(2)[2]} + \bar{c}_1^{(2)}, \quad (\text{B8b})$$

690 and the closure problems for the four closure variables as

$$\text{Pe}^{(s)} (\mathbf{u}_0 - \langle \mathbf{u}_0 \rangle_{\mathcal{B}}) + \text{Pe}^{(s)} \mathbf{u}_0 \cdot \nabla_{\boldsymbol{\xi}} \boldsymbol{\chi}^{(i)[1]} - D^{(i)} \nabla_{\boldsymbol{\xi}} \cdot \left( \mathbf{I} + \nabla_{\boldsymbol{\xi}} \boldsymbol{\chi}^{(i)[1]} \right) = \mathbf{0} \quad \text{for } \boldsymbol{\xi} \in \mathcal{B}, \quad (\text{B9a})$$

691 subject to

$$-\mathbf{n} \cdot D^{(i)} \left( \mathbf{I} + \nabla_{\boldsymbol{\xi}} \boldsymbol{\chi}^{(i)[1]} \right) = \mathbf{0} \quad \text{for } \boldsymbol{\xi} \in \Gamma, \quad (\text{B9b})$$

692 and

$$-\frac{|\Gamma|}{|\mathcal{B}|} + \text{Pe}^{(s)} \mathbf{u}_0 \cdot \nabla_{\boldsymbol{\xi}} \boldsymbol{\chi}^{(i)[2]} - D^{(i)} \nabla_{\boldsymbol{\xi}}^2 \boldsymbol{\chi}^{(i)[2]} = 0 \quad \text{for } \boldsymbol{\xi} \in \mathcal{B}, \quad (\text{B10a})$$

693 subject to

$$-\mathbf{n} \cdot D^{(i)} \nabla_{\boldsymbol{\xi}} \boldsymbol{\chi}^{(i)[2]} = 1 \quad \text{for } \boldsymbol{\xi} \in \Gamma. \quad (\text{B10b})$$

Finally, we collect terms of  $\mathcal{O}(\epsilon^0)$  from system (B1) to write

$$\begin{aligned} \frac{\partial c_0^{(1)}}{\partial t} + \frac{\partial c_1^{(1)}}{\partial \tau_1} + \frac{\partial c_2^{(1)}}{\partial \tau_2} + \nabla_{\mathbf{x}} \cdot \left( \text{Pe}^{(s)} \mathbf{u}_1 c_0^{(1)} + \text{Pe}^{(s)} \mathbf{u}_0 c_1^{(1)} - D^{(1)} \nabla_{\mathbf{x}} c_0^{(1)} - D^{(1)} \nabla_{\boldsymbol{\xi}} c_1^{(1)} \right) \\ + \nabla_{\boldsymbol{\xi}} \cdot \left( \text{Pe}^{(s)} \mathbf{u}_2 c_0^{(1)} + \text{Pe}^{(s)} \mathbf{u}_1 c_1^{(1)} + \text{Pe}^{(s)} \mathbf{u}_0 c_2^{(1)} - D^{(1)} \nabla_{\mathbf{x}} c_1^{(1)} - D^{(1)} \nabla_{\boldsymbol{\xi}} c_2^{(1)} \right) \\ = 0 \quad \text{for } \mathbf{x} \in \Omega, \boldsymbol{\xi} \in \mathcal{B}, \end{aligned} \quad (\text{B11a})$$

$$\begin{aligned} \frac{\partial c_0^{(2)}}{\partial t} + \frac{\partial c_1^{(2)}}{\partial \tau_1} + \frac{\partial c_2^{(2)}}{\partial \tau_2} + \nabla_{\mathbf{x}} \cdot \left( \text{Pe}^{(s)} \mathbf{u}_1 c_0^{(2)} + \text{Pe}^{(s)} \mathbf{u}_0 c_1^{(2)} - D^{(2)} \nabla_{\mathbf{x}} c_0^{(2)} - D^{(2)} \nabla_{\boldsymbol{\xi}} c_1^{(2)} \right) \\ + \nabla_{\boldsymbol{\xi}} \cdot \left( \text{Pe}^{(s)} \mathbf{u}_2 c_0^{(2)} + \text{Pe}^{(s)} \mathbf{u}_1 c_1^{(2)} + \text{Pe}^{(s)} \mathbf{u}_0 c_2^{(2)} - D^{(2)} \nabla_{\mathbf{x}} c_1^{(2)} - D^{(2)} \nabla_{\boldsymbol{\xi}} c_2^{(2)} \right) \\ = 0 \quad \text{for } \mathbf{x} \in \Omega, \boldsymbol{\xi} \in \mathcal{B}, \end{aligned} \quad (\text{B11b})$$

subject to the boundary conditions (i.e., at  $\mathcal{O}(\epsilon)$ )

$$-\mathbf{n} \cdot D^{(1)} \left( \nabla_{\mathbf{x}} c_1^{(1)} + \nabla_{\boldsymbol{\xi}} c_2^{(1)} \right) = \text{Da}_{SL}^{(1,s)} c_1^{(1)} - \text{Da}_{SL}^{(2,s)} c_1^{(2)} \quad \text{for } \mathbf{x} \in \Omega, \boldsymbol{\xi} \in \Gamma, \quad (\text{B11c})$$

$$-\mathbf{n} \cdot D^{(2)} \left( \nabla_{\mathbf{x}} c_1^{(2)} + \nabla_{\boldsymbol{\xi}} c_2^{(2)} \right) = \text{Da}_{SL}^{(2,s)} c_1^{(2)} - \text{Da}_{SL}^{(1,s)} c_1^{(1)} \quad \text{for } \mathbf{x} \in \Omega, \boldsymbol{\xi} \in \Gamma. \quad (\text{B11d})$$

After substituting in the solutions for  $c_1^{(i)}$  (system (B8)), we again apply the averaging operator  $\langle \cdot \rangle_{\mathcal{B}}$  (equation (11)) to equations (B11a)-(B11b), and implement the divergence theorem to incorporate the boundary conditions (equations (B11c)-(B11d)) and the no-slip condition. Further simplifications regarding the periodicity of the dependent variables in  $\boldsymbol{\xi}$  are also made to write

$$\begin{aligned} \frac{\partial c_0^{(1)}}{\partial t} + \frac{\partial \bar{c}_1^{(1)}}{\partial \tau_1} + \frac{\partial \langle c_2^{(1)} \rangle_{\mathcal{B}}}{\partial \tau_2} + \left[ \text{Pe}^{(s)} \left( \langle \mathbf{u}_1 \rangle_{\mathcal{B}} + \text{Da}_{SL}^{(1,s)} \langle \mathbf{u}_0 \chi^{(1)[2]} \rangle_{\mathcal{B}} \right) \right. \\ \left. + \text{Da}_{SL}^{(1,s)} \frac{|\Gamma|}{|\mathcal{B}|} \langle \chi^{(1)[1]} \rangle_{\Gamma} - \text{Da}_{SL}^{(1,s)} D^{(1)} \langle \nabla_{\boldsymbol{\xi}} \chi^{(1)[2]} \rangle_{\mathcal{B}} \right] \cdot \nabla_{\mathbf{x}} c_0^{(1)} + \text{Pe}^{(s)} \langle \mathbf{u}_0 \rangle_{\mathcal{B}} \cdot \nabla_{\mathbf{x}} \bar{c}_1^{(1)} \\ - \text{Da}_{SL}^{(2,s)} \left[ \frac{|\Gamma|}{|\mathcal{B}|} \langle \chi^{(2)[1]} \rangle_{\Gamma} - D^{(1)} \langle \nabla_{\boldsymbol{\xi}} \chi^{(1)[2]} \rangle_{\mathcal{B}} + \text{Pe}^{(s)} \langle \mathbf{u}_0 \chi^{(1)[2]} \rangle_{\mathcal{B}} \right] \cdot \nabla_{\mathbf{x}} c_0^{(2)} \\ - \nabla_{\mathbf{x}} \cdot \left[ \left( D^{(1)} \mathbf{I} + D^{(1)} \langle \nabla_{\boldsymbol{\xi}} \chi^{(1)[1]} \rangle_{\mathcal{B}} - \text{Pe}^{(s)} \langle \mathbf{u}_0 \otimes \chi^{(1)[1]} \rangle_{\mathcal{B}} \right) \cdot \nabla_{\mathbf{x}} c_0^{(1)} \right] \\ + \text{Da}_{SL}^{(1,s)} \frac{|\Gamma|}{|\mathcal{B}|} \left[ \text{Da}_{SL}^{(1,s)} \langle \chi^{(1)[2]} \rangle_{\Gamma} + \text{Da}_{SL}^{(2,s)} \langle \chi^{(2)[2]} \rangle_{\Gamma} \right] c_0^{(1)} \\ - \text{Da}_{SL}^{(2,s)} \frac{|\Gamma|}{|\mathcal{B}|} \left[ \text{Da}_{SL}^{(1,s)} \langle \chi^{(1)[2]} \rangle_{\Gamma} + \text{Da}_{SL}^{(2,s)} \langle \chi^{(2)[2]} \rangle_{\Gamma} \right] c_0^{(2)} \\ + \text{Da}_{SL}^{(1,s)} \frac{|\Gamma|}{|\mathcal{B}|} \bar{c}_1^{(1)} - \text{Da}_{SL}^{(2,s)} \frac{|\Gamma|}{|\mathcal{B}|} \bar{c}_1^{(2)} = 0 \quad \text{for } \mathbf{x} \in \Omega, \end{aligned} \quad (\text{B12a})$$

$$\begin{aligned}
& \frac{\partial c_0^{(2)}}{\partial t} + \frac{\partial \bar{c}_1^{(2)}}{\partial \tau_1} + \frac{\partial \langle c_2^{(2)} \rangle_{\mathcal{B}}}{\partial \tau_2} + \left[ \text{Pe}^{(s)} \left( \langle \mathbf{u}_1 \rangle_{\mathcal{B}} + \text{Da}_{SL}^{(2,s)} \langle \mathbf{u}_0 \chi^{(2)[2]} \rangle_{\mathcal{B}} \right) \right. \\
& + \text{Da}_{SL}^{(2,s)} \frac{|\Gamma|}{|\mathcal{B}|} \langle \chi^{(2)[1]} \rangle_{\Gamma} - \text{Da}_{SL}^{(2,s)} D^{(2)} \langle \nabla_{\xi} \chi^{(2)[2]} \rangle_{\mathcal{B}} \left. \right] \cdot \nabla_{\mathbf{x}} c_0^{(2)} + \text{Pe}^{(s)} \langle \mathbf{u}_0 \rangle_{\mathcal{B}} \cdot \nabla_{\mathbf{x}} \bar{c}_1^{(2)} \\
& - \text{Da}_{SL}^{(1,s)} \left[ \frac{|\Gamma|}{|\mathcal{B}|} \langle \chi^{(1)[1]} \rangle_{\Gamma} - D^{(2)} \langle \nabla_{\xi} \chi^{(2)[2]} \rangle_{\mathcal{B}} + \text{Pe}^{(s)} \langle \mathbf{u}_0 \chi^{(2)[2]} \rangle_{\mathcal{B}} \right] \cdot \nabla_{\mathbf{x}} c_0^{(1)} \\
& - \nabla_{\mathbf{x}} \cdot \left[ \left( D^{(2)} \mathbf{I} + D^{(2)} \langle \nabla_{\xi} \chi^{(2)[1]} \rangle_{\mathcal{B}} - \text{Pe}^{(s)} \langle \mathbf{u}_0 \otimes \chi^{(2)[1]} \rangle_{\mathcal{B}} \right) \cdot \nabla_{\mathbf{x}} c_0^{(2)} \right] \\
& + \text{Da}_{SL}^{(2,s)} \frac{|\Gamma|}{|\mathcal{B}|} \left[ \text{Da}_{SL}^{(2,s)} \langle \chi^{(2)[2]} \rangle_{\Gamma} + \text{Da}_{SL}^{(1,s)} \langle \chi^{(1)[2]} \rangle_{\Gamma} \right] c_0^{(2)} \\
& - \text{Da}_{SL}^{(1,s)} \frac{|\Gamma|}{|\mathcal{B}|} \left[ \text{Da}_{SL}^{(2,s)} \langle \chi^{(2)[2]} \rangle_{\Gamma} + \text{Da}_{SL}^{(1,s)} \langle \chi^{(1)[2]} \rangle_{\Gamma} \right] c_0^{(1)} \\
& + \text{Da}_{SL}^{(2,s)} \frac{|\Gamma|}{|\mathcal{B}|} \bar{c}_1^{(2)} - \text{Da}_{SL}^{(1,s)} \frac{|\Gamma|}{|\mathcal{B}|} \bar{c}_1^{(1)} = 0 \quad \text{for } \mathbf{x} \in \Omega.
\end{aligned} \tag{B12b}$$

701 We now add equations (B4a), (B6a), and (B12a) together, and equations (B4b), (B6b), and (B12b) to-  
702 gether. Upon making the substitutions  $\text{Pe}^{(s)} = \text{Pe}\epsilon$ ,  $\text{Da}_{SL}^{(1,s)} = \text{Da}_{SL}^{(1)}$ , and  $\text{Da}_{SL}^{(2,s)} = \text{Da}_{SL}^{(2)}$ , we obtain

$$\begin{aligned}
& \epsilon^{-2} \frac{\partial c_0^{(1)}}{\partial \tau_2} + \epsilon^{-1} \left( \frac{\partial c_0^{(1)}}{\partial \tau_1} + \frac{\partial \bar{c}_1^{(1)}}{\partial \tau_2} \right) + \frac{\partial c_0^{(1)}}{\partial t} + \frac{\partial \bar{c}_1^{(1)}}{\partial \tau_1} + \frac{\partial \langle c_2^{(1)} \rangle_{\mathcal{B}}}{\partial \tau_2} \\
& + \text{Pe} \left[ \langle \mathbf{u}_0 \rangle_{\mathcal{B}} \cdot \nabla_{\mathbf{x}} c_0^{(1)} + \epsilon \left( \langle \mathbf{u}_1 \rangle_{\mathcal{B}} \cdot \nabla_{\mathbf{x}} c_0^{(1)} + \langle \mathbf{u}_0 \rangle_{\mathcal{B}} \cdot \nabla_{\mathbf{x}} \bar{c}_1^{(1)} \right) \right] \\
& + \text{Da}_{SL}^{(1)} \left[ \frac{|\Gamma|}{|\mathcal{B}|} \langle \chi^{(1)[1]} \rangle_{\Gamma} - D^{(1)} \langle \nabla_{\xi} \chi^{(1)[2]} \rangle_{\mathcal{B}} + \text{Pe}\epsilon \langle \mathbf{u}_0 \chi^{(1)[2]} \rangle_{\mathcal{B}} \right] \cdot \nabla_{\mathbf{x}} c_0^{(1)} \\
& - \text{Da}_{SL}^{(2)} \left[ \frac{|\Gamma|}{|\mathcal{B}|} \langle \chi^{(2)[1]} \rangle_{\Gamma} - D^{(1)} \langle \nabla_{\xi} \chi^{(1)[2]} \rangle_{\mathcal{B}} + \text{Pe}\epsilon \langle \mathbf{u}_0 \chi^{(1)[2]} \rangle_{\mathcal{B}} \right] \cdot \nabla_{\mathbf{x}} c_0^{(2)} \\
& - \nabla_{\mathbf{x}} \cdot \left[ \left( D^{(1)} \mathbf{I} + D^{(1)} \langle \nabla_{\xi} \chi^{(1)[1]} \rangle_{\mathcal{B}} - \text{Pe}\epsilon \langle \mathbf{u}_0 \otimes \chi^{(1)[1]} \rangle_{\mathcal{B}} \right) \cdot \nabla_{\mathbf{x}} c_0^{(1)} \right] \\
& + \text{Da}_{SL}^{(1)} \frac{|\Gamma|}{|\mathcal{B}|} \left[ \text{Da}_{SL}^{(1)} \langle \chi^{(1)[2]} \rangle_{\Gamma} + \text{Da}_{SL}^{(2)} \langle \chi^{(2)[2]} \rangle_{\Gamma} \right] c_0^{(1)} \\
& - \text{Da}_{SL}^{(2)} \frac{|\Gamma|}{|\mathcal{B}|} \left[ \text{Da}_{SL}^{(1)} \langle \chi^{(1)[2]} \rangle_{\Gamma} + \text{Da}_{SL}^{(2)} \langle \chi^{(2)[2]} \rangle_{\Gamma} \right] c_0^{(2)} \\
& + \epsilon^{-1} \text{Da}_{SL}^{(1)} \frac{|\Gamma|}{|\mathcal{B}|} \left[ c_0^{(1)} + \epsilon \bar{c}_1^{(1)} \right] - \epsilon^{-1} \text{Da}_{SL}^{(2)} \frac{|\Gamma|}{|\mathcal{B}|} \left[ c_0^{(2)} + \epsilon \bar{c}_1^{(2)} \right] = 0 \quad \text{for } \mathbf{x} \in \Omega,
\end{aligned} \tag{B13a}$$

$$\begin{aligned}
& \epsilon^{-2} \frac{\partial c_0^{(2)}}{\partial \tau_2} + \epsilon^{-1} \left( \frac{\partial c_0^{(2)}}{\partial \tau_1} + \frac{\partial \bar{c}_1^{(2)}}{\partial \tau_2} \right) + \frac{\partial c_0^{(2)}}{\partial t} + \frac{\partial \bar{c}_1^{(2)}}{\partial \tau_1} + \frac{\partial \langle c_2^{(2)} \rangle_{\mathcal{B}}}{\partial \tau_2} \\
& + \text{Pe} \left[ \langle \mathbf{u}_0 \rangle_{\mathcal{B}} \cdot \nabla_{\mathbf{x}} c_0^{(2)} + \epsilon \left( \langle \mathbf{u}_1 \rangle_{\mathcal{B}} \cdot \nabla_{\mathbf{x}} c_0^{(2)} + \langle \mathbf{u}_0 \rangle_{\mathcal{B}} \cdot \nabla_{\mathbf{x}} \bar{c}_1^{(2)} \right) \right] \\
& + \text{Da}_{SL}^{(2)} \left[ \frac{|\Gamma|}{|\mathcal{B}|} \langle \chi^{(2)[1]} \rangle_{\Gamma} - D^{(2)} \langle \nabla_{\xi} \chi^{(2)[2]} \rangle_{\mathcal{B}} + \text{Pe}\epsilon \langle \mathbf{u}_0 \chi^{(2)[2]} \rangle_{\mathcal{B}} \right] \cdot \nabla_{\mathbf{x}} c_0^{(2)} \\
& - \text{Da}_{SL}^{(1)} \left[ \frac{|\Gamma|}{|\mathcal{B}|} \langle \chi^{(1)[1]} \rangle_{\Gamma} - D^{(2)} \langle \nabla_{\xi} \chi^{(2)[2]} \rangle_{\mathcal{B}} + \text{Pe}\epsilon \langle \mathbf{u}_0 \chi^{(2)[2]} \rangle_{\mathcal{B}} \right] \cdot \nabla_{\mathbf{x}} c_0^{(1)} \\
& - \nabla_{\mathbf{x}} \cdot \left[ \left( D^{(2)} \mathbf{I} + D^{(2)} \langle \nabla_{\xi} \chi^{(2)[1]} \rangle_{\mathcal{B}} - \text{Pe}\epsilon \langle \mathbf{u}_0 \otimes \chi^{(2)[1]} \rangle_{\mathcal{B}} \right) \cdot \nabla_{\mathbf{x}} c_0^{(2)} \right] \\
& + \text{Da}_{SL}^{(2)} \frac{|\Gamma|}{|\mathcal{B}|} \left[ \text{Da}_{SL}^{(2)} \langle \chi^{(2)[2]} \rangle_{\Gamma} + \text{Da}_{SL}^{(1)} \langle \chi^{(1)[2]} \rangle_{\Gamma} \right] c_0^{(2)} \\
& - \text{Da}_{SL}^{(1)} \frac{|\Gamma|}{|\mathcal{B}|} \left[ \text{Da}_{SL}^{(2)} \langle \chi^{(2)[2]} \rangle_{\Gamma} + \text{Da}_{SL}^{(1)} \langle \chi^{(1)[2]} \rangle_{\Gamma} \right] c_0^{(1)} \\
& + \epsilon^{-1} \text{Da}_{SL}^{(2)} \frac{|\Gamma|}{|\mathcal{B}|} \left[ c_0^{(2)} + \epsilon \bar{c}_1^{(2)} \right] - \epsilon^{-1} \text{Da}_{SL}^{(1)} \frac{|\Gamma|}{|\mathcal{B}|} \left[ c_0^{(1)} + \epsilon \bar{c}_1^{(1)} \right] = 0 \quad \text{for } \mathbf{x} \in \Omega.
\end{aligned} \tag{B13b}$$

703 Considering the expansions

$$\frac{\partial \langle c^{(i)} \rangle_{\mathcal{B}}}{\partial t} = \epsilon^{-2} \frac{\partial c_0^{(i)}}{\partial \tau_2} + \epsilon^{-1} \left( \frac{\partial c_0^{(i)}}{\partial \tau_1} + \frac{\partial \bar{c}_1^{(i)}}{\partial \tau_2} \right) + \frac{\partial c_0^{(i)}}{\partial t} + \frac{\partial \bar{c}_1^{(i)}}{\partial \tau_1} + \frac{\partial \langle c_2^{(i)} \rangle_{\mathcal{B}}}{\partial \tau_2} + \mathcal{O}(\epsilon), \quad (\text{B14a})$$

$$\text{Pe} \langle \mathbf{u} \rangle_{\mathcal{B}} \cdot \nabla_{\mathbf{x}} \langle c^{(i)} \rangle_{\mathcal{B}} = \text{Pe} \left[ \langle \mathbf{u}_0 \rangle_{\mathcal{B}} \cdot \nabla_{\mathbf{x}} c_0^{(i)} + \epsilon \left( \langle \mathbf{u}_1 \rangle_{\mathcal{B}} \cdot \nabla_{\mathbf{x}} c_0^{(i)} + \langle \mathbf{u}_0 \rangle_{\mathcal{B}} \cdot \nabla_{\mathbf{x}} \bar{c}_1^{(i)} \right) \right] + \mathcal{O}(\epsilon), \quad (\text{B14b})$$

$$\langle c^{(i)} \rangle_{\mathcal{B}} = c_0^{(i)} + \epsilon \bar{c}_1^{(i)} + \mathcal{O}(\epsilon^2), \quad (\text{B14c})$$

$$\langle \mathbf{u} \rangle_{\mathcal{B}} = \mathbf{u}_0 + \mathcal{O}(\epsilon), \quad (\text{B14d})$$

704 obtained using equations (10), (12), and system (13), for  $i \in \{1, 2\}$ , we can simplify system (B13) to  
 705 write the homogenized system as

$$\begin{aligned} \phi \frac{\partial \langle c^{(1)} \rangle_Y}{\partial t} + \mathbf{U}^{(1)} \cdot \nabla_{\mathbf{x}} \langle c^{(1)} \rangle_Y - \mathbf{V}^{(1)} \cdot \nabla_{\mathbf{x}} \langle c^{(2)} \rangle_Y - \nabla_{\mathbf{x}} \cdot \left( \mathbf{D}^{(1)} \cdot \nabla_{\mathbf{x}} \langle c^{(1)} \rangle_Y \right) \\ = \mathcal{R}^{(2)} \langle c^{(2)} \rangle_Y - \mathcal{R}^{(1)} \langle c^{(1)} \rangle_Y + \mathcal{O}(\epsilon) \quad \text{for } \mathbf{x} \in \Omega, \end{aligned} \quad (\text{B15a})$$

$$\begin{aligned} \phi \frac{\partial \langle c^{(2)} \rangle_Y}{\partial t} + \mathbf{U}^{(2)} \cdot \nabla_{\mathbf{x}} \langle c^{(2)} \rangle_Y - \mathbf{V}^{(2)} \cdot \nabla_{\mathbf{x}} \langle c^{(1)} \rangle_Y - \nabla_{\mathbf{x}} \cdot \left( \mathbf{D}^{(2)} \cdot \nabla_{\mathbf{x}} \langle c^{(2)} \rangle_Y \right) \\ = \mathcal{R}^{(1)} \langle c^{(1)} \rangle_Y - \mathcal{R}^{(2)} \langle c^{(2)} \rangle_Y + \mathcal{O}(\epsilon) \quad \text{for } \mathbf{x} \in \Omega, \end{aligned} \quad (\text{B15b})$$

706 where the effective parameters are defined as

$$\mathbf{U}^{(i)} = \text{Pe} \langle \mathbf{u} \rangle_Y + \text{Da}_{SL}^{(i)} \left[ \phi \frac{|\Gamma|}{|\mathcal{B}|} \langle \chi^{(i)[1]} \rangle_{\Gamma} - D^{(i)} \langle \nabla_{\xi} \chi^{(i)[2]} \rangle_Y + \text{Pe} \epsilon \langle \mathbf{u} \chi^{(i)[2]} \rangle_Y \right], \quad (\text{B15c})$$

$$\mathbf{V}^{(1)} = \text{Da}_{SL}^{(2)} \left[ \phi \frac{|\Gamma|}{|\mathcal{B}|} \langle \chi^{(2)[1]} \rangle_{\Gamma} - D^{(1)} \langle \nabla_{\xi} \chi^{(1)[2]} \rangle_Y + \text{Pe} \epsilon \langle \mathbf{u} \chi^{(1)[2]} \rangle_Y \right], \quad (\text{B15d})$$

$$\mathbf{V}^{(2)} = \text{Da}_{SL}^{(1)} \left[ \phi \frac{|\Gamma|}{|\mathcal{B}|} \langle \chi^{(1)[1]} \rangle_{\Gamma} - D^{(2)} \langle \nabla_{\xi} \chi^{(2)[2]} \rangle_Y + \text{Pe} \epsilon \langle \mathbf{u} \chi^{(2)[2]} \rangle_Y \right], \quad (\text{B15e})$$

$$\mathbf{D}^{(i)} = \phi D^{(i)} \mathbf{I} + D^{(i)} \langle \nabla_{\xi} \chi^{(i)[1]} \rangle_Y - \text{Pe} \epsilon \langle \mathbf{u} \otimes \chi^{(i)[1]} \rangle_Y, \quad (\text{B15f})$$

$$\mathcal{R}^{(i)} = \text{Da}_{SL}^{(i)} \mathcal{R}, \quad (\text{B15g})$$

$$\mathcal{R} = \phi \frac{|\Gamma|}{|\mathcal{B}|} \left[ \epsilon^{-1} + \text{Da}_{SL}^{(1)} \langle \chi^{(1)[2]} \rangle_{\Gamma} + \text{Da}_{SL}^{(2)} \langle \chi^{(2)[2]} \rangle_{\Gamma} \right], \quad (\text{B15h})$$

707 for  $i \in \{1, 2\}$ . We note that  $\text{Da}_{SL}^{(1)}$  and  $\text{Da}_{SL}^{(2)}$  are left in the homogenized model, but are required to be  
 708 of order  $\mathcal{O}(\epsilon^0)$ . As shown, we successfully homogenized the system for moderate reaction rates using the  
 709 generalized closure form strategy.

## 710 **Appendix C Linearly Separated Systems for $\mathbf{c}_1^{(i)[1]}$ and $\mathbf{c}_1^{(i)[2]}$**

711 In this Appendix, we provide the linearly separated systems from the first order system of differ-  
 712 ential equations (system (B7)) in the second problem.

### C1 Linearly Separated System for $c_1^{(1)[1]}$

$$\begin{aligned} \frac{\partial c_1^{(1)[1]}}{\partial \tau_2} - \frac{\partial \langle c_1^{(1)[1]} \rangle_{\mathcal{B}}}{\partial \tau_2} + \text{Pe}^{(s)} (\mathbf{u}_0 - \langle \mathbf{u}_0 \rangle_{\mathcal{B}}) \cdot \nabla_{\mathbf{x}} c_0^{(1)} + \text{Pe}^{(s)} \mathbf{u}_0 \cdot \nabla_{\mathbf{x}} c_1^{(1)[1]} \\ - \nabla_{\boldsymbol{\xi}} \cdot \left( D^{(1)} \nabla_{\mathbf{x}} c_0^{(1)} + D^{(1)} \nabla_{\boldsymbol{\xi}} c_1^{(1)[1]} \right) = 0 \quad \text{for } \mathbf{x} \in \Omega, \boldsymbol{\xi} \in \mathcal{B}, \end{aligned} \quad (\text{C1})$$

$$-\mathbf{n} \cdot D^{(1)} \left( \nabla_{\mathbf{x}} c_0^{(1)} + \nabla_{\boldsymbol{\xi}} c_1^{(1)[1]} \right) = 0 \quad \text{for } \mathbf{x} \in \Omega, \boldsymbol{\xi} \in \Gamma, \quad (\text{C2})$$

### C2 Linearly Separated System for $c_1^{(1)[2]}$

$$\begin{aligned} \frac{\partial c_1^{(1)[2]}}{\partial \tau_2} - \frac{\partial \langle c_1^{(1)[2]} \rangle_{\mathcal{B}}}{\partial \tau_2} - \frac{|\Gamma|}{|\mathcal{B}|} \left( \text{Da}_{SL}^{(1,s)} c_0^{(1)} - \text{Da}_{SL}^{(2,s)} c_0^{(2)} \right) + \text{Pe}^{(s)} \mathbf{u}_0 \cdot \nabla_{\mathbf{x}} c_1^{(1)[2]} \\ - \nabla_{\boldsymbol{\xi}} \cdot \left( D^{(1)} \nabla_{\boldsymbol{\xi}} c_1^{(1)[2]} \right) = 0 \quad \text{for } \mathbf{x} \in \Omega, \boldsymbol{\xi} \in \mathcal{B}, \end{aligned} \quad (\text{C3})$$

$$-\mathbf{n} \cdot D^{(1)} \nabla_{\boldsymbol{\xi}} c_1^{(1)[2]} = \text{Da}_{SL}^{(1,s)} c_0^{(1)} - \text{Da}_{SL}^{(2,s)} c_0^{(2)} \quad \text{for } \mathbf{x} \in \Omega, \boldsymbol{\xi} \in \Gamma, \quad (\text{C4})$$

### C3 Linearly Separated System for $c_1^{(2)[1]}$

$$\begin{aligned} \frac{\partial c_1^{(2)[1]}}{\partial \tau_2} - \frac{\partial \langle c_1^{(2)[1]} \rangle_{\mathcal{B}}}{\partial \tau_2} + \text{Pe}^{(s)} (\mathbf{u}_0 - \langle \mathbf{u}_0 \rangle_{\mathcal{B}}) \cdot \nabla_{\mathbf{x}} c_0^{(2)} + \text{Pe}^{(s)} \mathbf{u}_0 \cdot \nabla_{\mathbf{x}} c_1^{(2)[1]} \\ - \nabla_{\boldsymbol{\xi}} \cdot \left( D^{(2)} \nabla_{\mathbf{x}} c_0^{(2)} + D^{(2)} \nabla_{\boldsymbol{\xi}} c_1^{(2)[1]} \right) = 0 \quad \text{for } \mathbf{x} \in \Omega, \boldsymbol{\xi} \in \mathcal{B}, \end{aligned} \quad (\text{C5})$$

$$-\mathbf{n} \cdot D^{(2)} \left( \nabla_{\mathbf{x}} c_0^{(2)} + \nabla_{\boldsymbol{\xi}} c_1^{(2)[1]} \right) = 0 \quad \text{for } \mathbf{x} \in \Omega, \boldsymbol{\xi} \in \Gamma, \quad (\text{C6})$$

### C4 Linearly Separated System for $c_1^{(2)[2]}$

$$\begin{aligned} \frac{\partial c_1^{(2)[2]}}{\partial \tau_2} - \frac{\partial \langle c_1^{(2)[2]} \rangle_{\mathcal{B}}}{\partial \tau_2} - \frac{|\Gamma|}{|\mathcal{B}|} \left( \text{Da}_{SL}^{(2,s)} c_0^{(2)} - \text{Da}_{SL}^{(1,s)} c_0^{(1)} \right) + \text{Pe}^{(s)} \mathbf{u}_0 \cdot \nabla_{\mathbf{x}} c_1^{(2)[2]} \\ - \nabla_{\boldsymbol{\xi}} \cdot \left( D^{(2)} \nabla_{\boldsymbol{\xi}} c_1^{(2)[2]} \right) = 0 \quad \text{for } \mathbf{x} \in \Omega, \boldsymbol{\xi} \in \mathcal{B}, \end{aligned} \quad (\text{C7})$$

$$-\mathbf{n} \cdot D^{(2)} \nabla_{\boldsymbol{\xi}} c_1^{(2)[2]} = \text{Da}_{SL}^{(2,s)} c_0^{(2)} - \text{Da}_{SL}^{(1,s)} c_0^{(1)} \quad \text{for } \mathbf{x} \in \Omega, \boldsymbol{\xi} \in \Gamma. \quad (\text{C8})$$

- 718 Ahmed, E. N., Bottaro, A., & Tanda, G. (2022). A homogenization approach for buoyancy-induced  
719 flows over micro-textured vertical surfaces. *J. Fluid Mech.*, *941*, A53. doi: 10.1017/jfm.2022  
720 .320
- 721 Allaire, G., Brizzi, R., Mikelić, A., & Piatnitski, A. (2010). Two-scale expansion with drift approach  
722 to the Taylor dispersion for reactive transport through porous media. *Chem. Eng. Sci.*, *65*,  
723 2292-2300.
- 724 Allaire, G., Mikelić, A., & Piatnitski, A. (2010). Homogenization approach to the dispersion theory  
725 for reactive transport through porous media. *SIAM J. Math. Anal.*, *42*, 125-144.
- 726 Allaire, G., & Raphael, A.-L. (2007). Homogenization of a convection-diffusion model with reaction  
727 in a porous medium. *C. R. Acad. Sci. Paris*, *344*, 523-528.
- 728 Alnaes, M., Blechta, J., Hake, J., Johansson, A., Kehlet, B., Logg, A., ... Wells, G. (2015). The fen-  
729 ics project version 1.5. *Archive of Numerical Software*, *3*.
- 730 Arunachalam, H., Onori, S., & Battiato, I. (2015). On veracity of macroscopic lithium-ion battery  
731 models. *J. Electrochem. Soc.*, *162*, A1940-A1951.
- 732 Auriault, J.-L., & Adler, P. (1995). Taylor dispersion in porous media: Analysis by multiple scale ex-  
733 pansions. *Adv. Water Resour.*, *18*, 217-226.
- 734 Bachmat, Y., & Bear, J. (1986). Macroscopic modeling of transport phenomena in porous media. 1:  
735 The continuum approach. *Transp. Porous Media*, *1*, 213-240.
- 736 Battiato, I., Ferrero V, P. T., O'Malley, D., Miller, C. T., Takhar, P. S., Valdés-Parada, F. J., &  
737 Wood, B. D. (2019). Theory and applications of macroscale models in porous media. *Transp.*  
738 *Porous Media*, *130*, 5-76.
- 739 Battiato, I., & Tartakovsky, D. (2011). Applicability regimes for macroscopic models of reactive  
740 transport in porous media. *J. Contam. Hydrol.*, *120-121*, 18-26.
- 741 Battiato, I., Tartakovsky, D. M., Tartakovsky, A. M., & Scheibe, T. (2009). On breakdown of macro-  
742 scopic models of mixing-controlled heterogeneous reactions in porous media. *Adv. Water Re-*  
743 *sour.*, *32*, 1664-1673.
- 744 Battiato, I., Tartakovsky, D. M., Tartakovsky, A. M., & Scheibe, T. D. (2011). Hybrid models of re-  
745 active transport in porous and fractured media. *Adv. Water Resour.*, *34*, 1140-1150.
- 746 Becker, B., Guo, B., Buntic, I., Flemisch, B., & Helmig, R. (2022). An adaptive hybrid vertical  
747 equilibrium/full-dimensional model for compositional multiphase flow. *Water Resour. Res.*,  
748 *58*(1). doi: e2021WR030990
- 749 Berkowitz, B., Cortis, A., Dentz, M., & Scher, H. (2006). Modeling non-fickian transport in geologi-  
750 cal formations as a continuous time random walk. *Rev. Geophys.*, *44*(2). doi: [https://doi.org/](https://doi.org/10.1029/2005RG000178)  
751 [10.1029/2005RG000178](https://doi.org/10.1029/2005RG000178)
- 752 Bloch, J.-F., & Auriault, J.-L. (2019). Upscaling of diffusion–reaction phenomena by homogenisation  
753 technique: Possible appearance of morphogenesis. *Transp. Porous Media*, *127*, 191-209.
- 754 Boso, F., & Battiato, I. (2013). Homogenizability conditions for multicomponent reactive transport.  
755 *Adv. Water Resour.*, *62*, 254-265.
- 756 Bourbatache, M. K., Le, T.-D., Millet, O., & Moyne, C. (2021). Limits of classical homogeniza-  
757 tion procedure for coupled diffusion-heterogeneous reaction processes in porous media. *Transp.*  
758 *Porous Media*, *140*, 437-457.
- 759 Bourbatache, M. K., Millet, O., & Moyne, C. (2020). Upscaling diffusion-reaction in porous media.  
760 *Acta Mech.*, *231*, 2011-2031.
- 761 Cushman, J. H., & Ginn, T. R. (1993). Nonlocal dispersion in media with continuously evolving  
762 scales of heterogeneity. *Transp. Porous Media*, *13*(1), 123–138.
- 763 Diffusion in random media. (1995). In J. Keller, D. McLaughlin, & G. Papanicolaou (Eds.), *Surveys*  
764 *in applied mathematics* (p. 205-253). Springer.
- 765 Donato, P., & Piatnitski, A. (2005). Averaging of nonstationary parabolic operators with large lower  
766 order terms. *Math. Sci. Appl.*, *24*, 153-165.
- 767 Garnier, J. (1997). Homogenization in a periodic and time-dependent potential. *SIAM J. Appl.*  
768 *Math.*, *57*, 95-111.
- 769 Gelhar, L. W., & Axness, C. L. (1983). Three-dimensional stochastic analysis of macrodispersion in  
770 aquifers. *Water Resour. Res.*, *19*(1), 161-180. doi: <https://doi.org/10.1029/WR019i001p00161>
- 771 Golfier, F., Wood, B., Orgogozo, L., Quintard, M., & Buès, M. (2009). Biofilms in porous media:  
772 Development of macroscopic transport equations via volume averaging with closure for local  
773 mass equilibrium conditions. *Adv. Water Resour.*, *32*, 463-485.
- 774 Gray, W. G., & Miller, C. T. (2014). *Introduction to the thermodynamically constrained averaging*  
775 *theory for porous medium systems*. Switzerland: Springer.

- 776 Haggerty, R., McKenna, S. A., & Meigs, L. C. (2000). On the late-time behavior of tracer test  
777 breakthrough curves. *Water Resour. Res.*, *36*(12), 3467-3479. doi: [https://doi.org/10.1029/](https://doi.org/10.1029/2000WR900214)  
778 2000WR900214
- 779 Hormung, U. (1997). *Homogenization and porous media*. New York: Springer.
- 780 Iliev, O., Mikelić, A., Prill, T., & Sherly, A. (2020). Homogenization approach to the upscaling of a  
781 reactive flow through particulate filters with wall integrated catalyst. *Adv. Water Resour.*, *146*.  
782 doi: 103779
- 783 Le, T.-D., Moyne, C., Bourbatache, K., & Millet, O. (2022). A spectral approach for homogenization  
784 of diffusion and heterogeneous reaction in porous media. *Appl. Math Model.*, *104*, 666-681.
- 785 Lewandowska, J., Auriault, J.-L., Empereur, S., & Royer, P. (2002). Solute diffusion in fractured  
786 porous media with memory effects due to adsorption. *C. R. Mecanique*, *330*, 879-884.
- 787 Logg, A., Mardal, K.-A., & Wells, G. (2012). *Automated solution of differential equations by the fi-*  
788 *nite element method*. Springer.
- 789 Lubbers, N., Agarwal, A., Chen, Y., Son, S., Mehana, M., Kang, Q., . . . Viswanathan, H. S. (2020).  
790 Modeling and scale-bridging using machine learning: Nanoconfinement effects in porous media.  
791 *Sci. Rep.*, *10*. doi: 13312
- 792 Marušić-Paloka, E., & Piatnitski, A. (2005). Homogenization of a nonlinear convection-diffusion  
793 equation with rapidly oscillating coefficients and strong convection. *J. London Math. Soc.*, *2*,  
794 391-409.
- 795 Mauri, R. (1991). Dispersion, convection, and reaction in porous media. *Phys. Fluids A*, *3*, 743-756.
- 796 Mehmani, Y., Anderson, T., Wang, Y., Aryana, S. A., Battiato, I., Tchelepi, H. A., & Kovscek,  
797 A. R. (2021). Striving to translate shale physics across ten orders of magnitude: What have we  
798 learned? *Earth Sci. Rev.*, *223*. doi: 103848
- 799 Mehmani, Y., Castelletto, N., & Tchelepi, H. A. (2021). Multiscale formulation of frictional contact  
800 mechanics at the pore scale. *J. Comput. Phys.*, *430*. doi: 110092
- 801 Mei, C. (1992). Method of homogenization applied to dispersion in porous media. *Transp. Porous*  
802 *Media*, *9*, 261-274.
- 803 Mikelić, A., Devigne, V., & Van Duijn, C. (2006). Rigorous upscaling of the reactive flow through a  
804 pore, under dominant pecelet and damkohler numbers. *SIAM J. Math. Anal.*, *38*.
- 805 Miller, C., Valdés-Parada, F., Ostvar, S., & Wood, B. (2018). A priori parameter estimation for  
806 the thermodynamically constrained averaging theory species transport in a saturated porous  
807 medium. *Transp. Porous Media*, *122*, 611-632.
- 808 Miller, C. T., Bruning, K., Talbot, C. L., McClure, J. E., & Gray, W. G. (2019). Nonhysteretic  
809 capillary pressure in two-fluid porous medium systems: Definition, evaluation, validation, and  
810 dynamics. *Water Resour. Res.*, *55*, 6825-6849.
- 811 Molins, S., & Knabner, P. (2019). Multiscale approaches in reactive transport modeling. *Rev. Min-*  
812 *eral. Geochem.*, *85*.
- 813 Molins, S., Trebotich, D., Arora, B., Steefel, C. I., & Deng, H. (2019). Multi-scale model of reactive  
814 transport in fractured media: Diffusion limitations on rates. *Transp. Porous Media*, *128*(2),  
815 701-721. doi: 10.1007/s11242-019-01266-2
- 816 Morse, J. W., & Arvidson, R. S. (2002). The dissolution kinetics of major sedimentary carbonate  
817 minerals. *Earth Sci. Rev.*, *58*, 51-84.
- 818 Municchi, F., & Icardi, M. (2020). Macroscopic models for filtration and heterogeneous reactions in  
819 porous media. *Adv. Water Resour.*, *141*. doi: 103605
- 820 Neuman, S. P. (1993). Eulerian-lagrangian theory of transport in space-time nonstationary velocity  
821 fields: Exact nonlocal formalism by conditional moments and weak approximation. *Water Re-*  
822 *sour. Res.*, *29*(3), 633-645.
- 823 Pietrzyk, K., Korneev, S., Behandish, M., & Battiato, I. (2021). Upscaling and automation: Push-  
824 ing the boundaries of multiscale modeling through symbolic computing. *Transp. Porous Media*,  
825 *140*, 313-349.
- 826 Rubinstein, J., & Mauri, R. (1986). Dispersion and convection in periodic porous media. *SIAM J.*  
827 *Appl. Math.*, *46*, 1018-1023.
- 828 Salles, J., Thovert, J.-F., Delannay, R., Prevors, L., Auriault, J.-L., & Adler, P. (1993). Taylor dis-  
829 persion in porous media. determination of the dispersion tensor. *Phys. Fluids A*, *5*, 2348-2376.
- 830 Scheibe, T. D., Murphy, E. M., Chen, X., Rice, A. K., Carroll, K. C., Palmer, B. J., . . . Wood, B. D.  
831 (2015). An analysis platform for multiscale hydrogeologic modeling with emphasis on hybrid  
832 multiscale methods. *Groundwater*, *53*(1), 38-56. doi: <https://doi.org/10.1111/gwat.12179>
- 833 Schiller, U., & Wang, F. (2018). Multiscale simulation of transport phenomena in porous media:  
834 From toy models to materials models. *MRS Commun.*, *8*, 358-371.

- 835 Tang, Y., Valocchi, A. J., & Werth, C. J. (2015). A hybrid pore-scale and continuum-scale model for  
836 solute diffusion, reaction, and biofilm development in porous media. *Water Resour. Res.*, *51*(3),  
837 1846-1859.
- 838 Wang, Z., & Battiato, I. (2020). Patch-based multiscale algorithm for flow and reactive transport in  
839 fracture-microcrack systems in shales. *Water Resour. Res.*, *56*(2). doi: e2019WR025960
- 840 Wang, Z., & Battiato, I. (2021). Upscaling reactive transport and clogging in shale microcracks by  
841 deep learning. *Water Resour. Res.*, *57*(4). doi: e2020WR029125
- 842 Whitaker, S. (1999). *The method of volume averaging*. P.O. Box 17, 3300 AA Dordrecht, The  
843 Netherlands: Kluwer Academic Publishers.
- 844 Wood, B. (2009). The role of scaling laws in upscaling. *Adv. Water Resour.*, *32*, 723-736.
- 845 Yan, Z., Liu, C., Liu, Y., & Bailey, V. L. (2017). Multiscale investigation on biofilm distribution  
846 and its impact on macroscopic biogeochemical reaction rates. *Water Resour. Res.*, *53*(11),  
847 8698-8714.
- 848 Yousefzadeh, M., & Battiato, I. (2017). Physics-based hybrid method for multiscale transport in  
849 porous media. *J. Comput. Phys.*, *344*, 320-338.